

# Numerical modelling of spray and combustion processes using the Euler Eulerian multiphase approach

---

**Petranović, Zvonimir**

**Doctoral thesis / Disertacija**

**2016**

*Degree Grantor / Ustanova koja je dodijelila akademski / stručni stupanj:* **University of Zagreb, Faculty of Mechanical Engineering and Naval Architecture / Sveučilište u Zagrebu, Fakultet strojarstva i brodogradnje**

*Permanent link / Trajna poveznica:* <https://urn.nsk.hr/urn:nbn:hr:235:810384>

*Rights / Prava:* [In copyright](#) / [Zaštićeno autorskim pravom.](#)

*Download date / Datum preuzimanja:* **2025-04-03**

*Repository / Repozitorij:*

[Repository of Faculty of Mechanical Engineering and Naval Architecture University of Zagreb](#)





Sveučilište u Zagrebu

Faculty of Mechanical Engineering and Naval Architecture

Zvonimir Petranović

**NUMERICAL MODELLING OF SPRAY AND  
COMBUSTION PROCESSES USING THE  
EULER EULERIAN MULTIPHASE  
APPROACH**

DOCTORAL THESIS

Zagreb, 2016



Sveučilište u Zagrebu

Fakultet strojarstva i brodogradnje

Zvonimir Petranović

**NUMERIČKO MODELIRANJE PROCESA  
SPREJA I IZGARANJA KORIŠTENJEM  
EULER EULEROVOG VIŠEFAZNOG  
PRISTUPA**

DOKTORSKI RAD

Zagreb, 2016.



Sveučilište u Zagrebu

Faculty of Mechanical Engineering and Naval Architecture

Zvonimir Petranović

**NUMERICAL MODELLING OF SPRAY AND  
COMBUSTION PROCESSES USING THE  
EULER EULERIAN MULTIPHASE  
APPROACH**

DOCTORAL THESIS

Supervisor:  
Asst. prof. dr. sc. MILAN VUJANOVIĆ

Zagreb, 2016



Sveučilište u Zagrebu

Fakultet strojarstva i brodogradnje

Zvonimir Petranović

**NUMERIČKO MODELIRANJE PROCESA  
SPREJA I IZGARANJA KORIŠTENJEM  
EULER EULEROVOG VIŠEFAZNOG  
PRISTUPA**

DOKTORSKI RAD

Mentor:  
Doc. dr. sc. MILAN VUJANOVIĆ

**BIBLIOGRAPHY DATA**

UDC: 519.876.5  
Keywords: Multiphase, spray, combustion, CFD, modelling  
Scientific area: TECHNICAL SCIENCES  
Scientific field: Mechanical engineering  
Institution Faculty of Mechanical Engineering and Naval Architecture  
Thesis supervisor: Asst. prof. dr.sc. Milan Vujanović (FMENA, Zagreb)  
Number of pages: 176  
Number of figures: 63  
Number of tables: 17  
Number of references: 118  
Date of examination: 05 December 2016

## Jury members:

Asst. prof. dr.sc. Milan Vujanović (FMENA, Zagreb)

Prof. dr. sc. Neven Duić (FMENA, Zagreb)

Asst. prof. dr.sc. Darko Kozarac (FMENA, Zagreb)

Dr. sc. Wilfried Edelbauer – (AVL AST, Graz)

Dr. sc. Peter Priesching – (AVL AST, Graz)

Archive: Faculty of Mechanical Engineering and Naval Architecture

## **ACKNOWLEDGMENT**

This work was carried out at the Department of Energy, Power Engineering and Environment in the Faculty of Mechanical Engineering and Naval Architecture, University of Zagreb. I hereby declare that this thesis is entirely the result of my own work and knowledge obtained during my studies, except where otherwise indicated.

First, I would like to express my gratitude to the supervisor of this thesis, Associate Professor Milan Vujanović, for the opportunity, guidance, patience and support throughout this work. I would also like to thank Professor Neven Duić, for giving me the opportunity to work in his group, full of extremely bright, intelligent people that I consider as experts in their scientific field.

I would also like to thank the AVL AST team in Graz, Dr. Reinhard Tatschl, Dr. Klaus Pachler, Eberhard Von Berg, and others in the CFD development group, for the continuous support and accessibility. I would also like to acknowledge the financial support of AVL AST Zagreb. Very special thanks in this regard to its director, Mr. Goran Mirković.

I am very thankful for the valuable comments from jury members, Professor Darko Kozarac, Dr. Peter Priesching and Dr. Wilfried Edelbauer.

With this opportunity I would like to acknowledge special thanks to Dr. Wilfried Edelbauer and Professor Milan Vujanović for leading me through this work, for showing me hints and tips in programming, for sharing their knowledge, for helping me in publishing scientific papers, and for being full of understanding and support. This I will never forget.

I would also like to extend my appreciation to my colleagues, Dr. Marko Ban, Dr. Luka Perković, Dr. Hrvoje Mikulčić, Dr. Jakov Baleta, and Tibor Bešenić who also played a part in this work through helpful discussions.

My beloved parents, who supported this venture, deserve also the deepest gratitude. As I like to say, the opportunity is all I need, and they provided me the one. Thank you for your understanding, for your support, and unconditional love. I would like to thank Sanjin, Eduard and Zinka for being supportive and proud on my accomplishments. Also, I would like to thank Drago and Vesna for their support.

Finally, hereby I acknowledge my greatest thanks to my wife, Iva, and to our daughter Ana for giving me strength. Therefore, I dedicate this work to them, my two shining stars.

Zagreb, December 2016

*Zvonimir Petranović*

## TABLE OF CONTENTS

BIBLIOGRAPHY DATA .....	I
ACKNOWLEDGMENT .....	II
TABLE OF CONTENTS .....	III
SUMMARY .....	VI
SAŽETAK.....	VII
PROŠIRENI SAŽETAK.....	VIII
KEYWORDS .....	XIII
KLJUČNE RIJEČI .....	XIV
LIST OF ABBREVIATIONS .....	XV
NOMENCLATURE.....	XVII
LIST OF FIGURES.....	XXIV
LIST OF TABLES .....	XXVII
1. INTRODUCTION .....	1
1.1. Background .....	1
1.2. Overview .....	2
1.2.1. Compression Ignition Processes .....	2
1.2.2. Fuel Injection and Spray Processes.....	4
1.2.3. Combustion Processes .....	16
1.2.4. Emissions from IC diesel engines.....	18
1.2.5. Modelling Spray Processes .....	20
1.2.6. Modelling Reactive Spray Processes .....	22
1.3. Objective and hypothesis of research.....	24
1.4. Materials and methodology of research .....	24
1.5. Scientific contribution.....	27
2. NUMERICAL MODELLING.....	28
2.1. Fundamental equations of fluid flow and heat transfer.....	28
2.2. Turbulent flows .....	29
2.2.1. Averaging of the conservation equations.....	30
2.2.2. $k - \varepsilon$ turbulence model .....	33
2.2.3. $k - \zeta - f$ turbulence model .....	34
2.3. Multiphase flows.....	36
2.4. The Euler Lagrangian formulation.....	36



2.5.	The Euler Eulerian formulation .....	37
2.5.1.	Averaging in multiphase flows .....	38
2.5.2.	Mass conservation.....	40
2.5.3.	Momentum conservation .....	41
2.5.4.	Enthalpy conservation.....	42
2.5.5.	Species transport conservation.....	42
2.6.	Euler Eulerian spray sub – models.....	43
2.6.1.	Primary atomization.....	43
2.6.2.	Secondary atomization.....	46
2.6.3.	Droplet collision.....	48
2.6.4.	Droplet evaporation .....	49
2.6.5.	Momentum exchange via drag force.....	53
2.6.6.	Combustion .....	55
3.	RESULTS AND DISCUSSION.....	59
3.1.	Eulerian Lagrangian engine modelling .....	59
3.1.1.	Experimental data and numerical setup .....	60
3.1.2.	Results and discussion .....	63
3.2.	Euler Eulerian spray model parametric studies.....	67
3.2.1.	Experimental data and numerical setup .....	68
3.2.2.	Results and discussion .....	70
3.3.	Nozzle – flow spray coupling .....	75
3.4.	Primary atomization modelling.....	80
3.4.1.	DNS data and numerical setup.....	80
3.4.2.	Results and discussion .....	83
3.5.	Secondary atomization modelling.....	86
3.5.1.	Experimental data and numerical setup .....	86
3.5.2.	Results and discussion .....	89
3.6.	O’Rourke collision model.....	92
3.7.	Reactive multiphase spray modelling .....	95
3.7.1.	Euler Eulerian reactive spray method verification.....	96
3.7.2.	Experimental data and numerical setup .....	98
3.7.3.	Results and Discussion .....	101
3.8.	Euler Eulerian engine modelling.....	111

---

3.8.1. Experimental data and numerical setup .....	111
3.8.2. Results and discussion .....	116
4. CONCLUDING REMARKS, CONTRIBUTION AND FUTURE WORK RECOMMENDATIONS.....	122
4.1. Thesis conclusion.....	122
4.1.1. Eulerian Lagrangian modelling.....	122
4.1.2. Parametric study of spray sub – models .....	123
4.1.3. Validation of the WAVE secondary atomization model .....	124
4.1.4. O'Rourke collision model.....	125
4.1.5. Verification of the developed multiphase combustion method .....	125
4.1.6. Validation of the developed multiphase combustion method.....	126
4.2. Thesis contributions .....	127
4.3. Recommendations for future research .....	128
LITERATURE .....	131
CURRICULUM VITAE .....	142
ŽIVOTOPIS .....	144

## **SUMMARY**

The goal of this thesis is to develop advanced engineering method for numerical modelling of highly turbulent multiphase combustion processes.

The first objective was to use the commercial 3D Computational Fluid Dynamics (CFD) code FIRE<sup>®</sup> and model real engineering system by changing various combustion parameters. In this section, the spray process was modelled by employing the widely used Euler Lagrangian discrete Droplet Method (DDM). The focus was to gain insight into advantages and disadvantages of that approach. In the second section, the Euler Eulerian multiphase approach sub – models, namely the liquid jet primary atomization and droplet secondary atomization model were thoroughly analysed and parametrized. Furthermore, the primary atomization model was validated against Direct Numerical Simulation (DNS) data, a new inlet boundary condition was developed, and the nozzle flow – spray interface was enhanced within the Euler Eulerian spray module. In the third section, the validation and enhancement of the WAVE secondary break – up model within the Euler Eulerian framework was performed. The modelled spray cloud shape, spray cone angle, liquid penetration, and droplet size distributions were compared to the available experimental data. In the fourth section, the stochastic O'Rourke collision model was modified and implemented into the Euler Eulerian spray code. In the fifth section, the multiphase module was enhanced with the combustion model where the combustion process was described through general gas phase reactions and chemistry mechanisms. The developed method was verified by numerical modelling of constant volume reactor filled with liquid – gas mixture under elevated pressure and temperature conditions. In the last section, the newly developed method was extensively validated by comparing the simulation results to the available experimental data from the Engine Combustion Network (ECN) database. The liquid and vapour phase penetration, mixture distribution, spray cloud shape and temperature field were examined for various combustion parameters. To find the most suitable spray sub – model coefficients, a high pressure liquid fuel injection into the non – reactive environment was modelled. Finally, the developed method was used to model internal combustion engine compression and expansion stroke. The given results imply that the developed method can be reliably used in a modern engineering development processes.

## SAŽETAK

Cilj ovog rada je razviti naprednu inženjersku metodu za računalno modeliranje turbulentnih višefaznih strujanja i procesa izgaranja.

U prvom dijelu teze modelirani su realni inženjerski sustavi uz varijacije parametara izgaranja. U ovom dijelu teze, za opisivanje procesa spreja korišten je Euler Lagrangeov pristup izoliranih čestica (DDM). Navedeni model spreja korišten je s ciljem stjecanja razumijevanja njegovih prednosti i nedostataka. U drugom dijelu teze provedena je parametrizacija postojećih modela primarnog raspada mlaza goriva i sekundarnog raspada kapljica korištenjem Euler Eulerovog višefaznog pristupa. Modeli su parametrizirani računalnim modeliranjem ubrizgavanja goriva u nereaktivnu okolinu s povišenom temperaturom. Nadalje, primarni model raspadanja mlaza goriva validiran je usporedbom s rezultatima izravnih numeričkih simulacija (DNS), razvijen je novi rubni uvjet za ubrizgavanje goriva i unaprijeđeno je postojeće sučelje sapnica – sprej unutar Euler Eulerovog modela spreja. U trećem dijelu teze verificiran je, validiran i modificiran WAVE model sekundarnog raspada kapljica unutar Euler Eulerovog pristupa. Izračunati oblik isparenog goriva, kut spreja, penetracija goriva te distribucija kapljica uspoređeni su s dostupnim eksperimentalnim podacima. U četvrtom dijelu teze modificiran je i unaprijeđen O'Rourke model sudaranja kapljica unutar Euler Eulerovog sprej modela. U petom dijelu teze Euler Eulerov model nadograđen je s modelom za opisivanja procesa izgaranja. Verifikacija razvijene metode izvršena je računalnim modeliranjem reaktora s konstantnim volumenom ispunjenog smjesom goriva i plinova u uvjetima povišenog tlaka i temperature. U šestom dijelu teze novo razvijena metoda validirana je usporedbom modeliranih rezultata s eksperimentalnim podacima grupe koja se bavi istraživanjem procesa izgaranja u motorima s unutarnjim izgaranjem (*eng. Engine Combustion Network – ECN*). Uspoređeni su podaci penetracije kapljevite i plinovite faze, radijalna i aksijalna distribucija isparenog goriva, oblik isparenog goriva te temperaturna polja. Kako bi se definirali odgovarajući koeficijenti korištenih modela spreja, provedeno je istraživanje ubrizgavanja kapljevito goriva u nereaktivnu okolinu. Nakon toga, izvršena je validacija razvijene metode računalnim modeliranjem realnih sustava ubrizgavanja. U završnom dijelu rada, novo razvijena metoda korištena je za računalne simulacije motora s unutarnjim izgaranjem.

## PROŠIRENI SAŽETAK

Kao rezultat izgaranja fosilnih goriva velika količina emisija ispušta se u atmosferu. Veliki dio tih emisija dolazi iz transportnog sektora u kojem je u posljednjem desetljeću zabilježen značajan porast potrošnje energije. Zbog toga, važno je pronaći rješenje i utjecati na smanjenje štetnih emisija iz rastućeg transportnog sektora. U posljednje vrijeme propisane su stroge regulative vezane uz štetne emisije, a još se strože očekuju u budućnosti. Štetne emisije iz motora s unutarnjim izgaranjem ovise o procesu spreja i atomizaciji goriva, pogotovo o kvaliteti miješanja goriva i zraka. Razumijevanje i poboljšavanje tih procesa predstavlja jedno od rješenja u daljnjem razvoju motora s unutarnjim izgaranjem te u razvoju drugih sustava gdje dolazi do procesa spreja i izgaranja. Zbog dugog vremenskog perioda i visoke cijene eksperimentalnih ispitivanja, kombinirana primjena eksperimenata i Računalne Dinamike Fluida (RDF) postao je uobičajeni razvojni pristup. Zbog toga se odgovarajuće i pouzdano numeričko modeliranje interakcije goriva i zraka smatra kao važna stavka za uvid u proces spreja i za razumijevanje turbulentnih strujanja fluida. Razumijevanjem procesa spreja i interakcije goriva i zraka moguće je pristupiti unaprijedenu različitih inženjerskih sustava.

Postoji nekoliko računalnih pristupa koji se koriste za modeliranje turbulentnih višefaznih strujanja, kao što su: računalno zahtjevne izravne numeričke simulacije (*eng. Direct Numerical Simulations – DNS*), pristup izoliranih čestica (*eng. Discrete Particle Model – DPM*), Euler Lagrangeov pristup praćenja kapljica, Euler Eulerov višefazni pristup, itd. Euler Lagrangeov pristup uobičajen je i često korišten pristup za računanje procesa spreja u kojem se kapljevito gorivo grupira u skupine kapljica (parcele) sličnog promjera i sličnih fizikalnih svojstava. Za svaku parcelu rješavaju Lagrangeove jednadžbe te se računa njihova trajektorija, dok se plinovita faza tretira kao kontinuum te se modelira pomoću jednadžbi očuvanja mase, količine gibanja i energije. Ovakav pristup ima nedostatke kao što su ovisnost o prostornoj diskretizaciji u blizini točke ubrizgavanja goriva te porast računalnog opterećenja s povećanjem broja parcela. Također, takav pristup modeliranja spreja ima i nedostatak vezan uz statističku konvergenciju. Unatoč navedenim nedostacima, Lagrangeov pristup pogodan je za modeliranje područja raspršenog spreja gdje je koncentracija kapljevite faze dovoljno niska.

Proces spreja može se opisati korištenjem metoda praćenja površine interakcije kapljevite i plinovite faze, kao što su Volume of Fluid (VOF) i „level-set“ metode. Takve metode, unatoč visokoj razini točnosti, računalno su zahtjevne i trenutačno nisu u tolikoj mjeri zastupljene u razvoju realnih inženjerskih sustava.

Kako bi se zaobišli nedostaci Euler Lagrangeovog pristupa može se koristiti Euler Eulerov višefazni pristup. U ovom pristupu, postignuta je jača fizikalna sprega između kapljevite i plinovite faze te je kao takav pogodniji za računalno modeliranje područja gustog spreja. Jača fizikalna sprega postignuta je pretpostavkom da su kapljevita i plinovita faza kontinuumi, te rješavanjem Eulerovih jednadžbi očuvanja za obje faze. Za efikasno numeričko modeliranje procesa spreja potrebno je razumjeti utjecaj pojedinih parametara na proces spreja. Neki od parametara su strujanje unutar sapnice, tlak ubrizgavanja, tlak komore izgaranja, temperatura goriva, itd.

Kako bi se iskoristile prednosti Euler Eulerovog i Euler Lagrangeovog pristupa, oni se mogu koristiti istovremeno u spregnutim računalnim simulacijama – ACCI metoda (AVL Code Coupling Interface). Na taj način, rezultati dobiveni u jednoj računalnoj simulaciji koriste se, ili kao rubni uvjet, ili kao izvorski član/ponor u drugoj simulaciji. U posljednje vrijeme razvijan je još jedan pristup spregnutih simulacija - ELSA (Euler Lagrangian Spray Atomization) model. Glavna prednost ELSA modela je bolje opisivanje područja gustog spreja. Razlika između ELSA i ACCI modela je što se u ELSA modelu, u blizini sapnice, plinovita i kapljevita faza modeliraju kao smjesa kapljevite i plinovite.

Trenutno postoji nekoliko različitih pristupa modeliranju izgaranja gorivih para nastalih prilikom procesa spreja kao što su eddy dissipation, flamelet, PDF (eng. Probability Density Function), modeli izgaranja uz korištenje detaljne kemijske kinetike, itd. Mogućnost korištenja Euler Eulerovog višefaznog pristupa u kombinaciji s kemijskom kinetikom za opisivanje višefaznih reaktivnih strujanja do sada nije obrađena i objavljena u literaturi. Stoga, glavni cilj ovog doktorskog rada bio je razviti i implementirati takav pristup koji će biti korišten za pouzdano računalno modeliranje procesa turbulentnog višefaznog procesa spreja i procesa izgaranja.

## *CILJ I HIPOTEZA*

Hipoteza ovog rada je da su numeričke simulacije ubrizgavanja kapljevito goriva i procesa izgaranja, korištenjem Euler Eulerovog pristupa u kombinaciji s kemijskom kinetikom izvedive, te da se mogu koristiti u razvoju različitih inženjerskih sustava s postojećim reaktivnim tokovima fluida. Rezultati ovog rada omogućuju pouzdan opis procesa spreja u području gustog i razrijeđenog spreja. Nadalje, s detaljnim opisom procesa spreja dobiven je i pouzdan opis procesa izgaranja. Cilj ovog rada je bio uspostaviti pristup koji će potvrditi

hipotezu opsežnom usporedbom rezultata računalnog modeliranja i dostupnih eksperimentalnih podataka.

### ZNANSTVENI DOPRINOS

Rezultat ovog rada je nova metoda za računalno modeliranje višefaznih procesa spreja i procesa izgaranja. Metoda je razvijena kombiniranjem Euler Eulerovog višefaznog modela s kemijskom kinetikom za opisivanje procesa izgaranja. Postojeće sučelje sapnica – sprej unaprijeđeno je za višeprosorsko računanje i razvijen je novi rubni uvjet za Eulerov model spreja. Nadalje, Euler Eulerov model spreja unaprijeđen je s O'Rourke modelom za opisivanje procesa sudaranja kapljica te je validiran primarni model raspadanja mlaza goriva usporedbom s rezultatima izravnih numeričkih simulacija dostupnih iz literature. S ciljem boljeg opisivanja spreja u vidu predviđanja volumne i brojčane distribucije kapljica spreja, model sekundarnog raspadanja kapljica goriva unaprijeđen je s opcijom stvaranja satelitskih kapljica (*eng. child droplet*). Na temelju prikazanih rezultata može se zaključiti da razvijena metoda može proširiti područje korištenja Euler Eulerovog modela spreja, metode klase kapljica, na različite inženjerske aplikacije gdje postoje višefazni reaktivni tokovi fluida.

### METODE I POSTUPCI

Postoji nekoliko računalnih pristupa za rješavanje turbulentnih višefaznih strujanja kao što su izravne numeričke simulacije, pristup izoliranih čestica, Euler Lagrangeov pristup praćenja kapljica, Euler Eulerov višefazni pristup, itd. Euler Lagrangeov pristup je uobičajen i često korišten numerički pristup korišten za računanje procesa spreja, ali ima neke nedostatke. Da bi se izbjegli ti nedostaci može se koristiti Euler Eulerov višefazni pristup. U tom pristupu, kapljevit i plinovita faza smatraju se kontinuumom te se obje faze rješavaju Eulerovim pristupom. Ista diskretizacija, slične numeričke tehnike i jednačbe očuvanja koriste se za obje faze. Kako bi se što točnije opisalo ponašanje spreja, kapljice se dijele u konačan broj klasa karakteriziranih promjerom kapljica. Takav model, ujedno korišten i razvijan u ovome radu, uobičajeno se naziva model klasa kapljica. Za svaku klasu kapljica rješava se set jednačbi očuvanja s dodatnim izvorskim članovima za opis dinamike kapljica. Matematički modeli računanja procesa spreja i izgaranja korišteni su unutar Eulerovog sprej koda, prilikom čega se termo kemijske reakcije računaju unutar plinovite faze u pojedinom kontrolnom volumenu. Kemijske reakcije unutar plinovite faze rješavaju se korištenjem rješavača diferencijalnih jednačbi pomoću kojeg se računaju izvorski i ponorski članovi za transportne jednačbe

kemijskih vrsta i entalpije. Prikazani modeli spreja integrirani su u komercijalni kod AVL FIRE<sup>®</sup> korištenjem korisničkih funkcija. Spajanje jednadžbi modela s RDF kodom omogućeno je korištenjem uobičajenih FORTRAN funkcija. Istraživanje je izrađeno u nekoliko koraka kako bi se dobio pouzdan pristup za modeliranje procesa spreja i izgaranja.

Prvi korak istraživanja je opsežan pregled literature vezan na područje spreja te su prikazani rezultati računalnih simulacija korištenjem Euler Lagrangeovog pristupa. Računalno je modeliran jednocilindrični eksperimentalni motor s unutarnjim izgaranjem uz variranje pojedinih parametra izgaranja. Nadalje, izrađena je analiza polja temperature i štetnih emisija. Model je uspješno validiran usporedbom izračunatih rezultata s dostupnim eksperimentalnim podacima te su prikazani prednosti i nedostaci Euler Lagrangeovog pristupa modeliranja spreja.

Drugi korak istraživanja je detaljna parametrizacija postojećih modela primarnog raspada mlaza goriva i sekundarnog raspada kapljica korištenjem Euler Eulerovog višefaznog pristupa. U ovome dijelu opisan je navedeni pristup rješavanja spreja te su prikazane korištene jednadžbe očuvanja. Istraženi su modeli primarnog i sekundarnog raspada te je odabran set koeficijenata modela koji je dalje korišten u računalnim simulacijama u ovom dijelu rada. Parametrizacija modela izrađena je računalnim modeliranjem ubrizgavanja kapljevito goriva u nereaktivnu okolinu povišene temperature. Na taj način, omogućen je proces isparavanja, ali je izbjegnuta proces izgaranja. Model je validiran usporedbom rezultata računalnih simulacija s dostupnim eksperimentalnim podacima, prilikom čega je ispitan utjecaj koeficijenata modela na penetraciju kapljevito i isparenog goriva. Modelirani slučajevi spreja razlikuju se u tlakovima ubrizgavanja i tlaku komore izgaranja. Nadalje, u ovome dijelu rada verificiran je model primarnog raspadanja mlaza kapljevito goriva usporedbom s rezultatima izravnih numeričkih simulacija, implementiran je rubni uvjet za ubrizgavanje kapljevito goriva uz korištenje dijagrama ubrizgavanja goriva te je unaprijeđeno sučelje za spajanje računalnih simulacija toka goriva kroz sapnicu i procesa spreja.

Treći korak istraživanja je verifikacija i validacija WAVE modela sekundarnog raspada kapljica goriva unutar Euler Eulerovog pristupa. Model je validiran usporedbom rezultata računalnog modeliranja raspada kapljica goriva s dostupnim eksperimentalnim podacima iz literature te istraživanjem visokotlačnog ubrizgavanja kapljevito goriva s detaljno definiranom selekcijom ulaska goriva. Rubni uvjet ubrizgavanja goriva u sprezi je s računalnom simulacijom toka goriva kroz mlaznicu korištenjem datoteke sapnice i sučelja razvijenog u drugome dijelu teze. U datoteci sapnice zapisani su podaci turbulencije, temperature, brzine, gustoće goriva i smjese plinova za svaku fazu kroz cijeli vremenski period ubrizgavanja goriva, te su ti podaci



preslikani na ulaznu selekciju u Euler Eulerovoj računalnoj simulaciji procesa spreja. Računalno su modelirani različiti slučajevi visokotlačnog ubrizgavanja goriva u komoru konstantnog volumena ispunjenu nereaktivnom smjesom plinova. Oblik isparenog goriva, kut spreja, penetracija goriva te distribucija kapljica uspoređeni su s dostupnim eksperimentalnim podacima.

Četvrti korak istraživanja je modifikacija i implementacija stohastičkog O'Rourke modela sudaranja kapljica za Euler Eulerov višefazni pristup. Sudaranje kapljica računa se za definirana sučelja klasa u svim kontrolnim volumenima gdje ima dovoljno kapljevite faze. Za svaku fazu aktivnog sučelja, na odgovarajući način, računa se promjer kapljice, brzina i temperatura slijedeći konzervativna svojstva mase, količine gibanja i energije. Implementirani model sudaranja kapljica korišten je za računanje procesa spajanja kapljica.

Peti korak istraživanja je razvoj Euler Eulerovog pristupa modeliranja spreja s ciljem opisivanja procesa izgaranja. Rezultati ovog dijela rada omogućuju korištenje homogenih kemijskih reakcija u računalnim simulacijama višefaznih strujanja prilikom čega je proces izgaranja opisan korištenjem kemijske kinetike. Razvijena metoda verificirana je računalnim modeliranjem reaktora s konstantnim volumenom ispunjenog smjesom goriva i plinova pod povišenim tlakom i temperaturom te je istražen utjecaj procesa isparavanja na masene bilance, razvoj topline, i na promjene temperature nastale uslijed procesa izgaranja.

Šesti korak istraživanja je detaljna validacija nove metode koja obuhvaća istovremeno korištenje Euler Eulerovog modela spreja i kemijske kinetike. Metoda je validirana uspoređivanjem rezultata računalnog modeliranja s dostupnim eksperimentalnim podacima iz ECN baze podataka. Istražen je utjecaj raznih parametara spreja na penetracije kapljevite i plinovite faze, radijalna i aksijalna distribucija isparenog goriva, oblik oblaka isparenog goriva te temperaturna polja. Inicijalno su istraženi slučajevi ubrizgavanja kapljevite goriva u nereaktivno okruženje. Nakon toga, računalno su modelirani različiti reaktivnih slučajevi ubrizgavanja kapljevite goriva te su rezultati simulacije uspoređeni s dostupnim eksperimentalnim podacima kao što su udaljenosti procesa izgaranja od sapnice, porast tlaka u komori izgaranja, polja koncentracije OH radikala, polja temperature te vrijeme početka izgaranja. U završnom dijelu teze, novo razvijena metoda korištena je za računalne simulacije realnog motora s unutarnjim izgaranjem.

## **KEYWORDS**

*Computational fluid dynamics;*

*Numerical modelling;*

*Euler Eulerian approach;*

*Euler Lagrangian approach;*

*Multiphase;*

*Spray process;*

*Primary break – up;*

*Secondary break – up;*

*Droplet collision;*

*Droplet evaporation;*

*Vapour combustion;*

*Compression ignition;*

*IC engine;*

*Diesel;*

*n – heptane;*

*n – dodecane;*

*Reaction kinetics;*

*Constant volume vessel;*

*Pollutant emission;*

---

## KLJUČNE RIJEČI

*Računalna mehanika fluida;*

*Modeliranje;*

*Euler Eulerov pristup;*

*Euler Lagrangeov pristup;*

*Višefazno strujanje;*

*Proces spreja;*

*Primarno raspadanje mlaza goriva;*

*Sekundarno raspadanje kapljica goriva;*

*Sudaranje kapljica;*

*Isparavanje;*

*Izgaranje;*

*Samozapaljenje;*

*Motor s unutarnjim izgaranjem;*

*Dizel;*

*n – heptane;*

*n – dodecane;*

*Kemijska kinetika;*

*Komora s konstantnim volumenom;*

*Štetne emisije;*

**LIST OF ABBREVIATIONS**

<b><u>Abbreviations</u></b>	<b><u>Description</u></b>
ACCI	AVL code coupling interface
AVL	Anstalt für Verbrennungskraftmaschinen List (German)
BDC	Bottom dead centre
CDS	Central differencing scheme
CEN	European Standards Committee
CFD	Computational fluid dynamics
CI	Compression ignition
CVV	Constant volume vessel
DDM	Discrete droplet method
DNS	Direct numerical simulations
DPF	Diesel particulate filter
DPM	Discrete particle model
ECN	Engine combustion network
EDC	Eddy dissipation concept
EGR	Exhaust gas residuals
ELSA	Euler Lagrangian spray atomization
EOI	End of injection
EVM	Eddy viscosity model
FIPA	Fractionnement Induit Par Acceleration
GHG	Greenhouse gases
HC	Hydrocarbons
IC	Internal combustion
ID	Ignition delay
KH	Kevin – Helmholtz instabilities
LES	Large eddy simulations
LNT	Lean NOx trap
LOL	Lift off length
PDF	Probability density function

---

PM	Particulate matter
RANS	Reynolds averaged Navier Stokes
RDF	Računalna dinamika fluida
RN <sub>1</sub> , RN <sub>2</sub>	collision model random numbers
ROHR	Rate of heat release
ROI	Rate of injection
RT	Rayleigh – Taylor instabilities
SAC	Sack area around the needle tip
SCR	Selective catalyst reduction
RSM	Reynolds stress model
SMD	Sauter mean diameter
SOI	Start of injection
TAB	Taylor analogy break – up model
TDC	Top dead centre
TED	Turbulent dissipation energy
TKE	Turbulent kinetic energy
VOF	Volume of fluid
WAVE	secondary break – up model WAVE

**NOMENCLATURE**

<b><u>Roman</u></b>	<b><u>Description</u></b>	<b><u>Unit</u></b>
$A_D$	droplet frontal area	[m <sup>2</sup> ]
$A_i$	Coefficient in the Arrhenius expression	[1/s]
$b_{cr}$	Critical impact parameter	[-]
$B_{S1}, B_{S2}$	Constants in secondary break-up model	[-]
$B_M$	Spalding mass number	[-]
$B_T$	Spalding heat number	[-]
$Ca$	Area contraction coefficient	[-]
$Cd$	Nozzle discharge coefficient	[-]
$c_D$	drag coefficient	[-]
$C_\mu$	Constant in turbulence model	[-]
$c_{pk}$	Specific heat capacity for phase $k$	[J/kg/K]
$\bar{C}_{pF}$	specific heat capacity of vapour phase	[J/kg/K]
$C_{\varepsilon1}, C_{\varepsilon2},$	Constants in turbulence model	[-]
$C_{\varepsilon3}, C_{\varepsilon4}, C_T,$		
$C_L, C_\eta, C_\mu$		
$B_{P1}, B_{P2}, B_{P3}$	Constants in primary break-up model	[-]
$, C_4, C_5, C_6,$		
$C_7$		
$d$	diameter	[m]
$D_{kl}$	Turbulent dissipation inter-phase exchange between phase $k$ and $l$	[W/m <sup>3</sup> /s]
$D_{Y_i}$	species diffusion coefficient	[m <sup>2</sup> /s]
$E_i$	activation energy,	[J/kmol]
$f_i$	Cartesian component of the force vector	[m/s <sup>2</sup> ]

$f$	Elliptic function	[kg/m <sup>3</sup> /s]
$f$	complex function used within the collision model	[-]
$F_D$	Drag force	[N]
$F_{St}$	Stokes drag force	[N]
$F_M, F_T$	Diffusional and thermal film correction factors	
$G$	production/destruction of quantity by body force	[kg/m/s <sup>3</sup> ]
$h$	Specific enthalpy	[J/kg]
$H$	Interfacial enthalpy exchange term	[W/m <sup>3</sup> ]
$H_{fk}$	Heat of formation of the species $k$	[kJ/kmol]
$I$	number of reactions in the system	[-]
$k$	Turbulent kinetic energy	[m <sup>2</sup> /s <sup>2</sup> ]
$k_b$	backward reaction rate coefficients	[-]
$k_f$	forward reaction rate coefficients	[-]
$\bar{k}_g$	Thermal conductivity	[W/m/K]
$k_i$	chemical reaction rate	[-]
$K_{kl}$	Turbulent kinetic energy inter-phase exchange term between phase $k$ and $l$	[W/m <sup>3</sup> ]
$l$	Mixing length	[m]
$l_m$	Turbulent mixing length	[m]
$L$	turbulent length	[m]
$L$	latent heat	[J/kg]
$L_A$	atomization length scale	[m]
$Le$	Lewis number	[-]
$L_{noz}$	Nozzle channel length	[m]
$L_T$	Turbulent length scale	[m]
$L_W$	Aerodynamic length scale	[m]
$M$	Molar mass	[kg/kmol]

$m$	mass	[kg]
$n$	number of collisions	[-]
$n$	sample range	[m]
$n_j$	Cartesian component of the unit normal vector	[-]
$N$	number of process/experiment realisations	
$N_j^{III}$	number density	[1/m <sup>3</sup> ]
Oh	Ohnesorge number	[-]
$P$	pressure	[Pa]
$P$	Production of transported property by mean flow deformation	[kg/m/s <sup>3</sup> ]
$P_n$	Probability of collision process	[-]
$P_o$	Probability that the collision process will not occur	[-]
$q_{kj}$	Cartesian component of the heat flux vector for phase $k$	[W/ m <sup>2</sup> ]
$q_i$	reaction rate of reaction $i$	
$Q_L$	heat transfer into to droplet	[J]
$R$	universal gas constant	[J/kmol/K]
Re	Reynolds number	[-]
$r$	radius	[m]
$\dot{\cdot}$	Reaction rate of species $i$	[1/s]
$S$	surface	[m <sup>2</sup> ]
$S$	additional term for definition of turbulent length and time scales	[s <sup>-1</sup> ]
$Sc^t$	Turbulent Schmidt number	[-]
$S_g$	soot surface growth source	[kg/s]
$S_H$	Source term for heat of reaction	[W]
$S_n$	soot nucleation source	[kg/s]
$S_k$	Mass source term for species $k$	[kg/s]



$S_{O_2}$	soot oxidation source	[kg/s]
$S_{\phi S}$	soot formation rate source	[kg/s]
$S_{Y_i}$	Species $i$ source term	[kg/s]
$t$	time	[s]
$T$	turbulent time	[s]
	Taylor number	[-]
	Temperature	[K]
$T_{ref}$	Reference temperature	[K]
$u$	velocity	[m/s]
$u_i$	Cartesian velocity component	[m/s]
$u_j$	Cartesian velocity component	[m/s]
$u_k$	Cartesian velocity component	[m/s]
$\bar{u}_{mol}$	Averaged velocity	[m/s]
$u_t$	Characteristic turbulent velocity	[m/s]
$V$	volume	[m <sup>3</sup> ]
$V_{cell}$	cell volume	[m <sup>3</sup> ]
$We$	Weber number	[-]
$W_k$	Molecular weight of species $k$	[kg/kmol]
$w_k^n$	starting value of species $k$ mass fraction	[kg/kg]
$w_k^{n+1}$	0D reactor model value of species $k$ mass fraction	[kg/kg]
$x_i$	Cartesian coordinate	[m]
$x_j$	Cartesian coordinate	[m]
$x_k$	Cartesian coordinate	[m]
$X_k$	molar concentration of species $k$	[kmol/kmol]
$\mathcal{Y}$	droplet distortion parameter	[-]
$Y_i$	Species mass fraction	[-]
$Y_F$	Fuel mass fraction	[-]

<b><u>Greek</u></b>	<b><u>Description</u></b>	<b><u>Unit</u></b>
$\alpha$	volume fraction	[-]
$\bar{D}_g$	Binary diffusion coefficient	[m <sup>2</sup> /s]
$\varepsilon$	Dissipation rate of the turbulent kinetic energy	[m <sup>2</sup> /s <sup>3</sup> ]
$\delta_{T0}$	Thermal film thickness	[m]
$\delta_{M0}$	Diffusion film thickness	[m]
$\kappa_k$	Thermal conductivity for phase $k$	[W/m/K]
$\kappa_k$	species $k$	[-]
$\nu$	Kinematic viscosity	[m/s <sup>2</sup> ]
$\Gamma$	Mass transfer between phases	[kg/m <sup>3</sup> /s]
$\Delta n$	droplet class range for SMD calculation	[m]
$\rho$	density	[kg/m <sup>3</sup> ]
$\mu$	Dynamic molecular viscosity	[Pas]
$\mu_t$	turbulent viscosity	[Pas]
$\nu_i$	collision frequency	[1/s]
$\nu'_{ki}$	stoichiometric coefficient of reactants	[kmol]
$\nu''_{ki}$	stoichiometric coefficient of products	[kmol]
$\Lambda$	wave length	[m]
$\Omega$	wave growth rate	[1/s]
$\omega_k$	rate of production of species $k$	[kg/m <sup>3</sup> /s]
$\sigma$	surface tension	N/m <sup>2</sup>
$\sigma_k$	Constant in turbulence model	[-]
$\sigma_\varepsilon$	Constant in turbulence model	[-]
$\sigma_T$	Turbulent Prandtl number	[-]
$\zeta$	Velocity scales ratio	[-]
$\tau_A$	Atomization time scale	[s]
$\tau_{ij}$	Tangential stress tensor component	[N/m <sup>2</sup> ]

$\tau_{kij}$	Viscous stress tensor of phase k	N/m <sup>2</sup>
$\tau'_{kij}$	Reynolds stress tensor of phase k	
$\varphi$	General transport scalar variable	[-]
$\overline{\varphi}$	Mean part of averaged general transport scalar variable	[-]
$\varphi'$	Fluctuating part of averaged general transport scalar variable	
$\Phi$	Quantity	
$\overline{\Phi}_k$	component-weighted average	
$\overline{\Psi}_k$	mass-weighted average	
$\chi$	phase indicator function	[-]

**Subscripts****Description**

<i>A</i>	atomization
<i>avg</i>	averaged
<i>cr</i>	critical
<i>drop</i>	droplet
<i>D</i>	drag
<i>g</i>	gas phase
<i>i</i>	species index reaction index collector class
<i>inj</i>	injection
<i>j</i>	droplet class in the collision model
<i>k</i>	phase index in multiphase flow index of liquid class within the Euler Eulerian size – of – classes approach
<i>K</i>	number of gas phase species
<i>l</i>	liquid phase
<i>mol</i>	number of moles

$n$	nozzle
	number of experiments/realisations for averaging procedure
	bulk liquid class
	starting value
$n+1$	reactor model results
$nph$	number of phases
$noz$	nozzle
$P$	Lagrangian particle
$S$	surface
$target$	target droplet class
$W$	aerodynamic
$\varphi$	Intensive property
$\varphi$	General variable
1	gas phase
$\infty$	ambient condition

<b><u>Superscripts</u></b>	<b><u>Description</u></b>
----------------------------	---------------------------

$b_i$	Coefficient in Arrhenius expression
$nph$	number of phases
'	Reynold fluctuation
"	Favre fluctuation
-	Reynolds average
~	Favre average
III	number density
*	Modified

## LIST OF FIGURES

Figure 1	Schematic of IC diesel engine combustion chamber.....	3
Figure 2	Schematic of fuel injection system and cavitation process .....	5
Figure 3	Schematic of spray regimes.....	6
Figure 4	Schematic of liquid jet atomization mechanisms .....	7
Figure 5	Schematic of liquid jet break – up regimes [11] .....	9
Figure 6	Schematic of droplet secondary break – up regimes reproduced from [13] .....	10
Figure 7	Schematic of catastrophic secondary break – up mechanisms reproduced from [14][12].....	11
Figure 8	Schematic of spray characteristics .....	14
Figure 9	Schematic of IC diesel engine working cycle .....	17
Figure 10	Schematic of spray modelling approaches and the Euler Eulerian spray sub – models.....	38
Figure 11	Computational mesh for engine calculation.....	62
Figure 12	Calculated temperature, NO mass fraction, and soot mass fraction field .....	64
Figure 13	Comparison of calculated and experimental in – cylinder mean pressure and mean temperature profiles.....	66
Figure 14	Comparison of calculated and measured soot and NO <sub>x</sub> emissions relative to the case <i>a</i> .....	67
Figure 15	Experimental data of injection velocity and fuel tip penetration .....	68
Figure 16	Computational mesh for Euler Eulerian spray model parameterization .....	69
Figure 17	Parameterization of the primary atomization model for operating point d .....	71
Figure 18	Parameterization of the secondary atomization model for operating point d.....	72
Figure 19	Comparison of calculated and experimental liquid and vapour spray tip penetration .....	73
Figure 20	Comparison of calculated and measured liquid and vapour penetration (top), and distribution (bottom) for case d.....	74
Figure 21	Results of nozzle file mapping for the liquid volume fraction .....	76
Figure 22	Results of nozzle file mapping for various quantities .....	77
Figure 23	Computational meshes used for validation of the nozzle file interface .....	78
Figure 24	Calculated mass flow profile.....	79
Figure 25	Cavitation influence on the spray inlet boundary selection captured with the mapping procedure .....	79

Figure 26	Computational mesh used for validation of the primary break – up model.....	81
Figure 27	2D Euler Eulerian simulation results and DNS diagrams of volume fraction distribution .....	82
Figure 28	Comparison of calculated and DNS radial mixture distribution at $x/d=5$ .....	83
Figure 29	Comparison of calculated and DNS radial mixture distribution at $x/d=10$ .....	84
Figure 30	Comparison of calculated and DNS radial mixture distribution at $x/d=20$ .....	84
Figure 31	Comparison of calculated and DNS axial mixture distribution .....	85
Figure 32	Comparison of calculated and DNS liquid volume fraction field.....	85
Figure 33	Measured spray tip penetration .....	86
Figure 34	Computational meshes used for validation of secondary break – up model .....	88
Figure 35	Comparison of calculated and measured spray tip penetration .....	90
Figure 36	Comparison of calculated and measured spray angle .....	90
Figure 37	Comparison of calculated and measured droplet number distribution (left) and droplet volume distribution (right) .....	91
Figure 38	Computational mesh used for verification of the collision model .....	92
Figure 39	Calculated volume fraction field, and the number of droplet collisions with implemented collision model .....	93
Figure 40	Calculated volume fraction field without implemented collision model .....	94
Figure 41	Calculated sauter mean diameter field without (left) and with implemented collision model (right).....	95
Figure 42	Computational mesh used for verification of the Euler Eulerian reactive spray method.....	97
Figure 43	Calculated profiles of fuel mass fraction, oxygen mass fraction, temperature and ROHR.....	98
Figure 44	Computational mesh used for the n – heptane spray simulation.....	100
Figure 45	Comparison of calculated and measured liquid and vapour penetration, and mixture radial distribution profiles (right) for Case_h.....	102
Figure 46	Comparison of calculated and measured mixture field for Case_h.....	103
Figure 47	Comparison of calculated and measured temperature field for Case_h.....	104
Figure 48	Comparison of calculated and measured liquid and vapour penetration for Case_d1 and Case_d2 .....	105
Figure 49	Comparison of calculated and measured fuel vapour radial (top) and axial distribution (bottom) for Case_d1 and Case_d2.....	106

Figure 50	Comparison of calculated mixture and temperature field for Case_d2.....	107
Figure 51	Comparison of calculated and measured lift off length and ignition delay for n – heptane spray cases .....	108
Figure 52	Comparison of calculated and measured vapour penetration for Case_d_r.....	109
Figure 53	Comparison of calculated and measured OH results of mass fraction field (left), pressure rise and rate of heat release profiles.....	110
Figure 54	Computational mesh used for engine calculation.....	112
Figure 55	Details of the computational mesh used for engine modelling .....	113
Figure 56	Injection velocity profile .....	115
Figure 57	Experimental results of mean pressure a), mean temperature traces b) and rate of heat release c) .....	117
Figure 58	Comparison of calculated and measured in – cylinder mean pressure.....	118
Figure 59	Comparison of calculated and measured in – cylinder mean temperature.....	118
Figure 60	Comparison of calculated and measured rate of heat release.....	119
Figure 61	Cutting plane used for analysing the calculated results .....	119
Figure 62	Calculated gas velocity field at different crank angle positions.....	120
Figure 63	Calculated gas temperature field at different crank angle positions .....	121

**LIST OF TABLES**

Table 1	Default values of $k - \varepsilon$ turbulence model.....	33
Table 2	Default values of $k - \zeta - f$ turbulence model.....	35
Table 3	Euler Eulerian size – of – classes approach class specification. ....	37
Table 4	Chemistry mechanisms used within this thesis .....	58
Table 5	Characteristics of the experimental engine and the BOSCH Piezo common rail injection system.....	61
Table 6	Combustion system parameters.....	61
Table 7	Pollutant emission concentrations measured in the exhaust pipe.....	61
Table 8	Computational mesh boundary conditions.....	62
Table 9	Parameters of the engine operating points .....	63
Table 10	Operating conditions for model parameterization.....	69
Table 11	Nozzle flow – spray interface validation cases.....	77
Table 12	Measured spray characteristics for the examined nozzle designs .....	87
Table 13	Operation conditions for the non-reactive and the reactive spray cases .....	99
Table 14	Engine specifications.....	112
Table 15	Combustion characteristics of the simulated operating point .....	114
Table 16	Initial conditions for engine simulation.....	115
Table 17	Time discretization for engine simulation.....	116



# 1. INTRODUCTION

## 1.1. Background

Due to a higher fuel conversion efficiency, the compression ignition Internal Combustion (IC) engines are a favourable choice on the transportation vehicle market in the European countries. In addition, there are several other factors for their favourable choice such as high power output, fuel consumption reduction, high durability, and their reliability. The IC engines are usually powered by burning the fossil fuels which results in emitting great amounts of pollutant emissions into the Earth atmosphere. Such pollution is a hot topic and a great challenge for modern society. Therefore, a special attention is given to this issue. In order to reduce the harmful pollutants, specifically soot and NO<sub>x</sub> emissions, more and more stringent regulations are being put in front of the IC engine manufacturers. Those regulations represent a huge motivation and obligation to improve the existing technology. European Union developed the Euro standards Euro 1 – 6 that are used as a benchmark for reducing the pollutant emissions. The latest Euro 6 standard prescribes 80 % lower pollutant emission amounts from diesel engines compared to the Euro 1 standard. To reach this goal several measures have to be taken.

One of the measures for reducing the pollutant emissions emitted from IC engines is the use of aftertreatment emission control systems, such as diesel oxidation catalyst, diesel particulate filter, and Selective Catalytic Reduction (SCR). With emission control, pollutants from the exhaust system can be eliminated after they leave the IC engine combustion chamber. The pollutant emission control systems that are being used to reduce the Nitrogen Oxide (NO<sub>x</sub>) emissions are Exhaust Gas Recirculation (EGR), Lean NO<sub>x</sub> Trap (LNT) [1], SCR, etc. In EGR systems, widely used in IC diesel engines, the burned gas mixture is recirculated in the combustion chamber. This reduces the combustion efficiency but decreases the in – cylinder temperature. Accordingly, the NO<sub>x</sub> concentration is lowered and the concentration of HC and CO species is increased. The EGR and LNT systems are not enough to meet the EURO 6 emission standards and therefore another strategies, such as SCR had to be developed. The SCR is used to minimize the NO<sub>x</sub> emissions in the exhaust system, mostly from high duty vehicles, by using ammonia NH<sub>3</sub> as reductant. The ammonia is obtained from the thermal decomposition of urea, which is added as aqueous solution, and hydrolysis of isocyanic acid (HNCO).

The amount of pollutant emissions released from a modern combustion system depend

on the spray process, especially on fuel atomization and air – fuel mixing process [2]. Besides, with the use of flue gas aftertreatment systems, pollutant emissions can be reduced through the optimization of these processes. Optimization can include system operation at higher injection pressures, different nozzle design, modified needle movement, occurrence of cavitation, multiple injections, swirl motion, blending diesel fuel with biofuels, different piston design, etc. In general, it can be concluded that a detailed understanding of spray process is of utmost importance for engine development. Such understanding is limited from experimental investigations and therefore the CFD tools are usually being employed.

The objective of this thesis was to develop an advanced engineering method for numerical simulations of highly turbulent multiphase spray and combustion processes. The spray was modelled with the Euler Eulerian size – of – classes approach. Additionally, the existing interface for coupling spray and nozzle flow computational simulations was further enhanced. Furthermore, the primary and secondary atomization models were verified by comparing the calculated results to DNS results and to the available experimental data. To take into account the influence of droplet collision on the overall spray process, the O'Rourke collision model was modified and implemented within the Euler Eulerian spray code. The model was verified on a computational simulation of two colliding droplet jets. The Eulerian spray code was further enhanced with the combustion model, where the combustion process was modelled by using chemistry mechanisms, and it was thoroughly validated against experimental research of Constant Volume Vessel (CVV), and by modelling the IC diesel engine compression and expansion stroke.

## 1.2. Overview

In this part of the thesis, the fundamentals regarding the injection, spray, and combustion processes will be discussed. Also, the introduction to the commonly used numerical modelling approaches will be given.

### 1.2.1. Compression Ignition Processes

In IC diesel engines the liquid fuel is injected into a pressurized combustion chamber by using various injection systems. The injected fuel disintegrates into a big number of small diameter droplets that rapidly evaporate. Furthermore, evaporated fuel tends to self – ignite due to the increased temperature conditions. At crank angle positions around the start of injection, temperature and pressure are in the levels of 1000 K and 50 bar, respectively. To ensure a good combustion process the liquid fuel have to be disintegrated into a fine droplets, which is

achieved by the atomization process. In IC diesel engines the liquid fuel is injected through a small diameter nozzles possessing a high velocity. This generates high liquid – air relative velocities, contributing to the fuel droplet break – up process. To achieve complete combustion of each fuel droplet a fuel lean environment has to be ensured, which can be done by increasing the air excess ratio. The choice of proper air excess ratio is not straight forward, since it contributes to the emission levels.

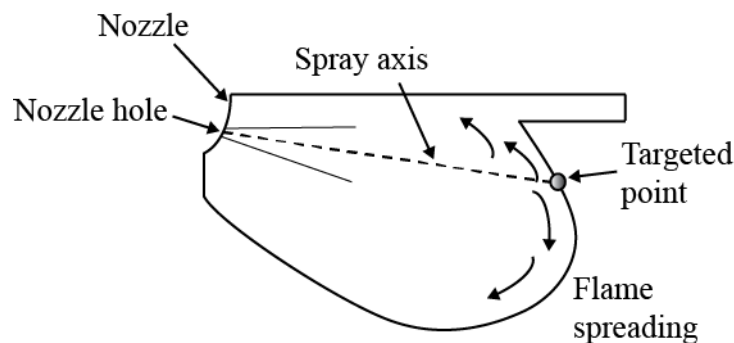


**Figure 1 Schematic of IC diesel engine combustion chamber**

In IC diesel engines the liquid fuel is injected into the combustion chamber and therefore, several conditions must be fulfilled. The IC engine is optimized in terms of start and end of fuel injection, injected mass, etc. It could be stated that, for achieving a good fuel – air mixing, droplet evaporation, flame propagation and pollutant emission formation, next conditions have to be fulfilled:

- 1) Injection of liquid fuel at a specific time.
- 2) Injection of a specific amount of fuel.
- 3) Ensuring of proper atomization process by using high injection pressures and engine compression stroke.
- 4) Injection of liquid jet in a specific direction, defined with angle relative to the horizontal axis.
- 5) Ensuring of flame spreading and excluding of excessive high temperature regions to reduce the  $\text{NO}_x$  emissions.

The liquid fuel injection, both the timing and injected mass, is regulated with the injection pressure and with the needle movement. The targeted point, shown in Figure 1, is

defined through detailed engine design investigations. Usually, the target is aimed with nozzle position and nozzle hole normal vector direction.

### 1.2.2. Fuel Injection and Spray Processes

Liquid sprays are used in a widespread field of technical applications, such as internal combustion engines, gas turbines, rockets, spray painting, spray cooling, fire extinction, spray quenching, waste treatment, etc. Usually, the liquid is delivered to the system as turbulent spray, which is defined as dynamic collection of liquid droplets dispersed in gas as a result of an intense atomization process. The spray process is used to distribute the liquid on a wider area, and to increase the surface needed for more intensive evaporation process. In this thesis the spray is produced by a high pressure liquid fuel injection through a small diameter nozzle, characteristic for real engineering combustion systems such as IC diesel engines. It is a common knowledge that the combustion efficiency, combustion stability, and pollutant formation depend on the spray process. Therefore an understanding of such process is necessary for further development of various engineering applications. Modelling the spray processes, which are considered highly turbulent and transient processes, is challenging since it involves modelling of turbulence, heat and mass transfer, phase change, chemical reactions, inter – phase coupling, etc. Next sections will provide a brief overview of the fuel injection systems, and also the basics regarding the spray and atomization regimes.

#### Fuel injection

To meet the high requirements on the pollutant emissions, regulated by the EU, the pollutant emission released from the IC diesel engines has to be somehow controlled and reduced under a certain thresholds. Such emissions can be reduced by ensuring a proper fuel air mixing process, which can be achieved by a high pressure liquid fuel injection through a small diameter nozzle. In a modern injection systems available on the market in 2016, fuel is injected under pressures over 2000 bar through the cylindrical nozzle holes which are around 0.1 mm in diameter. The schematic of injector nozzle is shown on left – hand side of Figure 2. Fluid flow under conditions characteristic for the injectors used in modern IC engines is a highly transient, turbulent, and subject to the cavitation process. The cavitation process is defined as phase change from the liquid to the gas phase when local pressure drops below the saturated vapour pressure of a liquid. Cavitation is one of the factors that can significantly affect the spray development in the combustion chamber. The phase change from liquid to gas phase occurs at

almost constant temperature, similar to the boiling process which occurs at constant pressure conditions.

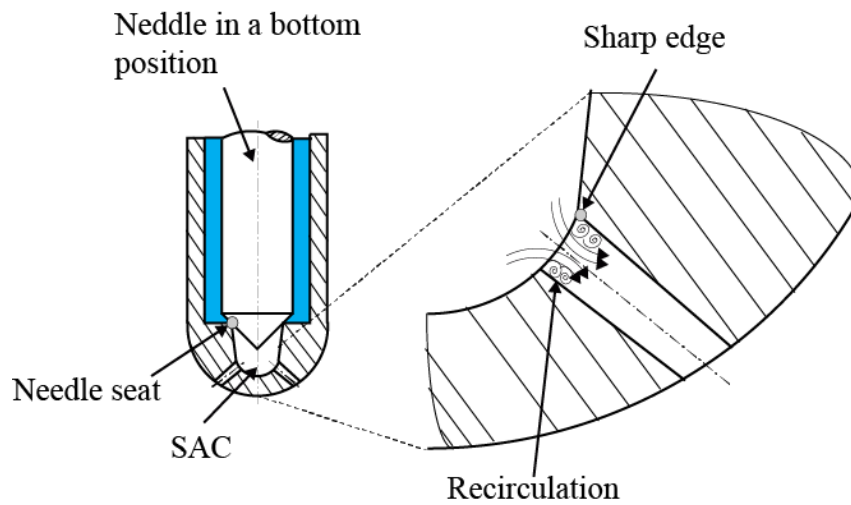


**Figure 2 Schematic of fuel injection system and cavitation process**

In liquid fuel injectors the cavitation usually occurs as a result of the injector design. As shown on the right – hand side in Figure 2, the liquid fuel flows through the small diameter nozzle channel with high velocity. At the entrance of the nozzle channel, the liquid fuel is suddenly curved and separation of the boundary layer could occur. This leads to a flow recirculation followed by a significant local pressure drop. As mentioned before, at the point when pressure is low enough, the cavitation process takes place. The occurrence of the gas phase within the nozzle channel, reduces the nozzle channel effective cross section and subsequently, a higher outflow velocity can be observed. If the vapour bubble collapse time is longer than the time necessary for vapour bubble to pass the whole nozzle channel, it can outflow and collapse in the combustion chamber. This leads to accelerated atomization of the liquid fuel and it could have a positive effect on the pollutant emissions. It is worth noting that in the multi hole injectors, due to the needle movement a vapour string connecting different nozzle holes can be created within the nozzle with sack area around the pintle tip (SAC). This process is commonly known as the string cavitation. It usually occurs upstream the nozzle channel cavitation, and it is a consequence of vortices created by the needle movement.

The influence of the nozzle cavitation on the spray characteristics by observing momentum and mass fluxes was reported in [3]. In this research the authors have found that with intensive cavitation, the liquid fuel velocity on the entrance of the combustion chamber increases. Such behaviour can be addressed to reduction of the nozzle hole effective cross

section due to presence of the vapour phase. The increase of the spray angle due to the cavitating nozzle flow is reported by [4], whilst the influence of the orifice geometry on the spray and combustion processes is presented by [2]. In that research, the authors have shown that with decreased cavitation, the dispersion and the break – up intensity is lower, whilst at the same time the liquid fuel jet penetration is more pronounced.

### Spray regimes

The atomization of liquid fuel jet plays a significant role in engine operation as it is responsible for creating fine droplets needed for efficient evaporation process. Sprays can be divided into several parts based on the mass fraction of the dispersed phase  $Y_F$ . According to such criterion, the spray can be divided into dense, thin, and diluted spray regions, as shown in Figure 3.

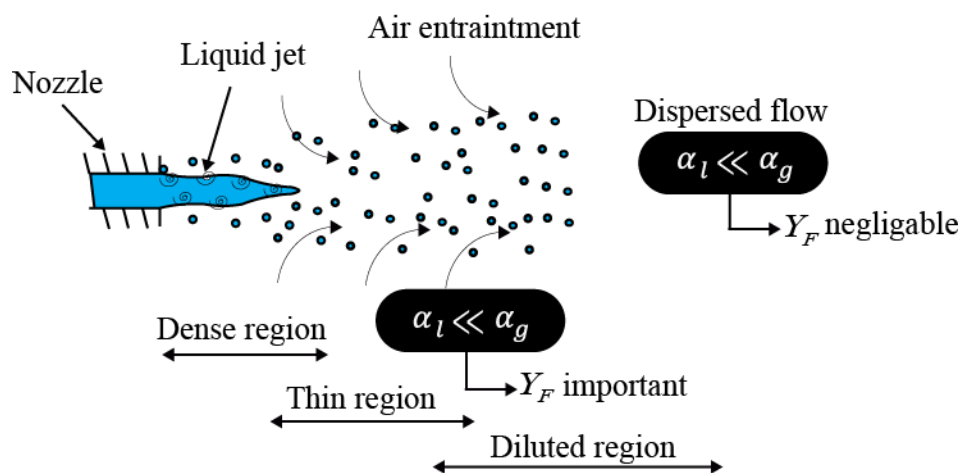


**Figure 3** Schematic of spray regimes

In the nozzle vicinity, where the dense spray is prevailing, the liquid core is disintegrated into unstable ligaments and bigger diameter droplets due to the primary atomization process. The liquid – gas density ratio and turbulence generated within the nozzle together define the mixing rate, droplet size distribution and flow structure of the dense spray region [5]. Further downstream from the nozzle, where the liquid fuel is completely atomized, a thin spray region is formed. It is a region where certain droplet population is already produced, and a dispersed phase volume fraction  $\alpha_l$  is low comparing to the gas phase volume fraction  $\alpha_g$ . However, due to the high liquid – gas density ratios, and a significant liquid mass fraction  $Y_F$ , there is still an influence of the dispersed phase on the gas phase. The diluted spray regime is defined in the region further downstream from the nozzle hole where the dispersed phase mass fraction is

negligible. In this region, fuel droplets are widely spread and isolated, and the droplet collision is not occurring anymore.

### Liquid core atomization process

The intense breakup of liquid jet is achieved through high velocity injection process from a plain – orifice small diameter nozzle hole into a pressurized environment. Such design and specific operating conditions result in creation of unstable ligaments and different sized droplets. This process, the disintegration of liquid jet, is called the primary atomization process. It is characterized as a multiphase flow, consisting of constantly interacting liquid and vapour phase over a wide range of spatial and temporal scales. The liquid jet atomization is a consequence of aerodynamic forces causing instabilities on the jet surface, turbulent velocity fluctuations, or a consequence of the cavitation bubbles implosion, as schematically shown in Figure 4.

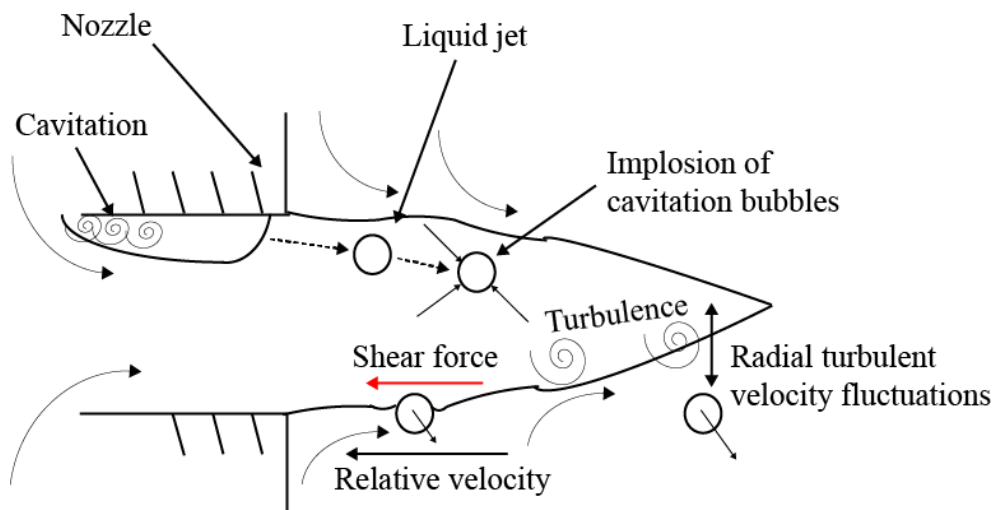


**Figure 4 Schematic of liquid jet atomization mechanisms**

A good review regarding the atomization mechanisms responsible for the liquid jet primary break – up process is shown in [6]. The cavitation occurring in the nozzle hole was examined by [7][8] and it was found that it strongly affects the injection velocity and spray droplet size distribution.

Liquid jet atomization can be diverse in nature, depending on the encountered physical conditions. Therefore, a liquid jet classification have been proposed based on the Reynolds, Weber and Ohnesorge dimensionless numbers.

The Reynolds number, widely used to characterize the turbulence and energy of a flow, relates the inertia forces arising from the droplet gas relative velocity to the viscous forces, as shown with next equation:

$$\text{Re} = \frac{u_l \rho_l d_n}{\mu_l}, \quad (1)$$

where the term  $d_n$  stands for the nozzle hole exit diameter,  $\rho_l$  is the liquid density,  $u_l$  is the liquid velocity, and  $\mu_l$  is the dynamic viscosity.

The second number that is used for characterization of liquid jet break – up nature is the liquid Weber number defined with next equation:

$$\text{We} = \frac{u_l^2 \rho_l d_n}{\sigma_l}, \quad (2)$$

where the variable  $\sigma_l$  stands for surface tension of the liquid. The Weber number correlates the inertia and surface tension forces. A detailed explanation of the Weber number and the jet stability is provided in [9].

The third relevant dimensionless number used for the liquid jet break – up classification is the Ohnesorge number defined with next equation:

$$\text{Oh} = \frac{\mu_l}{\sqrt{\sigma_l d_n \rho_l}}. \quad (3)$$

According to the increase of the liquid Weber number, four different liquid jet break – up regimes can be established, as depicted in Figure 5. At low Weber numbers (small injection velocity), the liquid jet disintegrates into droplets with bigger diameter than the jet itself. At such conditions, the liquid inertia and surface tension are in a balance but the surface of the liquid jet is unstable. This regime is called the Rayleigh break – up regime. With increase of the liquid jet injection velocity the inertia effect of the surrounding gas becomes significant. Increase in velocity also increases the unstable surface wave growth rate and therefore, amplifies the surface oscillations leading to a faster jet disintegration. The diameter of created droplets is of similar size like the nozzle hole diameter, and the liquid break – up process occurs many nozzle diameters downstream from the nozzle. This regime is called the First wind induced liquid jet break – up regime. By further increasing the injection velocity to a higher values, the Second wind break – up regime occurs. In this regime, the gas inertia is increased



and the liquid jet disintegrates due to the unstable growth of small wavelength surface waves. This implies that the droplet population from this regime consists of droplets with much smaller diameter comparing to the nozzle hole diameter. The liquid jet categorization that distinguished the first and second wind induced break – up was introduced by [10]. A regime that is of utmost importance in the IC diesel engine investigation is the atomization regime. It is characteristic for the liquid jet injection with high Weber number and sufficiently high gas density. When the conditions for the atomization regime are met, the fuel jet atomization starts immediately at the nozzle exit hole and a conical shaped spray characterized with small diameter droplets is produced.

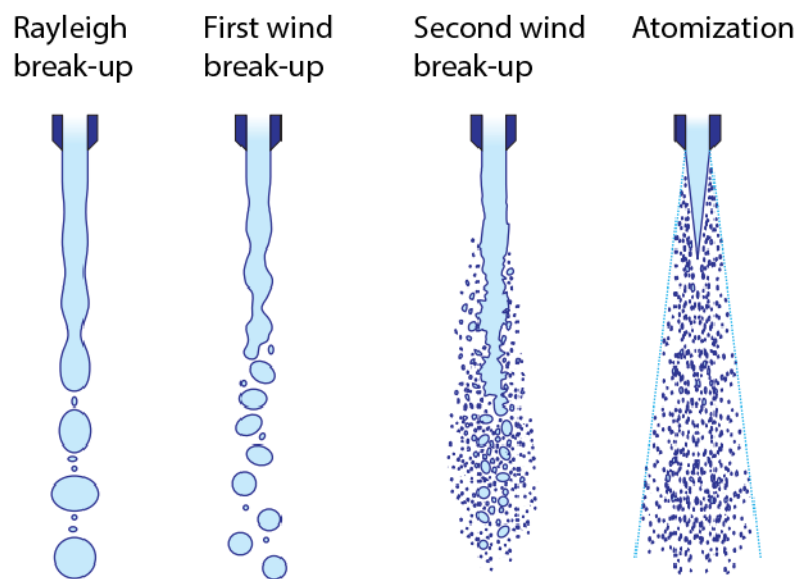


**Figure 5** Schematic of liquid jet break – up regimes [11]

In this thesis the spray generated by the high pressure liquid fuel injection into a pressurized gas environment is considered. Therefore, the atomization break – up regime is dominant where break – up of liquid jet starts directly at the nozzle exit. This process is referred as the primary break – up of the liquid core.

### Fuel droplet atomization

Products from the liquid jet primary atomization, ligaments and droplets, may further disintegrate into even smaller droplets, this process is called the secondary break – up. Liquid droplets generated with the secondary break – up process are subject to collision, evaporation and wall impingement processes. In modelling of the fuel injection systems, the secondary atomization model should consider two different disintegration mechanisms [12] that are

dominant for higher droplet – gas relative velocities. These mechanisms are known as the Rayleigh – Taylor (RT) accelerative instabilities and Kelvin – Helmholtz (KH) instabilities responsible for deformations on the droplets surface.

The secondary atomization process is characterized considering the gas Weber number. According to [13], there are five regimes of secondary break – up process, as illustrated in Figure 6. The gas Weber number correlates the aerodynamic and surface tension forces.

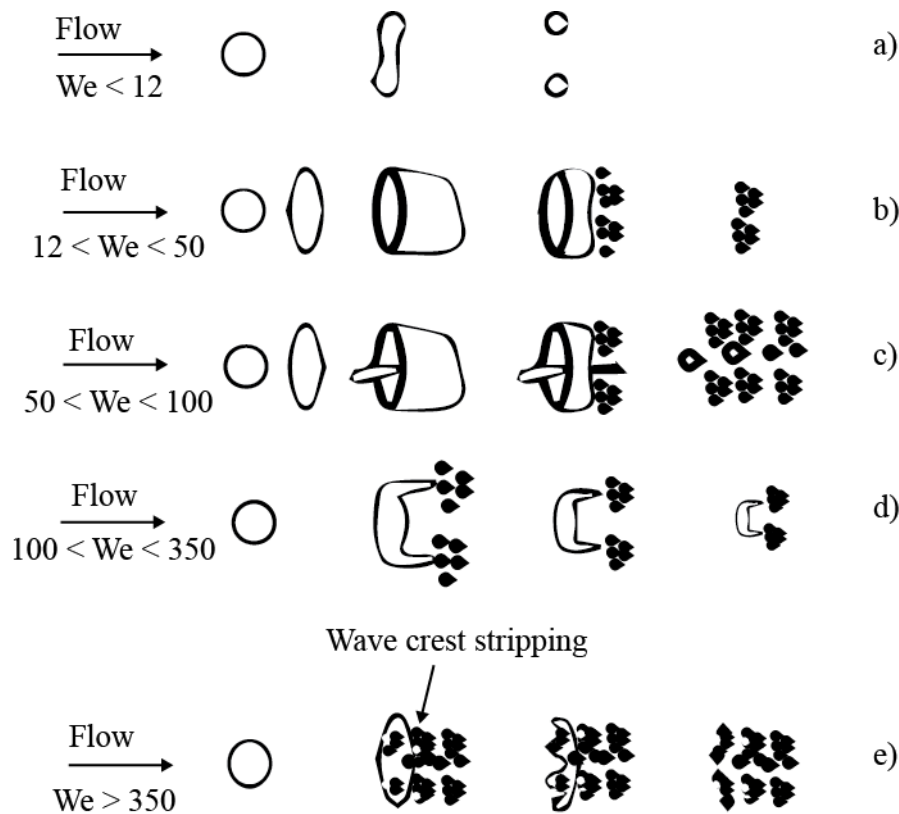


**Figure 6** Schematic of droplet secondary break – up regimes reproduced from [13]

- a) At low Weber numbers ( $We < 12$ ), droplet surface instabilities develop at natural frequency which is amplified by the surrounding flow. At such conditions, the droplet disintegration process occurs at relatively large time scales and only a small number of large fragments are being created. This regime is called the vibrational break – up, and usually it is not considered in droplet break – up studies.
- b) Increasing the Weber number ( $12 < We < 50$ ), liquid droplets undergo the bag break – up regime. Herein, a thin hollow bag is being formed and blown off the droplet surface as a result of aerodynamic forces. The bag bursts at some point creating toroidal

- rim which later disintegrates and forms bigger liquid ligaments. Also, the liquid thin bag – shaped structure bursts creating a number of fine, small diameter drops.
- c) With further increase of the Weber number ( $50 < We < 100$ ), liquid droplets undergo the bag – and – stamen break – up regime. This regime is similar to bag break – up regime with difference in creation of liquid column in the droplet axis parallel to the flow. The liquid column further disintegrates into a bigger liquid ligaments.
  - d) In the Weber number range between 100 and 350, droplets undergo the sheet stripping break – up regime. This regime is different to the bag break – up and the bag – and – stamen regime, since the bag shape is not created. Instead, the sheet disintegrates on the periphery of the droplet as a result of shear forces. This implies, that the KH instabilities are responsible for droplet atomization.
  - e) For high Weber number ( $> 350$ ), liquid droplets are subject to Wave stripping and catastrophic break – up regime. Large amplitude and long wavelength instabilities due to the inertia forces (RT instabilities) penetrate the droplet surface and create large fragments. The droplet penetration by the large amplitude surface waves is called the catastrophic break – up which occurs before the wave stripping mechanism, significantly reducing the droplet mass. For stripping mechanism the KH instabilities characterized with large amplitude and small wavelengths are responsible.

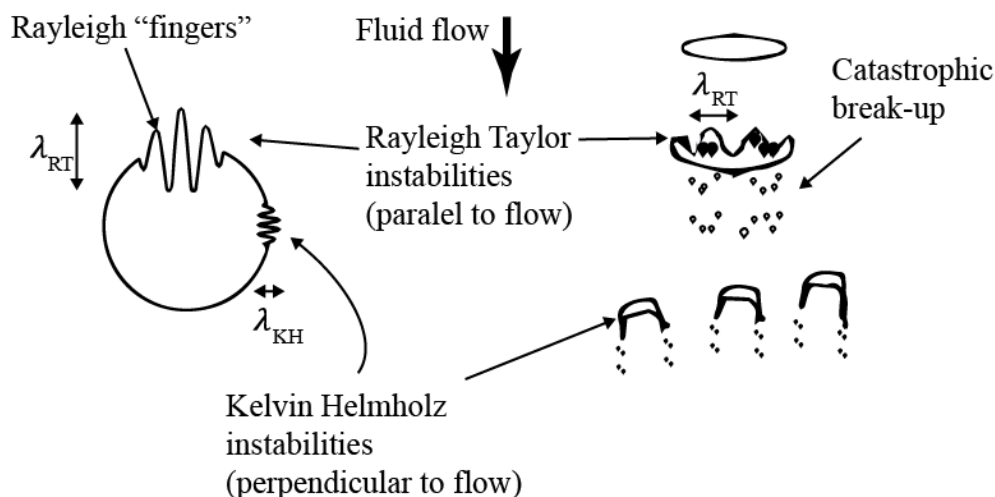


**Figure 7** Schematic of catastrophic secondary break – up mechanisms reproduced from [14][12]

As mentioned before, at high Weber number both the RT and KH instabilities are responsible for droplet break – up process. The RT instabilities lead to the formation of bigger ligaments due to the droplet deceleration (when the dense medium is accelerated with a less

dense one). They are characterized by large amplitude surface oscillations. On the other hand, the KH instabilities are associated with lower values of amplitude and wavelength. Both mechanisms are schematically shown in Figure 7.

### Spray characterization

To validate the developed mathematical models used for spray modelling, several spray properties have to be defined and experimentally recorded. Usually, the quantities of interest are fuel liquid and vapour penetrations, spray angle, droplet size and number distributions, etc. Regarding the reactive spray process characterization a lift – off length and ignition delay time are used. Roughly, the quality of atomization is determined by two parameters: level and uniformity of atomization. The level of atomization refers to the mean diameter of droplets, whilst the uniformity refers to the scatter of droplet diameters where a smaller scatter denotes higher uniformity level.

Spray penetration is not exactly defined and its quantification depends on the used measuring technique and measuring accuracy. Some authors define the liquid and vapour penetration as the furthest distance where their experimental apparatus recorded the fuel droplets or vaporized fuel. From this definition, it can be stated that the penetration depends on the measuring equipment accuracy. Furthermore, the liquid penetration could be defined as the distance where a certain mass of liquid fuel is penetrated into the domain, compared to the overall spray mass. During the CFD simulations and spray model development, of utmost importance is to correctly interpret the used experimental data. Otherwise, wrong conclusions may be drawn. For IC diesel engines it is characteristic that the liquid and vapour temporal and spatial penetrations are similar at early stage of injection. In later stages, when the liquid fuel reaches the quasi – steady (developed) state, the vaporized fuel continues to develop through the domain due to the momentum transferred from the liquid fuel. Another examined spray characteristic, closely related to the liquid tip penetration is the liquid core break – up length. It is measured as the axial distance between the tip of liquid jet and the nozzle orifice. Several investigations regarding the tip penetration and break – up length were reported in the literature. For example, the influence of ambient pressure on the liquid jet break – up length was investigated in [15][16] where the authors provided correlations between the liquid core break – up length, injection pressure and the surrounding gas density. The influence of the injection pressure on the spray properties was observed in the research conducted by [17]. In their research, the authors reported that the liquid penetration increases with the increase in

injection pressure, whilst it decreases with higher ambient pressure. The influence of the fuel properties and fuel temperature on liquid fuel penetration was described in the research carried out by [15].

Another spray characteristic that is used to define spray processes is the spray angle, which is defined as the opening angle of the fuel vapour cloud, as shown in Figure 8. The experimental measurement of this quantity is not straightforward due to the highly transient spray cloud development. In this thesis, the spray angle is quantified as a single value defined at 70 % of spray vapour cloud penetration in the axial direction recorded at the end of injection. In modelling of spray processes, the definition of the spray angle depends on the used approach. For instance, in Euler Lagrangian DDM approach the spray angle have to be pre – defined by the user, whilst in the Euler Eulerian size – of – classes approach the spray spreading is dynamically calculated through use of the turbulent dispersion model. The spray shape must ensure a proper droplet distribution through the combustion chamber [18]. In the literature, it is reported that the spray angle is affected by the environment density, but it is not dependent on the injection pressure [15][17][18]. A denser gas environment results in a wider spray cloud characterized with shorter liquid penetration length. This could be addressed to the fact that higher energy is acquired for the fuel propagation due to the increase of the surrounding gas density. As a result, instead of penetrating along the spray axis direction, the fuel droplets spread in the radial direction due to the increased dissipation forces.

The common spray characteristic recorded in the experimental research are liquid/vapour penetration and spray angle. This can be addressed to high expenses of experimental research for measuring spray microscopic characteristics, such as droplet number and volume distributions. To develop efficient computational models that are capable to capture the transient spray behaviour, a more detailed experimental data are necessary. For instance, the ECN [19] database offers additional data such as the mixture fraction distribution in the axial and radial direction on several distances from the injecting point. This data is valuable to quantify the accuracy of mass and momentum transfer from the liquid to the vapour phase. The cutting plane AA in Figure 8 is one example where the axial mixture fraction could be experimentally and computationally recorded, whilst planes B<sub>1</sub>B<sub>1</sub> and B<sub>2</sub>B<sub>2</sub> could be used for recording the radial mixture distribution.

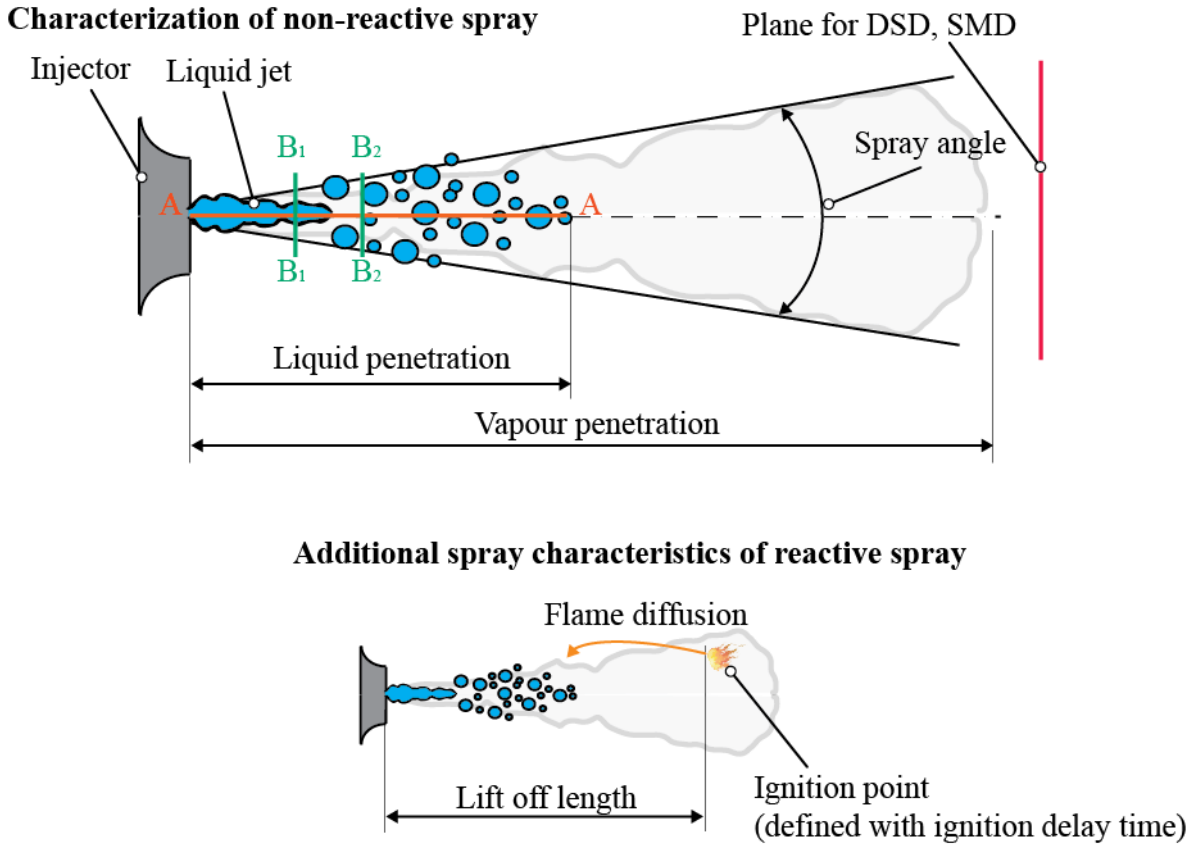


**Figure 8 Schematic of spray characteristics**

The above mentioned quantities belong to a group of macroscopic spray characteristics. A more detailed spray characterization is done by measuring spray microscopic characteristics such as internal structures in terms of Sauter Mean Diameter (SMD), and droplet number and volume distributions [20]. The SMD is the valuable quantity for spray characterization because it represents the diameter of a droplet which has the same ratio between volume and surface, taking into account the whole spray droplet population. Actually, it represents the surface available for evaporation. Smaller values of SMD mean a larger surface available for evaporation relative to the overall droplet mass. The SMD, considering  $n$  number of classes, is calculated according to next expression:

$$SMD = \frac{\sum_{i=1}^{n_{classes}} d_{drop}^3 \Delta n_i}{\sum_{i=1}^{n_{classes}} d_{drop}^2 \Delta n_i}, \quad (4)$$

where  $\Delta n_i$  is the sample  $i$  range. Measurements of spray SMD are rarely available since they require expensive measuring equipment. The SMD can be defined as global, measured from

the whole spray droplet population, or as SMD at a certain location of spray. Regarding the time scale, the SMD can be recorded instantaneously at any desired time frame, or it can be averaged over a certain time period. Experimental investigations regarding the SMD have been performed in [21][22][23][24], where the authors reported that with increase in injection pressure the SMD exhibits lower values, whilst with increase of ambient density the SMD increases. The authors also stated that the choice of the injection system influences the overall SMD value. Furthermore, in the literature it was addressed, that smaller droplets retain around the spray axis whilst bigger droplets form the edge of the spray cone [25]. In example discussed in this thesis, the SMD was defined as the global “planar cut” SMD, averaged for time period from 3 to 8 ms after start of injection.

The averaged SMD provides valuable information about the surface available for evaporation, but it does not provide information about the shape of the droplet size distribution. It is obvious that such detailed experimental data is of great importance for validation of new spray related models. Other microscopic spray characteristics used for model validation within this thesis are the droplet size probability density functions, which are either number or volume based, and they consider the whole spray droplet population.

In order to quantify the reactive spray process, two quantities are defined: the Ignition Delay (ID) and the Lift Off Length (LOL). In the literature there are several different definitions that are used for describing the ID. The ID can be defined as the highest gradient in the rate of heat release curve or the highest mean pressure gradient. On the other hand, it can be defined as time from start of injection to the time instance when first traces of the high temperature flame are recorded. Within this thesis, the ID was defined as the time period calculated from the SOI until a temperature higher than 1600 K was firstly recorded in the computational domain. It is worth to note that the ID definition should be carefully chosen by taking into account the used experimental technique. The same is valid for the LOL, which is defined as the smallest distance between the injection point and the spatial location where the gas temperature exceeds 1600 K. Alternatively, the LOL can be determined by observing the OH species concentration, which is beneficial if the OH chemiluminescence measurement technique was applied.

The rate of injected fuel correlated to the crankshaft angle is referred to the “Rate Of Injection (ROI) characteristics”. The integrated ROI curve provides the total fuel mass injected for each engine injection process. Such curve can be used as boundary condition of the spray inlet in CFD simulations, and therefore, it is of great importance to acquire a reliable ROI

characteristic. For the validation of the spray method developed within this thesis, a new type of spray boundary condition was developed and the ROI curve was used.

### 1.2.3. Combustion Processes

Reactive sprays are used in various engineering applications, and they are burned under a variety of circumstances. According to [26], different combustion models are used for different applications. For example, in liquid rocket engines, both, the liquid and the oxidizer, are injected from one end providing a premixed combustion process. For this kind of application a steady – state combustion model can be applied. Other examples are gas turbine combustor, which are similar to rocket engines but different since the combustion process is diffusion driven. The IC diesel engines are one of the most difficult application for modelling the combustion process. In such engines the combustion is a diffusion driven and highly transient process. Additionally, the flow is three – dimensional and the influence of the fuel impingement on the piston wall surface may have a significant influence on the overall engine performance.

#### Combustion process in IC diesel engines

The combustion process occurring inside the IC diesel engine combustion chamber is divided into several distinguished parts. The green curve in Figure 9 shows the mean in – cylinder pressure curve through the engine working cycle, including the compression and expansion strokes. In the compression stroke the engine piston moves towards Top Dead Centre (TDC) and compresses the cylinder working volume, which leads to pressure and temperature rise. At a certain crank angle position, in general several degrees before TDC, the liquid fuel is injected into the cylinder. The Start Of Injection is denoted with SOI in Figure 9. The abbreviation EOI stands for the End Of Injection, whilst the area below the rate of injection curve represents the liquid mass injected into the cylinder. Usually, the ROI curve has a “hat-like” shape, and it is defined by the nozzle needle movement and fuel pump pressure. Once the liquid fuel is injected, due to the elevated temperature conditions, the fuel starts to evaporate and to combust. The time between SOI and start of premixed combustion is denoted as ID, which depends on the fuel type, pressure conditions and piston bowl shape.

When the vaporized fuel is ignited, an uncontrolled and fast combustion process, characterized by a rapid pressure increase and a huge heat release, takes place. In this period, the fuel is partially oxidized to CO, H and C<sub>2</sub>H<sub>2</sub> which tend to diffuse towards nonpremixed regions. The premixed combustion speed depends on the air excess ratio and on the in - cylinder temperature.



After reaching the premixed peak, the in – cylinder pressure and temperature further increase due to the progressing combustion process. However, at this point the combustion is mixed controlled, where the diffusion flame occurs due to the established stoichiometric conditions around the spray flame areas. In the region near the liquid spray core, where a higher amount of vaporized fuel is present, the fuel rich conditions are suitable for generating soot pollutant emission. Such generated soot is later oxidized in the diffusion flame, but due to the higher local temperature conditions thermal  $\text{NO}_x$  is formed.

At later stages of the combustion process, the intensity of the heat release decreases and all of the vaporized fuel is consumed. After the heat is not released by the combustion process, and due to the piston movement towards Bottom Dead Centre (BDC) in the expansion stroke, the in s– cylinder pressure decreases. At the very end of the combustion process, a small remaining amount of the vaporized fuel reacts with the surrounding oxygen in the presence of high amount of combustion gas species.

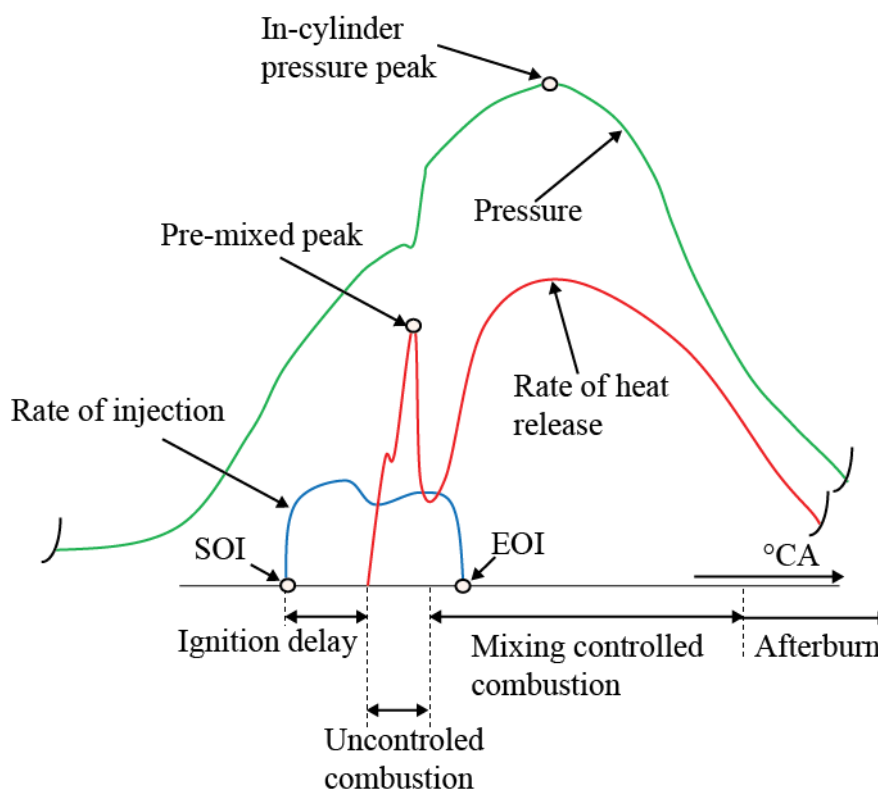


**Figure 9** Schematic of IC diesel engine working cycle

#### 1.2.4. Emissions from IC diesel engines

A vast amount of Green House Gasses (GHG) are released into the environment by combusting fossil fuels [27], and a rapid emission reduction (up to 85 %) has to be achieved by 2050 [28]. Both, the powering of diesel engines and fossil fuel combustion in a great amount contribute to the increase of atmosphere GHG concentrations. Most of the worldwide CO<sub>2</sub> emissions are released by burning the coal for power production and from the transportation sector. According to [29], in 2013 the share of transportation sector in global CO<sub>2</sub> emission was approximately 25 %. This can be addressed to a rapid increase of motor vehicles and limited use of emission control systems. Usually, running by the diesel engines is preferred comparing to the gas oil engines due their low operating costs, reliability, energy efficiency, etc. Therefore, in this section of the thesis, a description of emissions released from the IC diesel engines is provided. The special focus is given to Particulate Matter (PM) and NO<sub>x</sub> emissions, because diesel engine flue gases contain higher amounts of NO<sub>x</sub> and PM. In the later sections, a brief description of HC and CO emissions is provided.

Diesel fuel is comprised of carbon and hydrogen molecules in a certain ratio. For ideal conditions, the complete diesel fuel combustion would lead to generation of CO<sub>2</sub> and H<sub>2</sub>O species. In addition to CO<sub>2</sub> and H<sub>2</sub>O, in highly transient IC engine working conditions, a vast amount of other species is produced. The major part of these emissions are harmful pollutant species such as CO, HC, PM and NO<sub>x</sub>. In relative comparison to total flue gas amount, only 1 % of pollutant emissions is released from the engine exhaust system. A major part of these pollutant emissions, approximately 50 %, are the NO<sub>x</sub> pollutants whilst the second biggest emission share belongs to the PM emissions [30]. Even though other species such as CO, HC, and SO<sub>2</sub> are found in really small concentrations, they are not negligible due to their toxic influence on the human health and destructive behaviour towards the Earth ozone layers.

#### Nitrogen oxides (NO<sub>x</sub>)

Among various types of vehicles, diesel driven ones are the major contributors to NO<sub>x</sub> emissions. This is mostly a consequence of their higher in – cylinder temperatures compared to the gasoline engines. NO<sub>x</sub> emissions causes health problems, contribute to acidification, support destruction of the ozone layer, causes smog formation, etc. Their impact on human health is usually connected with lung and respiratory system diseases.

During the compression stroke of IC diesel engine the in – cylinder pressure and temperature increase, and consequently these conditions lead to auto ignition of the vaporized

fuel. In low temperature conditions, the nitrogen from the entrained air would not react with the surrounding oxygen. However, the in – cylinder temperatures found in the diesel engine combustion chamber reach locally values above 1850 K [31]. Such temperatures are enough to break – up nitrogen triple bonds and to form nitrogen oxides ( $\text{NO}_x$ ), which are referred as NO,  $\text{NO}_2$ ,  $\text{N}_2\text{O}$ ,  $\text{N}_2\text{O}_2$ ,  $\text{N}_2\text{O}_3$ ,  $\text{N}_2\text{O}_4$ , and  $\text{N}_2\text{O}_5$  [32]. Most of the  $\text{NO}_x$  emissions, approximately 85 - 95 %, is constituted of the hazardous nitrogen compound nitric oxide NO. Nitric oxide can be produced by several mechanisms such as thermal, prompt, and fuel mechanism. To model the thermal NO emissions, a reaction mechanism was previously developed by Zeldovich [33]. This mechanism is described by a set of chemical reactions where reaction constants are gained from the experimental research. Some authors noticed that the NO species concentration is much higher than those predicted by the Zeldovich mechanism, which was addressed to the prompt NO formation. The NO emissions formed by prompt mechanism occurs much earlier than the previously described thermal NO emissions. They are formed by the reaction of atmospheric nitrogen and hydrocarbon fragments, which is further oxidized to form NO. The third mechanism of NO formation is the fuel mechanism relevant when the liquid fuel contain organically bounded nitrogen, which is released during the combustion process. However, organically bounded nitrogen can be found only in heavy fuels and in coal.

### Particulate matter

PM emissions in the exhaust gases are formed during the combustion process within the engine combustion chamber. The PM has a wide range of potential environmental impacts, including health effects, ecological effects, climate change, etc. The new PM emission threshold limits are so low that they cannot be achieved solely by engine design and, therefore, engine flue gases require additional aftertreatment. The PM consists of two types of particles: (a) fractal – like agglomerates of primary particles 15 – 30 nm in diameter, composed of carbon and traces of metallic ash (partly burned fuel), and coated with condensed heavier end organic compounds and sulfate (partly burned lube oil); (b) nucleation particles composed of condensed hydrocarbons and sulfate [34]. Diesel PM are usually spherical with diameters of about 15 – 40 nm, and approximately more than 90 % of PM are smaller than 1  $\mu\text{m}$  in diameter. According to [35], the PM formation process is dependent on many factors such as combustion process and expansion stroke, fuel quality, lubrication oil quality, oil consumption, combustion temperature, exhaust gas cooling, etc. The PM emissions from IC diesel engines are approximately six to ten times higher than from gasoline engines.

The PM emissions can be divided into three main components: soot, Soluble Organic Fraction (SOF), and Inorganic Fraction (IF). More than 50 % of the total PM emissions are soot, which can be observed as black smoke.

### Carbon monoxide (CO)

The carbon monoxide (CO) is released into the Earth atmosphere due to the incomplete combustion where the oxidation process did not occurred completely. Usually, it is generated under the fuel rich conditions where carbon cannot convert to CO<sub>2</sub> due to oxygen deficiency. However, a small amount of CO can also occur in the fuel lean conditions, which is of particular importance for IC diesel engines. The CO can be also formed, if the right conditions are achieved, such as too high SMD, to low turbulence or swirl motion, etc.

Carbon monoxide emissions have a negative effect on the human health. If inhaled, it binds to haemoglobin and inhibits its capacity to transfer oxygen causing severe health issues.

### Hydrocarbons (HC)

Another pollutant compound that affect the Earth's environment and Human health are hydrocarbons. Regarding the influence on the environment, they are a huge contributor to ground level ozone formation and from the standpoint of human health, hydrocarbons are harmful to respiratory tract. They are usually formed from the unburned fuel in lower temperature regions near the cylinder walls. Therefore, a proper spray development and engine design could contribute to HC emission reduction. If the unburned HC outflow to the exhaust pipes and the conditions are adequate, they continue to react, and emitted HC concentration could be several times lower than those found inside the engine cylinder.

#### *1.2.5. Modelling Spray Processes*

Numerous studies about spray processes have helped engineers to establish the criteria needed to design and develop more efficient combustion devices while minimizing the pollutant emissions [36][37][38]. The understanding of the complex fuel spray process, which are mostly formed by high pressure injectors [39], in experimental research is limited and this understanding can be significantly improved with the numerical simulations. Compared to a single – phase flow modelling the modelling of the spray process, which represents a multiphase flow is a very challenging task. The challenges arise from the interaction between phases and property variations across the phase interfaces. Thus, computational spray models demand a complicated techniques to couple the dynamics of the liquid droplets with the carrier

gas. A variety of strategies have been formulated during the last years in order to address this problem. In general, most of these strategies fall into two basic methods that are commonly used to couple the dynamics of the liquid and the gas phase: the Euler Lagrangian and the Euler Eulerian method.

The Euler Lagrangian method has been firstly used in [40][41][42][43]. Currently, this method is the most common method for numerical modelling of spray processes in a wide range of engineering applications. In such method, the spray is represented by a finite numbers of grouped droplets called parcels. The assumption is that all droplets of a single parcel have the same size and physical properties. The transport of each parcel through the flow field is solved by using the Lagrangian formulation, whilst the continuous gas phase is described by solving the Eulerian conservation equations. The phase coupling is performed by introducing the source terms for interfacial mass, momentum and energy exchange. The Euler Lagrangian method has several limitations, as it is very sensitive to the numerical grid resolution in the near nozzle region [44]. The limitations on grid size also affect the modelling of heat transfer, momentum exchange, etc. Therefore, the numerical resolution is important in reproducing the structure of sprays [45]. This results in inadequate description of dense spray region in the vicinity of the nozzle. However, the Euler Lagrangian method is suitable for calculating the diluted region, where a lower liquid phase volume fraction is encountered. Other drawbacks of the Euler Lagrangian formulation are the increase of computational costs with higher number of introduced parcels, and the parallelization issues. The method also suffers from the statistical convergence problems, as discussed in [46] and [47].

A spray process can be modelled by employing the numerical methods used for tracking the liquid – gas interface, such as VOF and level – set methods. Authors in [48] examined the liquid jet break – up (constant injection velocity of 100 m/s, nozzle diameter 100  $\mu\text{m}$ ) on a 2.1 mm computational domain consisting of over 14 million control volumes by employing the level set/ VOF/ ghost fluid method. The authors in [49] used the level set method to solve the disintegration of a liquid jet with same injection conditions on a 2 mm computational domain consisting of several billions control volumes. The authors in [50] presented the modelling of primary atomization process by employing the refined level set grid method. They pointed out extremely high memory requirements (10 GB for every 50 ns) of such simulations. More detailed description of sharp interface techniques for multi – fluid flow modelling can be found in [51]. Based upon the literature review, despite their high accuracy, such models are highly

computationally expensive which represents a huge disadvantage for their usage in the industrial sector.

To overcome disadvantages of the Euler Lagrangian method, the Euler Eulerian multi – continuum method can be employed. In this method, both phases (liquid and gas) are treated as continuum, and conservation equations are solved for each phase separately. The Euler Eulerian method was firstly addressed by [52], and has been adopted and applied for computational simulations, e.g., [53][54][55], and others. Compared to the Euler Lagrangian method, the Euler Eulerian method is fairly efficient for calculation of flows with high droplet concentration. Driven by those facts, the two mentioned methods can be used in combination to overcome disadvantages inherent for both methods and to improve the accuracy of spray modelling. Coupling of the methods can be performed by using the AVL FIRE® Code Coupling Interface [56][57][58][59]. The coupling process means that the calculated results of both simulations are used either as boundary condition values, or as source/sink terms for the other simulation. The coupled modelling is performed on the two separate computational simulations with overlapping domains where a certain rules are applied for mass, momentum and energy source terms exchange. A detailed explanation on the mentioned spray modelling approach is described in [60].

An alternative to the coupled ACCI modelling approach is the ELSA model proposed in [61]. This approach has been under constant development, as discussed by [62], [63], and others. It is used for modelling the high speed turbulent sprays in order capture the processes within the dense spray region. Basically, ELSA model can be divided into three zones: Eulerian mixture zone, transition zone and the Lagrangian zone. The main difference between the ELSA and the ACCI approach is that in the ELSA model, in the vicinity of the nozzle the gas and the liquid phase are considered as one mixture phase.

#### *1.2.6. Modelling Reactive Spray Processes*

Reactive turbulent spray processes have been modelled by employing various approaches such as eddy dissipation model, flamelet models, PDF methods, reaction mechanisms, etc. The numerical modelling of a reactive methanol spray employing the Euler Lagrangian spray approach and the Eddy Dissipation Concept combustion model (EDC) was presented in [64]. The authors mentioned that the use of detailed chemistry would give a more reliable results for spray combustion. In recent years, researchers showed that detailed kinetic mechanisms are essential to properly predict spray burning characteristics such as lift off length. Combustion of diluted methanol sprays was performed in [65] and [66], whilst the diluted

ethanol/air spray combustion was presented in [67]. To account the influence of the turbulence on the spray combustion, a detailed investigation was performed by [68]. The authors used the steady flamelet model together with a detailed reaction mechanism in combination with the Euler Lagrangian method for spray modelling. The influence of the nozzle orifice geometry on combustion of the n – heptane spray, employing the same spray approach in combination with a detailed chemistry was discussed in [2]. The authors noticed a significant influence of injector design on spray combustion characteristics. Furthermore, the research of [69] showed the influence of injection timing on pollutant emissions, whilst the possibility of Euler Lagrangian spray approach to predict the NO and soot trends for various combustion parameters was shown in [70]. In the research of [71], the Euler Lagrangian spray approach in combination with the ECFM combustion model and presumed Probability Density Function (PDF) look – up table was used to model the dual fuel turbulence – chemistry interactions.

The Euler Eulerian reactive spray modelling was also researched in recent years. The simulation of reactive diluted sprays by employing the Euler Eulerian approach in combination with the eddy break – up combustion model was presented in [72]. Their method correctly described the spray combustion process, but discrepancies in modelled CO and CO<sub>2</sub> species concentrations have been recorded. The PDF Chemical equilibrium combustion model in combination with the Euler Eulerian spray approach, without discretisation of the liquid phase into droplet classes [73] was used for research of reactive sprays [74].

The LES studies, which can be used for studies of cyclic variabilities, need a high number of Lagrangian parcels to achieve accuracy, and therefore the Euler Eulerian approach could be used within the LES modelling framework [75]. To avoid the difficulties of near nozzle region, the authors introduced the downstream inflow turbulent boundary condition model [76]. The tabulated chemistry within the LES framework, where the discrete phase was described with the Eulerian modulation, was used for modelling the combustion process of a diluted n – heptane fuel [77]. The combustion of the mono dispersed spray, modelled with the Euler Eulerian spray approach within the LES framework was researched in [78]. The authors highlighted the influence of the dispersed phase on the flame propagation. The importance of the poly dispersed spray was shown in [79], where the flamelet generated manifold based on tabulated chemistry was coupled to an advanced spray module in order to investigate the partially premixed reacting acetone sprays. Combustion of two phase flows in the LES framework is still in its infancy and a good summary is presented in [80].

From the given literature review regarding modelling reactive spray processes, it can be concluded that the Euler Eulerian multi – continuum model extended to the size – of – classes approach has not been extensively tested on its ability to capture highly turbulent diesel spray and combustion processes. The main objective of this thesis was to develop a new computational method in order to resolve the dense spray region including the atomization, collision and evaporation processes, and to link it with the downstream vapour combustion.

### **1.3. Objective and hypothesis of research**

The hypothesis of this thesis is that numerical simulations of liquid fuel injection and combustion process are feasible, and that the Euler Eulerian multi continuum model size – of – classes approach in combination with chemistry kinetics can be used in development of various applications with reactive flow. The results of the thesis provide a reliable description of spray processes, especially in the near nozzle region. Furthermore, with a detailed spray characterisation a respectable description of the combustion process is achieved. The ultimate goal of thesis was to establish a model that confirms the hypothesis by comprehensive comparison of modelling results and the available experimental data.

### **1.4. Materials and methodology of research**

There are several existing approaches used for solving turbulent dispersed multiphase flows such as DNS resolving the particles, the Discrete Particle Model (DPM), the Euler Lagrangian, and the Euler Eulerian model, etc. [51]. The Euler Lagrangian approach is a common and widely used numerical approach for modelling the spray process, but it has some disadvantages. In order to overcome these disadvantages, the Euler Eulerian multi – continuum approach can be used. This approach considers the liquid and the gas phases as interpenetrating continuum, and both phases are treated from the Eulerian point of view. The same discretization, similar numerical techniques and conservation equations are used for both phases. For improved modelling accuracy, the droplet distribution is divided into a fixed number of droplet classes characterized by their droplet diameter. The complete set of conservation equations with additional source terms accounting for the droplet dynamics are solved for the gas phase and for each droplet class under consideration.

In this thesis the mathematical models used for calculation of the spray and combustion processes are treated in the Eulerian spray module of the applied CFD code, where thermochemical reactions occur in the gas phase within a certain control volume. The chemical



reactions of the gas phase are treated via an Ordinary Differential Equation (ODE) solver providing an additional sink and source terms for the species and enthalpy transport equations. The presented spray model is integrated into the commercial CFD code AVL FIRE® by using the user defined function capability based on FORTRAN subroutines. The conducted research is performed in several steps to get a reliable and accurate approach for modelling spray and combustion processes.

In the first step a comprehensive literature review regarding the spray modelling was shown and several computational simulations of the real engine configuration, using the Euler Lagrangian approach, are presented. The different combustion parameters were researched, and their influence on mean temperature and mean pressure is shown. Also, an investigation regarding the influence of the combustion parameters on the pollutant emission is shown. The validation process was conducted by comparing the calculated results to the available experimental data. In this section of the thesis the current status, advantages and disadvantages encountered by using the Euler Lagrangian approach were investigated.

In the second step of this research, a detailed parameterization of the atomization models was performed. The liquid jet primary break – up model and the droplet secondary break – up model were researched and parametrized. In this section the Euler Eulerian size – of – classes approach was used for spray modelling. The primary and secondary break – up models were thoroughly examined, and an adequate set of model coefficients was defined. The parameterization of the spray models was conducted by modelling several evaporative spray cases, where the liquid fuel is injected into non – reactive, high temperature gas environment. In the conducted simulations, the evaporation process was enforced, whilst the combustion of the vaporised fuel was avoided due to deficiency of the reactant species. The modelled results are compared with the available experimental data, where the influence of model coefficients on the liquid and vapour tip penetration is presented. Furthermore, for the nozzle flow – spray coupling interface a several new features were developed. A new type of boundary condition for spray injection was developed, and the primary atomization model was validated against the available DNS data.

In the third step, the validation and enhancement of the secondary WAVE break – up model within the Euler Eulerian framework was performed. The validation of the implemented code was conducted by comparing the modelled results to the available experimental data found in the literature, and by examining the high pressure liquid fuel injection with detailed spray inlet boundary condition. The spray inlet was coupled with the nozzle flow simulation through

the enhanced and modified nozzle file interface. In such interface the turbulence, temperature, velocity, volume fraction, and density information are recorded for each phase. In the spray simulation, the recorded data was adequately mapped to the spray inlet boundary selection, which was then used for representing a realistic fuel injection process. The results of high pressure liquid fuel injection into a constant volume chamber filled with an inert gases are presented. The spray cloud shape, spray cone angle, liquid penetration, and droplet size distribution are compared to the available experimental data.

In the fourth step, the stochastic O'Rourke collision model was modified for the Euler Eulerian size – of – classes approach and it was implemented into the CFD code FIRE<sup>®</sup>. The collision between droplets is considered for defined interfaces in all computational cells where a certain amount of liquid fuel is present. For each droplet class participating on the collisions process, the droplet diameter, velocity and temperature are properly defined according to the mass, momentum and energy conservation laws. The model is currently used to predict the coalescence of the colliding droplets.

In the fifth step the Euler Eulerian spray model was enhanced with the combustion model. The results of this section offer a new method that uses the general gas phase reactions for modelling the combustion process in combination with the Euler Eulerian size – of – classes approach. The method was developed by performing plausibility tests on a constant volume reactor filled with liquid – gas mixture under elevated pressure and temperature conditions. The influence of evaporation on the mass balance, heat release and temperature change due to the combustion is discussed.

In the sixth step, the developed and verified method was validated by comparing modelling results with the available experimental data from ECN database. The liquid and vapour phase penetrations, the radial and axial mixture distribution, the spray cloud shape and the temperature fields are compared with the experimental data. Initially, the modelling of high pressure liquid fuel injection into the non – reactive environment was performed. Afterwards, the validation of the developed method was conducted by numerical modelling of various reactive spray cases, and by comparing lift off length, pressure rise, OH radical concentration, and temperature fields to the available experimental data.

Finally, the developed method and validated spray sub models were used for 3D CFD modelling of a real engineering combustion system such as IC diesel engine. The engine working cycle (compression and expansion stroke) was modelled by including the mesh

movement and geometry mapping called mesh rezone. The simulated mean pressure and temperature traces, as well as the ROHR are compared to the available experimental data.

### **1.5. Scientific contribution**

The result of this thesis is a new method that can be used for modelling spray and combustion processes. The method was developed by combining the Euler Eulerian multi – continuum model size – of – classes approach with the chemical kinetics. The existing nozzle flow – spray interface was enhanced for MPI simulations and a new type of spray inlet boundary condition was developed. The Eulerian spray model was enhanced by the droplet collision model, and the primary atomization model was validated against the DNS data. To improve prediction of the droplet size distribution, the existing disintegration model was enhanced by taking into account child droplets. It can be stated that the developed method can be used to extend the applicability of the Euler Eulerian size – of – classes approach for various engineering applications with reactive multiphase flows.

## 2. NUMERICAL MODELLING

This section shows an introduction into 3D CFD modelling by discussing a general transport equation for single phase systems. Afterwards, a short introduction into turbulent flows is provided followed by the explanation of the averaging procedure applied on the conservation equations for the turbulent closure. Two different turbulence models are explained. Furthermore, a detailed explanation of the conservation equations for multiphase system are shown. The focus in this part of the thesis is put on the explanation of mass, momentum, enthalpy, and species transport equations with addition of two conservation equations needed for closing the equation system for turbulent flows, namely turbulent kinetic energy and dissipation rate.

### 2.1. Fundamental equations of fluid flow and heat transfer

Fundamental equations of fluid mechanics are based on mass, momentum and energy conservation laws. A general definition for conservation of physical flow properties is defined as: the temporal rate of change of a property is equal to the net rate “flux” at which the property flows through the control volume boundaries, plus the rate of property production/consumption due to some processes. The production/consumption term is known as the source/sink term.

The next equation shows the general conservation equation for any scalar property  $\varphi$  and for a fixed control volume  $V$  :

$$\int_V \frac{\partial}{\partial t} (\rho\varphi) dV + \int_S (\rho\varphi) u_j n_j dS = \int_S \left( \Gamma_\varphi \frac{\partial \varphi}{\partial x_j} \right) n_j dS + \int_V S_\varphi dV, \quad (5)$$

where the first term is the unsteady term and the second term is the convection term. The first term on the right – hand side is the diffusive flux, and the last term is the scalar property sink/source term. By using the Gauss’ divergence theorem and by defining the volume  $V$ , the above equation is transformed into the general transport equation of any scalar property  $\varphi$  :

$$\frac{\partial (\rho\varphi)}{\partial t} + \frac{\partial}{\partial x_j} (\rho\varphi u_j) = \frac{\partial}{\partial x_j} \left( \Gamma_\varphi \frac{\partial \varphi}{\partial x_j} \right) + S_\varphi, \quad (6)$$

where  $\Gamma$  and  $S$  are diffusion and source/sink terms, respectively.

## **2.2. Turbulent flows**

A turbulent flow is characterized by a broad range of temporal and spatial scales. Therefore, for direct solving of turbulent flows a fine computational mesh and small time steps should be used. Direct solving of turbulent flows is theoretically possible, but since it requires higher computational power, in a real engineering applications its use is currently limited. It is considered that a turbulent flow is composed of different sized eddies, where the largest ones possess most of the turbulent energy, and they are placed within the spatial scale named energy range. Energy from larger eddies is transferred towards smaller eddies with spatial scales placed within the initial subrange. Statistics of subrange eddies depend only on the energy transfer rate from the larger scale eddies. Furthermore, the energy is transferred towards the smallest scale eddies placed within the range of Kolmogorov scale. The Kolmogorov length scale becomes smaller with increase in turbulence, which implies that with turbulent flows characterized by high Reynolds number, a fine computational domain is required for adequate modelling. Computational solving of eddies covering the whole time and spatial scales is called DNS. Such approach is powerful, but currently too expensive for calculating combustion and spray processes in a real engineering applications. However, such approach can be used for simulation of simplified or small systems, in some cases with low Reynolds number. For instance, when the experimental research of a process is not available, or it is highly complicated, engineers could use DNS modelling results for development of computational models in LES or RANS framework. The LES stands for Large Eddy Simulations in which turbulent eddies are directly solved for the energy range, whilst smaller eddies are being modelled by using some turbulence modelling approach.

The abbreviation RANS stands for the Reynolds Averaged Navier Stokes equation approach in which all turbulent eddies are being modelled by means of the turbulence models. In such approach, the instantaneous variables of turbulent flow quantities are replaced with the time averaged value and its fluctuating part. Additionally, two terms are introduced into the conservation equations: the Reynolds stress tensor and the turbulent heat flux which result from the averaging processes. In order to solve a turbulent flow those terms have to be modelled, which is done by means of turbulence models. The next section shows the overview of statistical approaches used for conservation equations averaging within the RANS framework.

### 2.2.1. Averaging of the conservation equations

The DNS approach is still too expensive computational approach for modelling of real engineering applications, and therefore the RANS approach is used instead. The averaging of instantaneous quantity starts with its decomposition into mean and fluctuating part, as shown in next equation:

$$\varphi = \bar{\varphi} + \varphi'. \quad (7)$$

The averaged quantity  $\bar{\varphi}$  smoothly changes in time, which makes it is easier to solve than the instantaneous quantity. In a special case, when the averaged quantity is independent on time, a quasi – stationary flow is observed. The discussed averaging procedure is usually referred as the Reynolds averaging procedure. The continuity and momentum conservation equations, obtained by the Reynolds averaging, are shown in next equations:

$$\frac{\partial \bar{\rho}}{\partial t} + \frac{\partial}{\partial x_j} (\bar{\rho} u_j) = 0 \quad (8)$$

$$\rho \frac{\partial \bar{u}_i}{\partial t} + \frac{\partial}{\partial x_j} (\bar{\rho} u_j u_i) = -\frac{\partial \bar{p}}{\partial x_i} + \frac{\partial}{\partial x_j} \left[ \mu \left( \frac{\partial \bar{u}_i}{\partial x_j} + \frac{\partial \bar{u}_j}{\partial x_i} \right) - \overline{\rho u_i' u_j'} \right]. \quad (9)$$

The Reynolds averaging of the physical quantity produces additional terms (second moments) in the momentum transport equations by involving correlations of the fluctuating components. These terms have to be modelled, which is commonly known as turbulence closure. The closure terms are always one order higher than the averaged quantity. For instance, the averaging of the velocity vector will lead to a tensor of second order (Reynolds stress tensor). Turbulence models can be classified into first order (Eddy Viscosity/diffusivity Models – EVM) and second order models (Reynolds Stress Models – RSM). In the EVM models the turbulent fluxes are correlated to the mean flow field, whilst in the RSM models additional transport equations are being solved for each turbulent flux component. The EVM models can be further divided into zero, one or two equation models. In such models the Reynolds stress tensor is expressed in the same way as the viscous stress for Newtonian isotropic fluids, proportional to the mean strain rate tensor, but with difference that the molecular viscosity term is enhanced with the eddy viscosity term. The Reynolds stress tensor for EVM turbulence model is defined with the next expression:

$$-\overline{\rho u_i u_j} = \mu_t \left( \frac{\partial \bar{u}_i}{\partial x_j} + \frac{\partial \bar{u}_j}{\partial x_i} \right) - \frac{2}{3} \left( \mu_t \frac{\partial \bar{u}_k}{\partial x_k} + \bar{\rho k} \right) \delta_{ij}, \quad (10)$$

where  $\mu_t$  is the turbulent viscosity and  $\bar{k}$  is the turbulent kinetic energy defined according to next equation:

$$\bar{k} = \frac{\overline{u_i' u_i'}}{2}. \quad (11)$$

In processes with large density variations such as combustion process, the RANS equations are further complicated due to the velocity density fluctuation term  $\rho' u'$ . To reduce the system complexity the Favre averaging is introduced, as shown with eq. (12):

$$\bar{\varphi} = \frac{\overline{\varphi \rho}}{\bar{\rho}}. \quad (12)$$

Similarly to the Reynolds averaging, the instantaneous quantity is decomposed into Favre mean and fluctuating component, as shown with next equation:

$$\varphi = \bar{\varphi} + \varphi''. \quad (13)$$

Favre averaging is performed on all quantities except pressure and density, which are Reynolds averaged quantities. The continuity and momentum conservation equations, obtained by the Favre density averaging, are shown in next equations:

$$\frac{\partial \bar{\rho}}{\partial t} + \frac{\partial}{\partial x_j} (\bar{\rho} u_j) = 0 \quad (14)$$

$$\frac{\partial (\bar{\rho} u_i)}{\partial t} + \frac{\partial}{\partial x_j} (\bar{\rho} u_i u_j) = \bar{\rho} f_i - \frac{\partial \bar{p}}{\partial x_i} - \frac{\partial \bar{\rho} u_i'' u_j''}{\partial x_j} + \frac{\partial \bar{\tau}_{ij}}{\partial x_j}, \quad (15)$$

where term  $\bar{\rho} u_i'' u_j''$  represents the Reynold stress tensor which needs to be modelled by the turbulence model. The same conservation averaging principle is put upon the enthalpy and species conservation equations. In the averaged enthalpy conservation equation, the additional term  $\bar{\rho} h'' u_j''$  arises, which also needs to be modelled.

The Reynolds stress tensor shown for Reynolds and Favre averaging is modified according to next equation:

$$-\overline{\rho u_i u_j} = \mu_t \left( \frac{\partial u_i}{\partial x_j} + \frac{\partial u_j}{\partial x_i} \right) - \frac{2}{3} \left( \mu_t \frac{\partial u_k}{\partial x_k} + \overline{\rho k} \right) \delta_{ij}. \quad (16)$$

The Favre averaged turbulent kinetic energy is calculated according to next expression:

$$k = \frac{u_i u_i}{2}. \quad (17)$$

For calculating turbulent stresses and fluxes, the turbulent viscosity and conduction coefficients have to be known. Those coefficients are not fluid properties, but instead they are in a function of flow properties. Therefore, Prandtl defined those coefficients by postulating the turbulent viscosity  $\mu_t$  according to the gas kinetic theory. Consequently, the viscosity is calculated according to the next expression:

$$\mu = \frac{1}{3} \rho l \overline{u_{mol}}, \quad (18)$$

where  $l$  is the mixing length and  $\overline{u_{mol}}$  is the averaged velocity. Turbulent viscosity is defined as:

$$\mu_t = \rho l_m u_t, \quad (19)$$

where  $l_m$  is the turbulent mixing length and  $u_t$  is the characteristic turbulent velocity. The turbulent mixing length must be defined, and it is a function of the observed system and the flow characteristics. The above mentioned expression for turbulent viscosity is used in zero equation EVM models, whilst in more complex models (one or two equation), a different approach for calculation of  $\mu_t$  is used. In one equation models, an additional transport equation for the turbulent kinetic energy is solved, whilst the energy dissipation rate is modelled. In two equation models, both transport equation are being solved. In the following section a brief introduction into two equation turbulence models is shown, focusing on the widely used  $k - \varepsilon$  and the more advanced  $k - \zeta - f$  turbulence model.



### 2.2.2. $k-\varepsilon$ turbulence model

In the  $k-\varepsilon$  turbulence model the turbulent viscosity is calculated according to the next expression:

$$\mu_t = \bar{\rho} C_\mu \frac{k^2}{\varepsilon}, \quad (20)$$

where  $C_\mu$  is a model constant. To calculate the turbulent viscosity, two additional transport equations are being solved, for  $k$  and  $\varepsilon$ , according to next expressions:

$$\frac{\partial(\bar{\rho}k)}{\partial t} + \frac{\partial(\bar{\rho}k u_j)}{\partial x_j} = \frac{\partial}{\partial x_j} \left[ \left( \mu + \frac{\mu_t}{\sigma_k} \right) \frac{\partial k}{\partial x_j} \right] + P + G - \bar{\rho} \varepsilon \quad (21)$$

$$\frac{\partial(\bar{\rho}\varepsilon)}{\partial t} + \frac{\partial(\bar{\rho}\varepsilon u_j)}{\partial x_j} = \frac{\partial}{\partial x_j} \left[ \left( \mu + \frac{\mu_t}{\sigma_\varepsilon} \right) \frac{\partial \varepsilon}{\partial x_j} \right] + C_{\varepsilon 1} \frac{\varepsilon}{k} P + C_{\varepsilon 3} \frac{\varepsilon}{k} G - C_{\varepsilon 2} \frac{\varepsilon^2}{k} \rho, \quad (22)$$

where the terms on the left – hand side of both equations are the local change in time and the convective transport. The first term on the right – hand side stands for the diffusion, term  $P$  is the production of the transported quantity by mean flow deformation,  $G$  stands for production/destruction of the quantity by body forces, and the last term is the dissipation term. The model constants  $\sigma_k$ ,  $\sigma_\varepsilon$ ,  $C_{\varepsilon 1}$ ,  $C_{\varepsilon 2}$ , and  $C_{\varepsilon 3}$  are not universal and must be tuned for different applications. The recommended model coefficient values for the  $k-\varepsilon$  turbulence model are shown in Table 1 [81].

**Table 1 Default values of  $k-\varepsilon$  turbulence model.**

$C_\mu$	$\sigma_k$	$\sigma_\varepsilon$	$C_{\varepsilon 1}$	$C_{\varepsilon 2}$	$C_{\varepsilon 3}$
0.09	1	1.3	1.44	1.92	0.8

In case of multiphase flows the transport equations for  $k$  and  $\varepsilon$  are slightly modified. The transport equation for turbulent kinetic energy for multiphase flows is defined as:

$$\frac{\partial(\alpha_k \rho_k k_k)}{\partial t} + \frac{\partial(\alpha_k \rho_k k_k u_{kj})}{\partial x_j} = \frac{\partial}{\partial x_j} \left[ \alpha_k \left( \mu_k + \frac{\mu_{tk}}{\sigma_k} \right) \frac{\partial k_k}{\partial x_j} \right] + \alpha_k P_k - \alpha_k \rho_k \varepsilon_k + \sum_{l=1, l \neq k}^{npk} K_{kl} + \sum_{l=1, l \neq k}^{npk} k_{kl} \Gamma_{kl}, \quad (23)$$

where term  $P_k$  represents the production of turbulent kinetic energy by mean flow deformation for phase  $k$ . The transport equation of the turbulent dissipation rate is defined as

$$\frac{\partial(\alpha_k \rho_k \varepsilon_k)}{\partial t} + \frac{\partial(\alpha_k \rho_k \varepsilon_k u_{kj})}{\partial x_j} = \frac{\partial}{\partial x_j} \left[ \alpha_k \left( \mu_k + \frac{\mu_{tk}}{\sigma_\varepsilon} \right) \frac{\partial \varepsilon_k}{\partial x_j} \right] + \sum_{l=1, l \neq k}^{npk} D_{kl} + \varepsilon_{kl} \sum_{l=1, l \neq k}^{npk} \Gamma_{kl} + \alpha_k C_{\varepsilon 1} \frac{\varepsilon_k}{k_k} P_k - \alpha_k C_{\varepsilon 2} \frac{\varepsilon_k^2}{k_k} \rho_k + \alpha_k C_{\varepsilon 4} \rho_k \varepsilon_k \frac{\partial u_{kj}}{\partial k_j}. \quad (24)$$

Terms  $K_{kl}$  and  $D_{kl}$  are the inter – phase exchange terms and have to be modelled. In theory, the turbulent viscosity should be calculated for each Eulerian class. However, in this thesis the assumption is made that the level of turbulence of the droplet classes are equal to the continuous phase, and that the interaction between the phases is neglected [82]. In addition to the coefficient set shown in Table 1, a new coefficient  $C_{\varepsilon 4}$  is introduced with recommended value of -0.33. The used assumptions lead to the closure of  $k$  and  $\varepsilon$  equations similar to single phase flows. In the multiphase conservation equations, the averaged terms are shown as regular due to easier reading.

### 2.2.3. $k - \zeta - f$ turbulence model

In some parts of this thesis the eddy-viscosity  $k - \zeta - f$  turbulence model was employed for the description of the highly turbulent spray behaviour [83][84]. This turbulence model is based on Durbin's elliptic relaxation concept [85], and it solves an additional transport equation for the velocity scale ratio  $\zeta = \overline{v^2} / k$ . It is robust and suitable for spray process modelling, and for describing the swirl motion which is characteristic for IC diesel engines.

The eddy viscosity term is calculated according to the next equation:

$$\mu_t = \overline{\rho} C_\mu \zeta \frac{k^2}{\varepsilon}, \quad (25)$$

where  $C_\mu$  is the turbulence model constant. In addition to the abovementioned transports equations for  $k$  and  $\varepsilon$  quantities, the transport equation for the velocity scale ratio  $\zeta$  is calculated according to the next equation:

$$\frac{\partial(\bar{\rho}\zeta)}{\partial t} + \frac{\partial}{\partial x_j}(\bar{\rho}u_j\zeta) = \bar{\rho}f - \bar{\rho}\frac{\zeta}{k}P_k + \frac{\partial}{\partial x_j}\left[\left(\mu + \frac{\mu_t}{\sigma_\zeta}\right)\frac{\partial\zeta}{\partial x_j}\right], \quad (26)$$

where the term  $\sigma_\zeta$  is the model constant, the term  $f$  is the elliptic function calculated according to the expression:

$$f - \frac{\partial^2 f}{\partial x_i \partial x_j} L^2 = \left(C_1 + C_2 \frac{P_k}{\zeta}\right) \frac{(2/3 - \zeta)}{T}, \quad (27)$$

where  $L$  and  $T$  terms are the turbulent length and turbulent time scales, respectively. The model closure is achieved by imposing the Kolmogorov time and length scales as lower bounds combined with the Durbin realizability constraints:

$$T = \max\left[\min\left(\frac{k}{\varepsilon}, \frac{0.6}{\sqrt{6}C_\mu|S|\zeta}\right), C_T\left(\frac{\nu}{\varepsilon}\right)^{0.5}\right] \quad (28)$$

$$L = C_L \max\left[\min\left(\frac{k^{1.5}}{\varepsilon}, \frac{k^{0.5}}{\sqrt{6}C_\mu|S|\zeta}\right), C_\eta\left(\frac{\nu^3}{\varepsilon}\right)^{0.25}\right]. \quad (29)$$

Next table shows the default set of  $k-\zeta-f$  model constants used as starting point for modelling turbulent flows in various engineering applications.

**Table 2** Default values of  $k-\zeta-f$  turbulence model

$C_\mu$	$\sigma_k$	$C_{\varepsilon 1}$	$C_{\varepsilon 2}$	$\sigma_\varepsilon$	$\sigma_\zeta$	$C_1$	$C_2'$	$C_T$	$C_L$	$C_\eta$
0.22	1	$1.4(1+0.012/\zeta)$	1.9	1.3	1.2	0.4	0.65	6	0.36	85

### **2.3. Multiphase flows**

Multiphase flows are found in many engineering applications and in various industries such as transport, chemical, aerospace industry, etc. Such flows can be categorized as liquid – liquid, liquid – gas, liquid – solid, and gas – solid combinations. Furthermore, they can be divided into thin, diluted or dense multiphase flows. Due to such a variety, there are different computational methods that are being used for multiphase flow modelling. It should be mentioned, that none of the existing methods is suitable for solving all types of multiphase flows. On contrary, the models are developed specifically to describe a certain multiphase flow category. This implies, that each developed model has certain advantages and disadvantages, which have to be taken into account before approaching to CFD numerical modelling. A high pressure liquid fuel injection is considered as liquid – gas multiphase flow covering the dense, diluted and thin multiphase flow regime. To model such a complicated process, two distinguished modelling approaches are frequently used, the Euler Lagrangian and Euler Eulerian approach. For both approaches the Eulerian formulation is used to describe the gas phase, whilst for modelling the discrete phase the Lagrangian equations of motion, or the Eulerian conservation equations, are being used. For capturing the interfacial mass, momentum and enthalpy exchange in Lagrangian formulation a large number of liquid parcels have to be introduced into the computational domain, whilst in the Euler Eulerian formulation an increased number of classes is required.

In the next section the two above mentioned formulations for modelling multiphase flows are briefly described. The first one is the mostly used Lagrangian DDM approach which tracks liquid particle separately and calculates its trajectory. The second is the Euler Eulerian approach in which both phases are considered as inter – penetrating continuum.

### **2.4. The Euler Lagrangian formulation**

In the Euler Lagrangian DDM approach, a sample of individual droplets same in dimensions and physical quantities, are tracked through the calculation domain. Such defined groups are referred as parcels [40]. Instead of tracking each droplet, the grouping procedure allows tracking of parcels which reduces the computational effort. To track the spray spatial and temporal distribution, for each parcel a trajectory is calculated according to the next expression:

$$\rho_l \frac{du_p}{dt} = \sum F, \quad (30)$$

where the term  $du_p / dt$  represents the parcel acceleration, and the term on the right – hand side stands for the sum of all forces acting on the observed parcel  $P$ . This term gets contribution from drag, gravity and buoyancy forces, force arising from pressure difference, and external forces such as magnetic or electrostatic forces.

The Euler Lagrangian approach suffers from several limitation. It is very sensitive to the numerical grid resolution in the near nozzle region, which directly affects the modelling of mass, momentum and heat exchange between the defined phases. Furthermore, the computational costs increase with increase of the parcel number, and it suffers from parallelization issues and statistical convergence problems. Nevertheless, it is efficient and sufficiently accurate to be the mostly used spray modelling approach in the industrial development processes.

## 2.5. The Euler Eulerian formulation

To overcome the disadvantages of the Euler Lagrangian DDM approach, the Euler Eulerian multi – continuum approach can be employed. The basis of this formulation is the multiphase approach obtained through an ensemble averaging process of the conservation equations. Both, the gas and the liquid phase, are considered as continuum represented by their volume fraction. Within this thesis, the liquid phase is further divided into a defined number of droplet classes represented by their class diameter. Therefore, this model is called size – of – classes model. The total number of Eulerian classes and the class diameter range are chosen according to certain rules based on experience, and by taking into consideration the available CPU power. The diameter range of droplet classes is usually defined by taking into account expected SMD and nozzle hole diameter. A higher number of classes results in better spray resolution but also in higher computational effort. For proper model behaviour it is important to assign the nozzle diameter as class size of the bulk liquid phase  $k$ . The class specification for the Euler Eulerian size – of – classes approach is shown in Table 3.

**Table 3 Euler Eulerian size – of – classes approach class specification.**

<b>Class</b>	1	2, ..., k-1	k
<b>Content</b>	Gas mixture	Droplets	Bulk liquid

The Eulerian classes from 2 to  $k-1$  are defined as droplet classes sorted in increasing manner according to their diameter. The last Eulerian class, class  $k$ , is defined as the bulk liquid class representing the fuel jet flowing out from the nozzle hole. Within the Euler Eulerian size – of – classes approach, the liquid phase is expressed through the class volume fractions, according to the assumption that the discrete phase can be considered as continuum. Within one control volume and one Eulerian class, the assumption that all droplets have same velocity and physical properties is made. Figure 10 shows a schematic representation of the Euler Eulerian class specification and a brief description of the Eulerian sub – models for mass, momentum and enthalpy exchange. The primary atomization model is used to describe the mass transfer from liquid jet towards the droplet classes. The secondary atomization model is used to define mass transfer between droplet classes from class with bigger diameter towards class defined with smaller droplet diameter. The evaporation model is used to define the phase change and calculate the mass exchange between droplet classes and the gas phase. Finally, the collision model is used to model the coalescence process occurring between defined droplet classes.

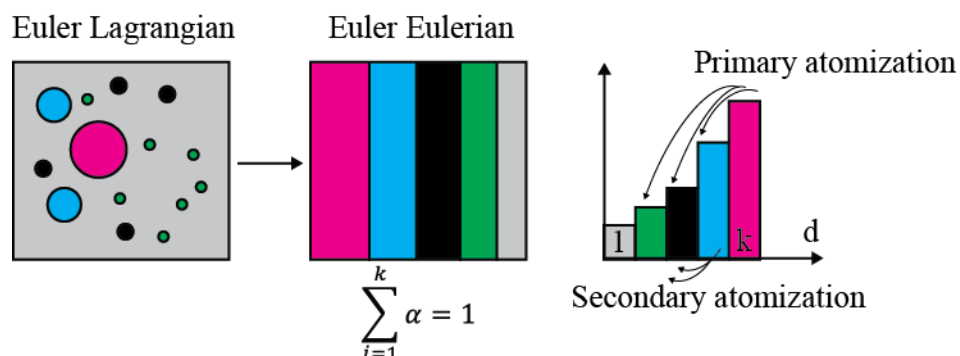


**Figure 10** Schematic of spray modelling approaches and the Euler Eulerian spray sub – models

### 2.5.1. Averaging in multiphase flows

In the Euler Eulerian size – of – classes approach, the droplet classes and the continuous gas phase are considered as continuum, and the same transport equations are being solved to describe the fluid flow. The conservation equations of the multiphase system are similar to the single phase equations, but with difference in addition of inter – phase exchange terms between the defined classes. Due to the a relatively big time and spatial scale range, that is characteristic for multiphase flows, the modelled system should be discretized with high resolution, both in time and space. This implies relatively small computational time steps and finer computational volumes. The need for fine spatial and time resolution lead to a high computational effort for

multiphase flows modelling. Another difficulty, arising from the continuum assumption and from dividing the discrete phase into classes, is the description of the physical processes occurring at the phase interfaces.

Depending on the turbulent flow characterization, three different averaging methods can be introduced [86][87]:

1. Time averaging
2. Spatial averaging
3. Ensemble averaging of identical processes/experiments

To average the multiphase conservation equations the ensemble averaging procedure is used. Ensemble averaging builds the simple sum of a quantity for all process/experiment realisations and divides them by the number realisations, as shown with next equation:

$$\Phi(x_i, t_i) = \frac{1}{N} \sum_{n=1}^N \Phi(x_n, t), \quad (31)$$

where  $N$  is the number of process/experiment realisations.

The averaging procedure is enhanced by introducing a phase indicator function  $\chi$  which ensures the contribution of a particular phase to the averaging procedure, only if this phase exists in the region of interest. The phase indicator function is defined as:

$$\chi_k(x, t) = 1 \rightarrow \text{if phase } k \text{ is present at location } x \text{ at time } t \quad (32)$$

$$\chi_k(x, t) = 0 \rightarrow \text{if phase } k \text{ is not present at location } x \text{ at time } t. \quad (33)$$

The volumetric concentration (or volume fraction, or relative residence time) of phase  $k$  is defined according to equation

$$\alpha_k = \overline{\chi_k}, \quad (34)$$

where  $\overline{\chi_k}$  stands for the ensemble averaged phase indicator function. In multiphase flows, two types of averaged variables are considered: the component weighted average  $\overline{\Phi_k}$ , and the mass weighted average  $\overline{\Psi_k}$ . The former mentioned averaging is defined as:

$$\overline{\Phi} = \frac{\overline{X_k \Phi}}{\alpha_k}, \quad (35)$$

whilst the latter mentioned one is defined as:

$$\overline{\Psi}_k = \frac{\overline{X_k \rho \Psi}}{\alpha_k \rho_k}. \quad (36)$$

The component weighted average is used to express the averaged phase density, whilst the mass average is used for expressing the averaged phase velocity. Due to the above mentioned difficulties, the multiphase conservation equations are derived by applying these averaging approaches on the transport equations, as described in the following section.

### 2.5.2. Mass conservation

The continuity equation for compressible single phase system is expressed by the next expression:

$$\frac{\partial \rho}{\partial t} + \frac{\partial}{\partial x_j} (\rho u_j) = 0, \quad (37)$$

which can be converted for multiphase systems by taking into account the ensemble averaging procedure, as shown in the previous section. Rearranging the upper equation, the continuity equation for phase  $k$  can be derived as:

$$\frac{\partial (\alpha_k \rho_k)}{\partial t} + \frac{\partial}{\partial x_j} (\alpha_k \rho_k u_{kj}) = \sum_{l=1, l \neq k}^{Nph} \Gamma_{kl}, \quad (38)$$

where  $\alpha_k$  is the Eulerian class volume fraction,  $\rho_k$  is class density and  $u_{kj}$  is the velocity at phase interface. The term on the right – hand side stands for the interfacial mass exchange between classes  $k$  and  $l$ .

In the Euler Eulerian size – of – classes approach an additional condition regarding the class volume fraction  $\alpha_k$  must be fulfilled. To achieve mass conservation, the sum of volume fractions must be equal to one, as shown with next equation:

$$\sum_{k=1}^{Nph} \alpha_k = 1. \quad (39)$$



### 2.5.3. Momentum conservation

The momentum conservation equations for multiphase system are defined as:

$$\frac{\partial(\alpha_k \rho_k u_{ki})}{\partial t} + \frac{\partial}{\partial x_j} (\alpha_k \rho_k u_{ki} u_{kj}) = -\alpha_k \frac{\partial p}{\partial x_i} + \frac{\partial}{\partial x_j} [\alpha_k (\tau_{kij} + \tau'_{kij})] + \alpha_k \rho_k f_i + \sum_{l=1, l \neq k}^{Nph} \mathbf{M}_{kli} + u_{kli} \sum_{l=1, l \neq k}^{Nph} \Gamma_{kl}, \quad (40)$$

where the terms on the left – hand side are the time derivative of momentum for class  $k$  and the convective momentum transport, respectively. The first term on the right – hand side is the pressure gradient term yielding the pressure forces on the droplets of class  $k$ . In this thesis the pressure was assumed identical for all phases. The second term represents the momentum exchange due to surface forces arising from molecular and turbulent stresses (viscous and Reynolds stresses). For a multiphase system the viscous stress tensor is calculated according to next expression:

$$\tau_{kij} = \mu_k \left[ \left( \frac{\partial u_{kj}}{\partial x_i} + \frac{\partial u_{ki}}{\partial x_j} \right) - \frac{2}{3} \delta_{ij} \frac{\partial u_{km}}{\partial x_m} \right], \quad (41)$$

where  $\mu_k$  is the molecular viscosity of phase  $k$ . The Reynolds stress tensor is calculated according to next expression:

$$\tau'_{kij} = \mu_k^t \left[ \left( \frac{\partial u_{kj}}{\partial x_i} + \frac{\partial u_{ki}}{\partial x_j} \right) - \frac{2}{3} \delta_{ij} \frac{\partial u_{km}}{\partial x_m} \right] - \frac{2}{3} \delta_{ij} \rho_k k_k, \quad (42)$$

where turbulent viscosity  $\mu_k^t$  of phase  $k$  is calculated according to next expression:

$$\mu_k^t = \rho_k C_\mu \frac{k_k^2}{\varepsilon_k} \text{ or } \mu_k^t = \rho_k C_\mu \zeta_k \frac{k_k^2}{\varepsilon_k}, \quad (43)$$

depending on the applied turbulence model. The third term on the right – hand side of momentum conservation equation is the gravity force term, term  $\mathbf{M}_{kli}$  represents the interfacial momentum transfer from the class  $k$  to gas phase, and term  $\Gamma_{kl}$  stands for momentum change due to the mass transfer between the Eulerian classes.

#### 2.5.4. Enthalpy conservation

The total enthalpy conservation for each Eulerian class is shown by the next expression:

$$\begin{aligned} \frac{\partial(\alpha_k \rho_k h_k)}{\partial t} + \frac{\partial}{\partial x_j} (\alpha_k \rho_k u_{kj} h_k) = \frac{\partial}{\partial x_j} [\alpha_k (q_{kj} + q_{kj}^t)] + \alpha_k \rho_k f_j u_{ki} + \\ + \frac{\partial}{\partial x_j} [\alpha_k u_{ki} (\tau_{kij} + \tau_{kij}^t)] + \alpha_k \frac{\partial p}{\partial t} + \sum_{l=1, l \neq k}^{Nph} H_{kl} + h_{kl} \sum_{l=1, l \neq k}^{Nph} \Gamma_{kl} \end{aligned} \quad (44)$$

where the terms on the left – hand side are the time derivative of the total enthalpy for phase  $k$  and the enthalpy convective transport, respectively. The first term on the right – hand side is the total enthalpy change from molecular and turbulent heat fluxes. The third term represents the enthalpy change due to surface forces. The heat flux vector  $q_{kj}$  is calculated according to next expression:

$$q_{kj} = \frac{\kappa_k}{c_{pk}} \frac{\partial h_k}{\partial x_j}, \quad (45)$$

where  $\kappa_k$  is phase  $k$  thermal conductivity. The turbulent heat flux vector  $q_{kj}^t$  is calculated as follows:

$$q_{kj}^t = \frac{\mu_k^t}{\sigma_T} \frac{\partial h_k}{\partial x_j}, \quad (46)$$

where  $\mu_k^t$  is turbulent viscosity of phase  $k$ , and  $\sigma_T$  is turbulent Prandtl number.

#### 2.5.5. Species transport conservation

In order to model chemical reactions within the gas phase, either by using combustion model or chemical mechanisms, the gas phase is divided into a desired number of chemical species. In order to transport chemical species additional transport equations need to be solved, named species transport equations. The FIRE<sup>®</sup> species transport module allows to transport an arbitrary number of species with a user defined set of properties to model general transport problems like multi – component mixing, flue gases aftertreatment, or combustion processes. The next equation represents the species transport equation for the chemical species  $i$  transported by the gas phase  $l$ :

$$\frac{\partial}{\partial t}(\alpha_1 \rho_1 Y_i) + \frac{\partial}{\partial x_j}(\alpha_1 \rho_1 u_j Y_i) = \frac{\partial}{\partial x_j} \left( \alpha_1 (\rho_1 D_{Y_i} + \frac{\mu_1^t}{Sc^t}) \frac{\partial Y_i}{\partial x_j} \right) + S_{Y_i}, \quad (47)$$

where the first term is the time derivative, whilst the second term is the species convective transport. The first term on the right – hand side is the diffusion term where  $D_{Y_i}$  is the effective diffusion coefficient of species  $i$ , whilst  $Sc^t$  is the turbulent Schmidt number with a default value of 0.7. The last term stands for the species mass source modelled by taking into account the species reaction rate  $\dot{m}_i$  and the molar mass  $M_i$ . The expression for the species mass source term is defined according to next expression:

$$S_{Y_i} = \dot{m}_i \quad . \quad (48)$$

## 2.6. Euler Eulerian spray sub – models

### 2.6.1. Primary atomization

In various engineering applications where the liquid fuel is injected through a small diameter nozzle holes as a result of high pressure difference, the liquid core is subject to a rapid disintegration process. This phenomenon, disintegration of the liquid core itself, is called the primary atomization process. It is a consequence of nozzle flow turbulence, aerodynamic surface instabilities occurring outside the nozzle channel, and the cavitation process.

The pressurized liquid fuel passes through small gaps determined by the nozzle needle movement, and the high pressure differences accelerate the fluid towards the nozzle exit hole. The fluid flow inside the nozzle is considered as a highly turbulent multiphase flow where the fluids aggregate state may change in regions with very low pressure – this process is called cavitation. At the entrance into the nozzle hole channel, the fluid changes its direction which results in velocity increase and a local pressure drop. When the pressure is reduced below the vapour saturation pressure, liquid fuel is vaporized and the cavitation process is induced. The bubbles created by the cavitation contribute to the break – up of the liquid core, and they can significantly reduce the effective outflow cross section area of the nozzle which influences the liquid jet velocity. The liquid fuel flows out from the nozzle channel, and aerodynamic forces act on the liquid jet surface contributing to the jet atomization.

The liquid core, within the Eulerian size – of – classes approach, is represented as a certain number of droplets characterized with the nozzle hole diameter. This assumption is

called the blob injection model. The liquid core is modelled as separate bulk liquid class, and it is the only class that is subject of the primary atomization process. The primary atomization model used within this thesis considers two independent mechanisms: the aerodynamic surface wave growth and internal stresses caused by turbulence. The applied model was developed by [88] and later modified by [89].

The liquid core disintegration rate can be modelled by estimating averaged values of nozzle flow turbulence or by using the AVL nozzle file interface where realistic boundary conditions on the inlet selection are prescribed. The turbulent perturbations initiate the surface instabilities which grow further as a result of aerodynamic pressure forces. Those instabilities results in creation of unstable fuel ligaments and bigger droplets.

The mass loss of the bulk liquid class in each computational cell is calculated according to equation:

$$\frac{dm}{dt} = 4\pi r_n^2 \rho_n \frac{dr}{dt}, \quad (49)$$

where the right – hand side denotes the artificial radius change rate of injected droplets or blobs. Within this model, the radius of the injected droplet remains constant, but the bulk liquid class volume fraction is reduced. The radius change rate is defined as ratio of atomization length scale  $L_A$  and overall break-up time scale  $\tau_A$ , as shown as in the next equation:

$$\frac{dr}{dt} = \frac{L_A}{\tau_A}. \quad (50)$$

The atomization length scale is considered equivalent to the liquid jet turbulent length scale, and it is related to the averaged turbulent kinetic energy and energy dissipation rate at the exit of the nozzle, as shown by the next equation:

$$L_T = B_{P2} C_\mu \frac{k_{avg}^{1.5}}{\varepsilon_{avg}} = L_A. \quad (51)$$

The atomization length scale can be modified to match the experimental data by changing model coefficient  $B_{P2}$ , whilst coefficient  $C_\mu$  is set to 0.09 in all simulations. The average turbulent kinetic energy and energy dissipation rate are calculated according to:

$$k_{avg} = \frac{u_{inj}^2 d_{noz}}{8L_{noz}} \left[ \frac{1}{C_7^2} - C_4 - (1 - C_6^2) \right] \quad (52)$$

$$\varepsilon_{avg} = C_5 \frac{u_{inj}^3}{2L_{noz}} \left[ \frac{1}{C_7^2} - C_4 - (1 - C_6^2) \right], \quad (53)$$

where  $u_{inj}$  is the injection velocity,  $L_{noz}$  is the nozzle channel length and  $d_{noz}$  is the nozzle hole diameter. The model coefficients  $C_4$  and  $C_5$  are held constant with values 0.45 and 0.27 respectively, whilst the area contraction coefficient  $C_6$  and the discharge coefficient  $C_7$  are chosen from the experimental research. The aerodynamic length scale is considered proportional to the turbulent length scale:

$$L_W = 2L_T. \quad (54)$$

The turbulent time scale is calculated according to the next equation:

$$\tau_T = C_\mu \frac{k_{avg}}{\varepsilon_{avg}}. \quad (55)$$

The aerodynamic time scale is calculated according to the KH instability model, as shown in the next equation:

$$\tau_W = \frac{L_W}{\sqrt{\frac{\rho_l \rho_n |u_n - u_l|^2}{(\rho_n + \rho_l)^2} - \frac{\sigma}{(\rho_n + \rho_l) L_W}}}, \quad (56)$$

where index  $l$  represents the gas phase and index  $n$  stands for the bulk liquid class. Term  $\rho$  stands for the class density,  $\sigma$  is the surface tension of the dispersed phase, and the term  $u_n - u_l$  stands for the relative liquid – gas velocity. The total atomization time scale is calculated as linear combination of the turbulent and aerodynamic time scale:

$$\tau_A = B_{P1} \tau_T + B_{P3} \tau_W, \quad (57)$$

or as a harmonic combination of turbulent and aerodynamic time scales, where the faster process dominates the break – up mechanism:

$$\tau_A = \left[ \frac{1}{B_{P1}\tau_T} + \frac{1}{B_{P3}\tau_W} \right]^{-1}. \quad (58)$$

The term  $B_{P1}$  is the model constant which defines the turbulent time scale, whilst  $B_{P3}$  defines the aerodynamic time scale. Both model constant are used to match the experimental data.

### 2.6.2. Secondary atomization

After the primary atomization of the liquid core, which causes generation of unstable ligaments and bigger droplets, a further disintegration into even smaller drops occurs – this process is called the secondary atomization process. The disintegration of liquid droplets is a consequence of instabilities resulting from aerodynamic and turbulent forces acting on the droplet surface. In the literature several secondary break – up models have been proposed, i.e. WAVE, TAB (Taylor Analogy Break-up), FIPA (Fractionnement Induit Par Acceleration), KHRT (Kevin Helmholtz – Rayleigh Taylor), HuhGosman, Chu [56]. All of these model are capable to reproduce the measured data with a right set of model coefficients. In this thesis, the WAVE secondary break – up model was used. The basis of this model is the linear stability analysis applied on a liquid jet penetrating into an incompressible and quiescent gas environment. To develop the model, an infinitesimal axisymmetric surface displacement was imposed onto the droplet surface, characterised by the fluctuating pressure and the radial and axial velocity components. Such fluctuations have been described by the continuity equation and the equation of motion, which were solved to obtain the dispersion relation for the wave growth rate and the corresponding wavelength. By use of the experimental investigation the semi empirical equations (curve fits of the numerical solution) were given for the wavelength  $\Lambda$  and for the maximum growth rate  $\Omega$  in function on local flow properties, as shown with next equations [9]:

$$\Lambda_k = 9.02r_k \frac{(1 + 0.45 \cdot Oh^{0.5})(1 + 0.4 \cdot T^{0.7})}{(1 + 0.87 \cdot We_1^{1.67})^{0.6}} \quad (59)$$

$$\Omega_k = \left( \frac{\rho_k r_k^3}{\sigma} \right)^{-0.5} \frac{0.34 + 0.38 \cdot We_1^{1.5}}{(1 + Oh)(1 + 1.4 \cdot T^{0.6})}, \quad (60)$$

where  $r_k$  is the droplet radius of the parent class,  $Oh$  is the Ohnesorge number,  $T$  is the Taylor number, and  $We$  is the gas phase Weber number. The break-up target radius  $r_{target}$  is modelled according to:

$$r_{target} = B_{S1} \Lambda, \quad (61)$$

following the assumption that the created droplet is proportional to the wavelength of the fastest growing instability acting on the droplet surface. In this thesis, the constant  $B_{S1}$  was set to 0.61. Due to the production of new droplets, the volume fraction of the parent class is reduced and the assumed change rate of the parent droplet diameter is defined as:

$$\frac{dr_k}{dt} = -\frac{r_k - r_{target}}{\tau_A}, r_{target} \leq r_k, \quad (62)$$

where term  $\tau_A$  is the break-up time defined according to:

$$\tau_a = 3.726 B_{S2} \frac{r_k}{\Lambda_k \Omega_k}. \quad (63)$$

The constant  $B_{S2}$  is the break – up time constant used to scale the break – up time. It varies from one injector to another with recommended values from 1.73 – 20. The expression for the modelled mass loss due to the secondary droplet break-up process is defined according to the next equation:

$$\frac{dm_k}{dt} = 4\pi r_k^2 \rho_k \frac{dr_k}{dt}, \quad (64)$$

where the left – hand side of the equation represents the mass loss rate  $k$ , and the last term is radius change rate described in equation (64).

Modelling the secondary droplet atomization within the Eulerian size – of – classes approach is highly dependent on the choice of the class diameters. It can occur that the target diameter lays within the parent class diameter boundaries, and therefore, droplets of smaller diameter will not be created. Thus, the common WAVE model is modified with the child droplet option to reduce its dependency on the choice of the droplet classes.

### 2.6.3. Droplet collision

From the viewpoint of the statistical particle method, which builds the basis of the common spray simulation module, the droplet collisions are modelled by a statistical approach. In the work carried out within tasks defined in this thesis the O'Rourke collision model [90] was implemented into the commercial CFD code FIRE<sup>®</sup> for the Eulerian size – of – classes spray modelling approach. The droplet collision process is modelled for a defined number of liquid class interfaces. Currently, the model is used to calculate the coalescence regime, where two droplets stick together and form a new droplet with bigger radius, according to the mass conservation law. The collision frequency is calculated by using the relative velocity between the colliding droplets. Thus, in the deficiency of the relative velocity, the collision between the droplets within the same class is not modelled. For each of the colliding droplets, the diameter, velocity and the temperature are appropriately modified to conserve the mass, momentum and energy. The model verification was performed on a 2 – dimensional geometry with two colliding jets.

Droplet collision is considered in each computational cell where the volume fraction of the colliding classes is greater than a defined threshold value. The bigger of two colliding droplets is referred as collector, whilst the smaller one is referred as droplet. The collision frequency  $\nu_i$  between collector and the surrounding droplets is calculated according to equation:

$$\nu_i = N_j^m \frac{(d_i + d_j)^2 \pi}{4} |u_i - u_j|, \quad (65)$$

where  $N_j^m$  is the number density of the droplet class,  $d_i$ ,  $d_j$ ,  $u_i$  and  $u_j$  are the diameters and velocities of the collector and the droplet classes, respectively. The probability  $P_n$  that the collector undergoes  $n$  number of collisions with the surrounding droplets follows a Poisson distribution according to the next equation:

$$P_n = e^{-\bar{n}} \frac{\bar{n}^n}{n!}, \quad P_0 = e^{-\bar{n}}. \quad (66)$$

The number of expected collisions in each computational time step is calculated according to equation:



$$\bar{n} = v\Delta t, \quad (67)$$

where  $\Delta t$  is the computational time step. The collision probability is zero, denoted with  $P_0$  in equation (66), when the mean value of expected collisions  $\bar{n}$  is equal to 0. Additionally, two random numbers  $RN_1$  and  $RN_2$  in the range between 0 and 1 are introduced. Both random numbers are defined at the beginning of each time step of the CFD simulation, and they are held constant for all collision interfaces. This contributes to the numerical stability, and leads to better convergence of the solution. The first random number  $RN_1$  is compared to the zero probability  $P_0$ . When  $RN_1$  is smaller than  $P_0$ , then droplet collision is not considered. In the other case, when  $RN_1 > P_0$ , a new random number  $RN_2$  is introduced. The  $RN_2$  determines the outcome of the collision process, either coalescence or grazing collision. In the Euler Eulerian approach, this number replaces the droplet impact parameter  $b$ , described in [91]. Furthermore, the critical impact parameter,  $b_{cr}$ , is calculated according to next equation, and its value is compared to  $RN_2$ :

$$b_{cr}^2 = \min[1.0, 2.4(f(y)/We_d)]. \quad (68)$$

The function  $f(y)$  is calculated according to [92], whilst the term  $We_d$  stands for the droplet class Weber number. When the critical impact parameter  $b_{cr}$  is greater than impact parameter  $b$ , the outcome of every collision is droplet coalescence.

#### 2.6.4. Droplet evaporation

Beside the aforementioned liquid jet primary atomization, droplet secondary atomization and droplet collision processes, the liquid fuel evaporation process plays a significant role in the IC engine overall efficiency in terms of fuel consumption and pollutant formation. Evaporation occurs when the thermodynamic conditions are not in equilibrium enforced by the high pressure and elevated temperature within the combustion chamber. As mentioned before, in the Eulerian size – of – classes approach the spray droplets are sorted into classes, where the first class is reserved for the gas phase. Other classes are dedicated to the spray droplet classes, and the last class represents the bulk liquid jet. Therefore, it is worth noting that the mass source modelled with the evaporation model gets its contribution from all droplet classes and from the bulk liquid class. The evaporation model used for the CFD

modelling in this thesis considers fuel droplets as isolated spheres, where a cross influence of surrounding droplets is neglected. Furthermore, according to the infinite conductivity model, it is assumed that the liquid droplet temperature is uniform for the whole droplet, and that the pressure change in the gas is negligible. Also, the radiative heat transfer is neglected. The mathematical expressions for modelling the evaporation process are derived by Abramzon and Sirignano [93].

To take into account the effect of convective transport caused by the droplet – gas relative motion, the authors apply the film theory. This theory assumes that heat and mass transfer between droplet surface and gas flow are analogous, and they take place within a certain gas film thickness, as shown by the next equations:

$$\delta_{T0} = \frac{2r_s}{Nu_0 - 2} \quad (69)$$

$$\delta_{M0} = \frac{2r_s}{Sh_0 - 2}, \quad (70)$$

where  $Nu_0$  is the Nusselt number derived for non – evaporating droplets, and  $Sh_0$  is the analogous Sherwood number, as proposed by Clift [94]. For taking into account the influence of Stefan flow, which leads to a thickening of the film, those parameters are corrected by the next expressions:

$$F_T = \frac{\delta_T}{\delta_{T0}} \quad (71)$$

$$F_M = \frac{\delta_M}{\delta_{M0}}. \quad (72)$$

The final droplet vaporization/condensation rate can be calculated according to the next expressions:

$$\dot{m} = 2\pi \overline{\delta_g} \overline{D_g} r_s Sh^* \ln(1 + B_M) \quad (73)$$

$$\dot{m} = 2\pi \frac{\overline{k_g}}{C_{pF}} r_s Nu^* \ln(1 + B_T), \quad (74)$$

where  $\bar{\delta}_g$ ,  $\bar{D}_g$  and  $\bar{k}_g$  are the average density, binary diffusion coefficient and thermal conductivity in the gas film. The term  $\bar{C}_{pF}$  represents the integral specific heat capacity of the vapour phase, whilst terms  $B_M$  and  $B_T$  are Spalding mass and heat transfer numbers calculated according to next equations:

$$B_M = \frac{Y_{Fs} - Y_{F\infty}}{1 - Y_{Fs}} \quad (75)$$

$$B_T = \frac{\bar{C}_{pF}(T_\infty - T_S)}{L(T_S) + Q_L / \dot{m}}, \quad (76)$$

where the term  $T$  stands for temperature, the term  $Y_F$  represents the fuel mass fraction, and subscripts  $S$  and  $\infty$  refer to droplet surface and ambient conditions, respectively. To calculate the average temperature and fuel mass fraction in the film, the 1/3 – rule was employed [95]. The terms  $Sh^*$  and  $Nu^*$  are the modified Nusselt and Sherwood numbers defined as the non - dimensional heat and mass transfer coefficients according to:

$$Sh^* = 2 + \frac{(Sh_0 - 2)}{F_M} \quad (77)$$

$$Nu^* = 2 + \frac{(Nu_0 - 2)}{F_T}. \quad (78)$$

The correction factors  $F_M$  and  $F_T$ , that represent the diffusional film correction, are approximated according to the next equation:

$$F_M = F(B_M); F_T = F(B_T). \quad (79)$$

The universal function  $F(B_x)$  is calculated according to:

$$F(B_x) = (1 + B_x)^{0.7} \frac{\ln(1 + B_x)}{B_x}, \quad (80)$$

where index  $x$  is either subscript  $M$  or  $T$ . The iterative calculation procedure of the evaporation rate and the heat transferred into the droplet classes is described by the following steps:

- 1) Calculation of the fuel vapour mass fraction at the droplet surface.
- 2) Calculation of the average physical film properties according to 1/3 – rules described in [95].
- 3) Calculation of the Nusselt number of non-vaporizing droplets and the corresponding Sherwood number for the initial state according to the next expressions:

$$Nu_0 = 2 + 0.552 Re^{1/2} Pr^{1/3} \quad (81)$$

$$Sh_0 = 2 + 0.552 Re^{1/2} Sc^{1/3}. \quad (82)$$

- 4) Calculation of  $\dot{m}$ ,  $B_M$ ,  $Sh^*$  and  $F_M$  according to equations (73), (75), (77), and (79).

At this point the droplet vaporization rate is calculated by using  $B_M$  and  $Sh^*$ .

- 5) Calculation of  $B_T$  by using values from the old time step; calculation of the correction factor  $F_T$ .
- 6) Calculation of the modified Nusselt number  $Nu^*$  and calculation of the corrected  $B_T$  according to expression:

$$B_T = (1 + B_M)^\Phi - 1, \quad (83)$$

where parameter  $\Phi$  is defined according to:

$$\Phi = \left( \frac{\bar{C}_{PF}}{\bar{C}_{PG}} \right) \left( \frac{Sh^*}{Nu^*} \right) \frac{1}{Le}. \quad (84)$$

- 7) Comparison of the calculated Spalding heat transfer number with the one assumed from the previous time step. If the relative value is over the predefined value, the iteration process continues – return to step 5).
- 8) Calculation of heat transferred into the droplet according to:

$$\dot{Q}_d = \dot{m} \left( \frac{(T_\infty - T_S)}{B_T} - L(T_S) \right). \quad (85)$$

The terms  $\dot{m}$  and  $\dot{Q}_d$  are used to calculate the total evaporation mass and heat transfer rates from all Eulerian classes (droplets), which is done by multiplying the calculated values with the total number of droplets in each control volume [56].

### 2.6.5. Momentum exchange via drag force

The relative motion between liquid droplets and the surrounding gas causes a drag force. This force points into the direction opposite to the relative velocity vector, and it is shown with the next equation:

$$F_D = \frac{\rho_g}{2} c_D A_D u_{rel}^2, \quad (86)$$

where  $\rho_g$  is the ambient gas density,  $c_D$  is the drag coefficient,  $A_D$  is the droplet frontal area, and  $u_{rel}$  is the relative velocity between droplet and gas. The drag coefficient is not constant, it varies with flow speed, direction, object size, density and viscosity. Therefore, it can be said that drag coefficient is in a function of the droplet Reynolds number, defined with the next equation:

$$\text{Re} = \frac{\rho_g \cdot |u_{rel}| \cdot d_D}{\mu_g}, \quad (87)$$

where  $d_D$  is the droplet diameter and  $\mu_g$  is the ambient gas viscosity. At low flow velocities, when inertial forces are negligible compared to the viscous ones, the Stokes' law is being used to calculate the drag coefficient. The total force acting on a spherical droplet is calculated as follows [96]:

$$F_{St} = 3\pi d_D \mu_g u_D. \quad (88)$$

The Stokes' drag force is usually normalized by the dynamic pressure (assumption of incompressible flow) and droplet area projected into direction of the droplet motion vector. Accordingly, the expression for the drag coefficient at low Reynolds number is given as follows:

$$c_D = \frac{24}{\text{Re}}. \quad (89)$$

For higher droplet Reynolds number, the drag coefficient is often modelled according to the next expression [97] and [98]:

$$c_D = \left\{ \begin{array}{l} \frac{24}{\text{Re}} (1 + 0.15 \cdot \text{Re}^{0.687}) \rightarrow \text{for } \text{Re} \leq 1000 \\ 0.44 \rightarrow \text{for } \text{Re} > 1000 \end{array} \right\}. \quad (90)$$

Furthermore, when a droplet enters a gas stream with a sufficiently large Reynolds and Weber numbers, it is being deformed as it interacts with the gas [97]. This effect can be modelled by the next equation:

$$c_D = c_D (1 + 2.632y), \quad (91)$$

where term  $y$  is the droplet distortion parameter. The expression (93) correlates the droplet drag coefficient and droplet distortion, calculated according to the equations of TAB droplet break – up model [99].

Within this thesis the drag coefficient for each Eulerian liquid class  $k$  was modelled according to modified drag coefficient expression:

$$c_{Dk} = \frac{24}{\text{Re}_k} \left( (1 - \alpha_k)^{-2.65} + \frac{\text{Re}_k^{0.66}}{6} (1 - \alpha_k)^{-1.78} \right) + c_{Dk,Def}, \quad (92)$$

where term  $\alpha_k$  denotes class volume fraction. When applied for the Lagrangian formulation, the subscript  $k$  vanishes from the above mentioned equation.

The next expression is used to calculate drag force of each Eulerian droplet class expressed per unit volume:

$$F_{Dk} = \rho_g \frac{u_{rel,kg}^2}{2} c_{Dk} A_{Dk} N_{dk}^{III} = \frac{3}{4} c_{Dk} \frac{\alpha_k}{D_{dk}} \rho_g u_{rel,kg}^2. \quad (93)$$

In general, the assumption that all droplets within one Eulerian class and one computational cell are same in the diameter and have same relative velocity was imposed. Term  $N^{III}$  stands for the number of droplets per unit volume. The same expression is used for the Lagrangian spray formulation but the subscript denoting the droplet classes is then excluded from the equation (95).

### 2.6.6. Combustion

The fuel combustion is a process of heat release due to the chemical reactions of the fuel vapour species and an oxidizer. The combustion process can be described through combustion models with different level of complexity or by employing the detailed/reduced chemical mechanisms. Within the used CFD code several combustion models are implemented, such as:

- 1) Eddy break up model.
- 2) Turbulent flame speed closure model.
- 3) Coherent flame model.
- 4) PDF model.
- 5) Characteristic timescale model.
- 6) Steady combustion model.
- 7) General gas phase reaction model.

In the following section of the thesis, the description of combustion modelling by employing the chemistry mechanisms is shown. In the literature, according to the authors' knowledge there are no published sources on the modelling the reactive spray processes by using the Euler Eulerian size – of – classes approach in combination with chemistry mechanism. Therefore, one goal of this thesis was to enhance the Euler Eulerian spray model with the general gas phase reaction model to solve the reactive multiphase processes.

The use of the general gas phase reaction model together with multiphase flow solver enables modelling of different types of kinetic problems. This feature opens a huge variety of applications involving multiphase reactive flows, e.g. the combustion processes in IC diesel engines. The combustion model is used in combination with the general species transport model, and it is used to calculate reaction rates of gas species. The reaction rates are dependent on the temperature and species concentrations, and they are used as source/sink terms in the species and enthalpy transport equations. The reaction rates are evaluated through the FIRE® internal chemistry interpreter [56].

To calculate chemical reactions within the gas phase, the Arrhenius expression is used. This expression correlates the reaction rate constant  $k_i$  of reaction  $i$  with the local temperature  $T$ , according to the next expression:

$$k_{fi} = A_i T^{b_i} \exp\left(\frac{-E_i}{RT}\right), \quad (94)$$

where term  $A_i T^{b_i}$  is the chemical reaction rate coefficient (composed of pre-exponential factor  $A$  and temperature  $T$ ), which can be physically interpreted as molecular collision number, term  $E_i$  is the activation energy, and  $R$  is the universal gas constant. The term  $\exp(-E_i / (RT))$  is the Boltzmann factor which shows the amount of molecules containing enough energy necessary for triggering chemical reactions. The individual quantities such as  $A_i$ ,  $b_i$ , and  $E_i$  have to be determined experimentally for each reaction. This leads to the conclusion that for modelling the combustion process of different fuels, separate reactions mechanism have to be employed. All above mentioned coefficients, together with the stoichiometry of the reactions, are provided within a chemistry input file. The general set of elementary reactions is expressed with next equation:

$$\sum_{k=1}^K \nu'_{ki} \kappa_k \xrightleftharpoons[k_{b,i}]{k_{f,i}} \sum_{k=1}^K \nu''_{ki} \kappa_k \quad (i = 1, I), \quad (95)$$

where term  $K$  is the total number of gas phase species in the system,  $\nu'$  and  $\nu''$  are the stoichiometric coefficients of reactants and products, respectively. Furthermore,  $k_f$  and  $k_b$  stand for the forward and backward reaction rate coefficients calculated according to the Arrhenius expression. The above mentioned equation is used to calculate the reaction rates of all species from  $I$  number of chemical reactions.

The rate of production of species  $k$  (the reaction rate) is calculated according to the next expression:

$$\omega_k = \sum_{i=1}^I \nu_{ki} q_i, \quad (96)$$

where term  $q_i$  is the reaction rate of reaction  $i$ , or commonly called the production rate of reaction  $i$ .

The production rate is defined as the difference of the forward and backwards reaction rates, according to the next expression:



$$q_i = k_{fi} \prod_{k=1}^K [X_k]^{v'_{ki}} - k_{bi} \prod_{k=1}^K [X_k]^{v''_{ki}}, \quad (97)$$

where term  $X_k$  is the molar concentration of species  $k$ .

In the FIRE<sup>®</sup> multiphase code the 0D reactor model is used to calculate source terms for species and enthalpy transport equations. The source terms for the species transport equations are calculated as:

$$S_k = \frac{\rho^{n+1} w_k^{n+1} - \rho^n w_k^n}{\Delta t} V_{cell}, \quad (98)$$

where the superscript  $n$  denotes the previous time step and  $n+1$  the new time step resulting from the single zone reactor model. The above equation is shown for species  $k$  and cell volume  $V_{cell}$ . The source term of the enthalpy transport equation, based on the species source terms, is calculated as:

$$S_H = \sum_{k=1}^K S_k H_{fk} \Big|_{T_{ref}} \frac{1}{W_k}, \quad (99)$$

which represents the sum of enthalpy sources arising from all gas species.

In the section “result and discussion”, the modelling results of different liquid fuel atomization, evaporation and combustion processes are shown. Initially, the developed method was validated on a constant volume vessel where the atomization and combustion process of n – dodecane and n – heptane fuel was simulated. Afterwards, the combustion of the diesel biofuel blend, named EN 590 B7, was modelled on a real engineering application. The EN 590 B7 is a diesel biodiesel fuel blend containing 7 % of biofuel, which is actually the maximum allowable biofuel addition for road transportation powering systems. Chemical reactions, their rates, and thermodynamic and transport properties have been introduced through the chemical reaction mechanisms.

Table 4 shows the number of chemical species, number of reactions, literature source, and the observed spray characteristics for the chemistry mechanisms used within the scope of this thesis.

**Table 4 Chemistry mechanisms used within this thesis**

	<b>Number of species</b>	<b>Number of reactions</b>	<b>Reference</b>	<b>Observed spray characteristics</b>
<b>n-dodecane</b>	106	420	[100]	<ul style="list-style-type: none"> <li>▪ Vapour penetration length observing OH radicals local concentrations; liquid penetration</li> <li>▪ OH mass fraction distribution at several time instances</li> <li>▪ Rate of heat release</li> <li>▪ Pressure rise</li> </ul>
<b>n-heptane</b>	68	283	[101]	<ul style="list-style-type: none"> <li>▪ Lift off length for different oxygen concentration in ambient gas mixture</li> <li>▪ Ignition delay</li> </ul>
<b>EN 590 B7</b>	45	193	<i>AVL confidential</i>	<ul style="list-style-type: none"> <li>▪ Pressure in the cylinder</li> <li>▪ Mean temperature in the cylinder</li> <li>▪ Total rate of heat release</li> </ul>

### 3. RESULTS AND DISCUSSION

In the next sections the results of 3D CFD numerical modelling are shown. In the first section the modelling results of spray, combustion and emission processes occurring in the IC engine by employing the Euler Lagrangian spray approach are shown. The second section shows the results obtained by modelling the non – reactive spray processes where the Euler Eulerian size – of – classes approach was utilized. This section was performed to understand the influence of spray sub model coefficients on the mass, momentum and enthalpy exchange occurring during the fuel atomization process. In the third section the nozzle flow – spray interface is described, whilst in the fourth section the validation of the primary atomization model is performed. In the fifth section the modelling results of non – reactive fuel spray process by using the modified WAVE model are shown. In the sixth section the results of two colliding droplet jets by taking into account droplet collision model are presented. In the seventh section the verification and validation results of the developed method are shown. Finally, in the last section, the developed method is used to model the real engineering application, and the modelling results are shown and discussed.

#### 3.1. Eulerian Lagrangian engine modelling

In this section the results of numerical modelling of an experimental IC engine are discussed. The physical models for the liquid fuel disintegration, evaporation and pollutant formation, existing within the commercial CFD code FIRE<sup>®</sup>, were utilized for the IC engine simulations. These models are capable to predict the complex in – cylinder processes and, ultimately, the formation of pollutant emissions. The aim of this section was to investigate the important thermos – chemical parameters, and the chemical kinetic mechanisms that describe the NO<sub>x</sub> formation process, and to gain insights into advantages and disadvantages of the Euler Lagrangian DDM models. The results from numerical simulations, such as in – cylinder pressure and temperature traces, and NO<sub>x</sub> and soot concentrations, are found to be in good agreement with the existing experimental data.

In the used Euler Lagrangian DDM approach the gas phase is described by the Eulerian formulation, whilst the discrete phase is described with the Lagrangian equations. The phase coupling is performed by introducing the adequate source terms for mass, momentum and energy exchange. Several physical models were used for calculation of dispersed spray flow, combustion and pollutant formation. For modelling the droplet break – up process, the common WAVE model was applied, whilst for modelling the NO<sub>x</sub> formation two different reaction mechanisms

were used: the thermal and the prompt NO<sub>x</sub> mechanism. The chemistry – turbulent interaction was modelled by integration of kinetic rates with respect to the fluctuating temperature using a presumed PDF approach [32].

There are several existing mathematical models for calculating the disintegration process, one of them is the WAVE model discussed in section 2.6.2. In the observed engineering application, WAVE model represents the appropriate modelling approach since the high pressure liquid fuel atomization is characterized with the KH instabilities. The evaporation process was modelled according to the Abramzon – Sirignano evaporation model, and the ECFM – 3Z combustion model [56] was used to describe the combustion process. Such combustion model considers the influence the IC engine combustion chamber inner surfaces on the flame propagation and on the flame temperature. The influence of the spray wall interaction was described by the wall – impingement sub model based on [42], which neglects the wall film formation, and in which the droplet diameter after the wall rebound is considered as a function of the Weber number.

The NO formation model was previously integrated into the commercial CFD code via user functions, as described in [60]. The NO<sub>x</sub> emissions are calculated by using additional transport equation for an active scalar, and their formation is modelled according to the chemistry mechanism derived by [33]. In such approach, the species reactions rates are calculated through the Arrhenius law. The effects of the turbulent fluctuations on nitrogen pollutant reaction scheme were taken into account by integrating the instantaneous pollutant reaction rates over the presumed beta PDF functions. At high temperatures and at fuel rich conditions, hydrocarbon fuels show the tendency to form carbonaceous particles, otherwise known as soot. In the early stage of the engine working cycle the soot is formed, and later it is being oxidised in the regions with higher oxygen concentrations. To determine the soot formation, an additional partial transport equation for the soot mass fraction must be solved. In this section, the Kinetic model with a reduced number of species and reactions was used for modelling the soot formation. The basis of such model is a chemical reaction mechanism for soot formation and oxidation including 1850 homogeneous reactions, 186 species and 100 heterogeneous reactions [56].

### *3.1.1. Experimental data and numerical setup*

The experimental research was performed in the frame of the bowl optimization project, and it was carried out by AVL GmbH researchers. A single cylinder engine with Electro-Hydraulic Valve Actuation and a  $\omega$ -shaped piston (EHVA) was researched by using the AVL's

single cylinder engine test bed. The pressure measurements were carried out by using the application-oriented automation system (PUMA Open), whilst pollutant emissions have been measured by using AVL's emission measurement system. The main engine and injection system characteristics are presented in Table 5.

**Table 5 Characteristics of the experimental engine and the BOSCH Piezo common rail injection system**

<b>Bore (mm)</b>	85	<b>Spray Angle (°)</b>	158
<b>Stroke (mm)</b>	94	<b>Displacement (mm<sup>3</sup>)</b>	533.4
<b>Compression ratio (-)</b>	16:1	<b>Nozzle (-)</b>	8-hole

For the research purposes, several combustion system parameters were varied, as presented in Table 6.

**Table 6 Combustion system parameters**

<b>Engine speed (min<sup>-1</sup>)</b>	3000	<b>Swirl (%)</b>	0 – 74
<b>SOI (°)</b>	1 – 10 before TDC	<b>Inj. pressure (bar)</b>	1200 – 1600
<b>EGR (%)</b>	12 – 20		

The NO<sub>x</sub> and soot mass fractions, expressed in kilograms of species per kilogram of engine exhaust gas, have been measured in the exhaust pipe and they are presented in Table 7. The experimental data were provided by AVL GmbH within the long term collaboration project with the Faculty of Mechanical Engineering and Naval Architecture, University of Zagreb, Croatia.

**Table 7 Pollutant emission concentrations measured in the exhaust pipe**

<b>Case</b>	<b>Soot (kg/kg)</b>	<b>NO (kg/kg)</b>	<b>Case</b>	<b>Soot (kg/kg)</b>	<b>NO (kg/kg)</b>
<b>a</b>	2.1x10 <sup>-5</sup>	5.6x10 <sup>-4</sup>	<b>d</b>	2.1x10 <sup>-5</sup>	9x10 <sup>-4</sup>
<b>b</b>	6.6x10 <sup>-5</sup>	3.6x10 <sup>-4</sup>	<b>e</b>	6.6x10 <sup>-5</sup>	6.7x10 <sup>-4</sup>
<b>c</b>	2.1x10 <sup>-5</sup>	5.5x10 <sup>-4</sup>	<b>f</b>	1.9x10 <sup>-5</sup>	5.6x10 <sup>-4</sup>

To research the capabilities of the DDM spray modelling approach, several high pressure diesel spray injection cases were modelled. In order to reduce computational costs, and due to the assumed non – cavitating symmetrical nozzle flow, the geometric model was reduced to the 1/8 sector of the whole cylinder bowl. The computational mesh contained

approximately 24000 control volumes at TDC, and approximately 80000 control volumes at BDC. During the piston movement, the mesh was rezoned several times. This is done in order to keep the deformation and aspect ratios of the computational cells low. The rezone procedure is a mesh replacement at the certain crank positions, where the new mesh has the same extension but with different number of cell volumes used to avoid undesirable cell distortions. To capture the wall influence on the simulation results, a 2 – cell boundary layer was created in the vicinity of wall selections.

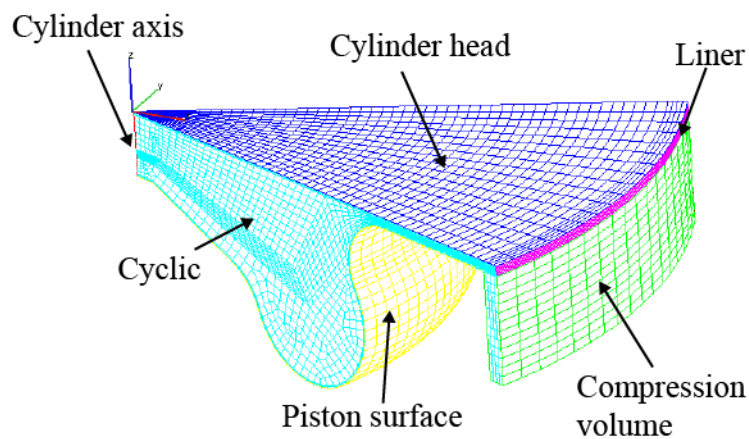


**Figure 11 Computational mesh for engine calculation**

On the engines' head and piston surfaces the impermeable wall boundary conditions were defined. The cylinder geometry was assumed to be symmetric around the cylinder axis, and a periodic boundary conditions was applied to the side surfaces of the sector model defined with the Cyclic boundary selection. The computational domain and the boundary surfaces are shown in Figure 11, whilst the defined boundary conditions are shown in Table 8.

**Table 8 Computational mesh boundary conditions**

<b>Selection</b>	<b>Boundary Type</b>	<b>Specific condition</b>
Piston surface	Mesh movement	Temperature 550 K
Cyclic	Periodic inlet/outlet	Periodic
Cylinder Head	Wall	Temperature 500 K
Comp. Volume	Wall	Thermal/ Adiabatic boundary
Cyl. Axis	Symmetry	-
Liner	Wall	Temperature 500 K

The Central Differencing Scheme (CDS) was used for the continuity equation, whilst the upwind differencing scheme was used for turbulence, energy and scalar transport equations. For the momentum equations, the blend between the CDS and upwind scheme, with blending factor of 0.5 was used [56]. The turbulence was modelled by using the advanced  $k-\zeta-f$  model discussed in section 2.2.3. Such model is sufficiently robust to be used for computations involving grids with moving boundaries and highly compressed flows, as it is the case in internal combustion engines. It guarantees a good solution for various computational meshes. The main parameters of the engine operating points are shown in Table 9.

<b>Case</b>	<b>SOI – EOI (°)</b>	<b>Swirl (min<sup>-1</sup>)</b>	<b>Injected mass (kg)</b>	<b>EGR mass fraction (%)</b>
a	713.5 – 734.8	5409	3.38x10 <sup>-06</sup>	0.19872
b	712.3 – 735.4	5832	3.37x10 <sup>-06</sup>	0.23839
c	714.4 – 736.9	4048	3.41x10 <sup>-06</sup>	0.16463
d	709.3 – 732.4	7062	3.41x10 <sup>-06</sup>	0.16140
e	714.6 – 734.4	4030	3.37x10 <sup>-06</sup>	0.16376
f	714.4 – 736.9	4072	3-38x10 <sup>-06</sup>	0.16160

### 3.1.2. Results and discussion

The following section discusses the calculation results where 3D plots of temperature flow field, the NO and the soot distribution are shown for three different crank angle positions (720, 724 and 730 °CA). In addition, the pressure and temperature curves are shown for the engine cycle from 640 °CA to 800 °CA. The results are shown for the referent case *a* defined in Table 9.

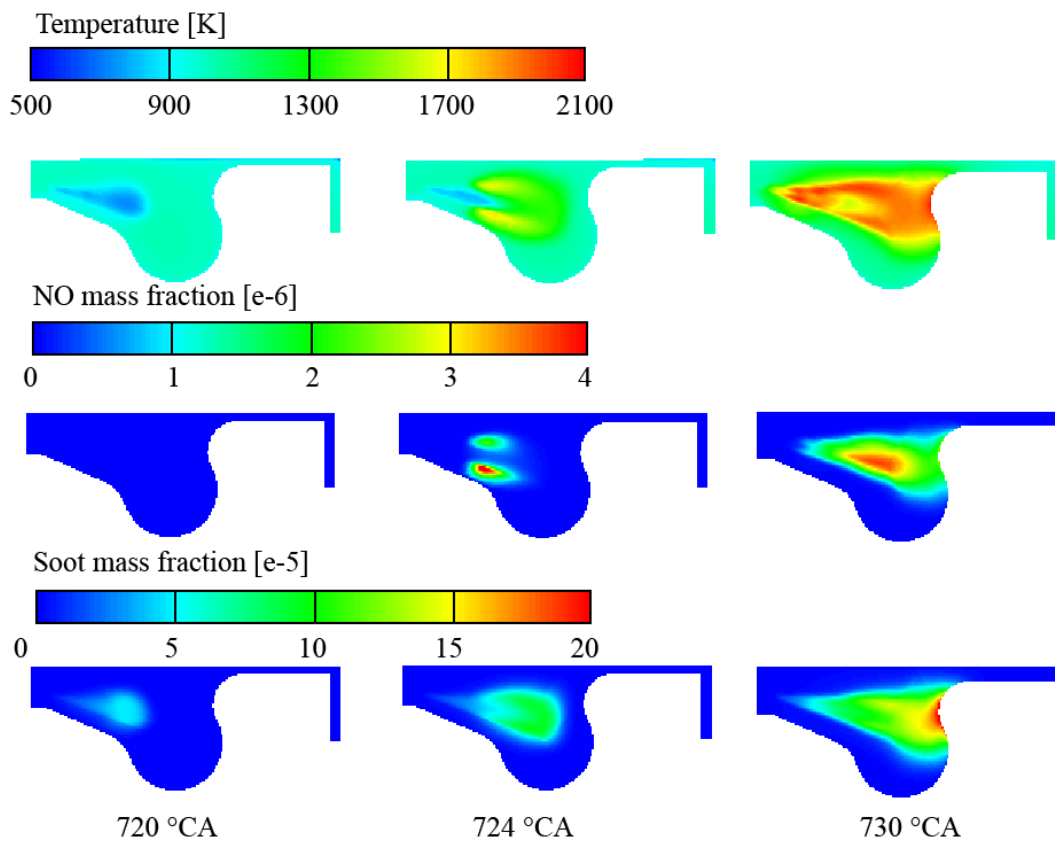


**Figure 12** Calculated temperature, NO mass fraction, and soot mass fraction field

The first column in Figure 12 shows the calculated temperature distribution and the pollutant emissions before the ignition has started. The second column shows results after fuel ignition, whilst the third column shows the results at an advanced stage of the combustion process. For the referent case, the liquid fuel is injected into the engine combustion chamber at 713.5 °CA. Initially, the liquid fuel undergoes the disintegration process, and the spray penetrates into the pressurized gas mixture enclosed within the cylinder boundaries. The created droplets are subject to evaporation, and thus, a conically shaped vapour cloud is formed. The vapour cloud is visible in the first column and first row of Figure 12. At approximately 724 °CA, the evaporated fuel ignites due to the elevated temperature conditions, and the combustion process starts at the periphery of the spray vapour cloud. Afterwards, the flame consumes the evaporated fuel, and the combustion process diffuses towards the injection point. As final outcome, the liquid fuel is completely evaporated and combusted. In the early stage of injection, the evaporated and the liquid fuel possess the same penetrating velocity. After the liquid fuel has reached its maximum penetration length, the fuel vapour still possesses a certain momentum and penetrates further into the combustion chamber. Additionally, due to turbulent



dissipation and gas entrainment effects, the fuel vapour diffuses away from the spray axis into the radial direction.

The NO formation process is shown in the second row of Figure 12. The NO pollutant species are formed under high temperature conditions within the flame region. The NO formation is more pronounced at higher temperatures and at higher flame propagation rates.

The soot formation is shown in the third row of Figure 12 where the influence of high temperature regions is visible. In later stages, the soot accumulates near the piston wall due to the wall cooling effect which is responsible for decreasing the soot oxidation intensity.

In the experimental research, the pollutant concentrations have been recorded at the time of the exhaust valve opening, whilst the pressure traces have been recorded during the whole compression and power strokes. All quantities measured in the experimental research are modelled by using the CFD tool, and were thoroughly analysed. Figure 13 shows the experimental temperature and pressure curves compared with the modelled results. The results are shown for cases *a*, *d* and *e*, but the given conclusions are also valid for the other operating points. The pressure and temperature curves from the CFD simulations are represented by black lines, whilst the experimental results are represented by red dashed lines. The mixture of air and exhaust gas residue are compressed in the engine compression stroke, the working volume is reduced and temperature and pressure are increased. In the researched cases, after fuel injection and disintegration, the fuel rapidly evaporates due to the increased temperature conditions. When the in – cylinder temperatures reaches the fuel ignition temperature level, the evaporated fuel ignites causing a rapid pressure and temperature increase. This behaviour is noticeable around 720 °CA. With further crankshaft motion, a mean temperature of approximately 1600 K is reached, locally over 2200 K. With the expansion stroke and further augmentation of cylinder working volume, the in – cylinder pressure and temperature decreases. This decrease is noticeable in Figure 13 at the crank angle positions just after reaching the in – cylinder temperature peaks. During the exhaust stroke, when the exhaust valves are opened, the pollutants flow out into the exhaust system pipes. The modelled and measured results show a good agreement throughout the whole engine working cycle. The overall agreement indicates that the initial and the boundary conditions were chosen appropriately. A slight discrepancies in the pressure and temperature results could be attributed to the limitations of the Euler Lagrangian DDM approach for modelling the dense spray region where a lower liquid fuel evaporation rate is noticeable. However, the overall results can be

further improved by adjusting spray model coefficients within the Lagrangian spray module, such as primary and secondary break – up, evaporation, etc.

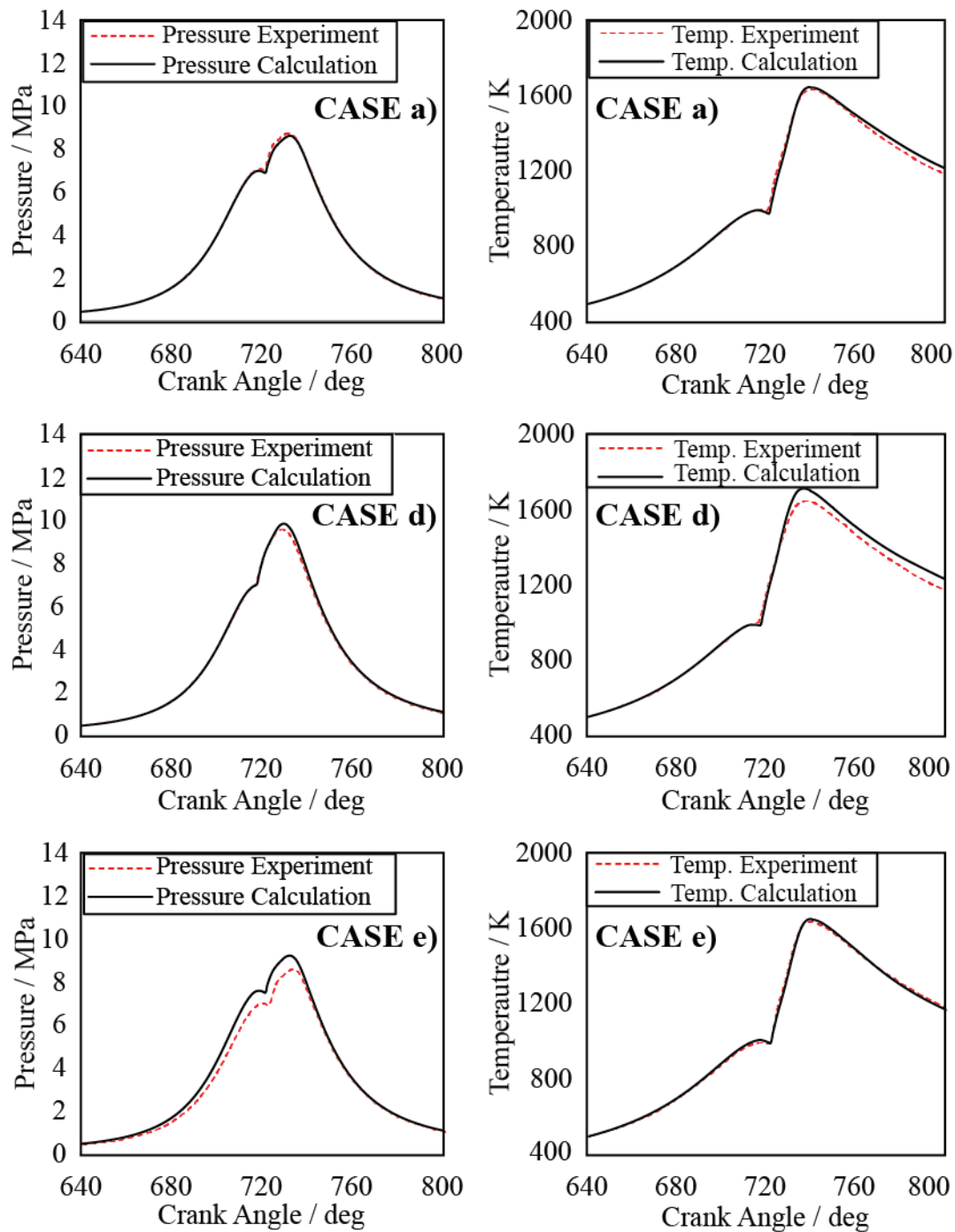


**Figure 13 Comparison of calculated and experimental in – cylinder mean pressure and mean temperature profiles**

Figure 14 shows the NO and soot emissions concentrations at the time of exhaust valve opening, expressed relative to the referent case *a*. A good agreement in the predicted emission trends is visible by comparing to the experimental data. Observing the results, it can be concluded that the pollutant formation processes occurring during the engine operation are well described by the used models. However, a peak in the relative soot emissions noticeable for operating point *b*, which is not captured by the CFD computer simulations. For this case, the mismatch in pollutant concentrations between the experiment and calculation is noticeable but the emission trend, pressure and temperature curves are well described.

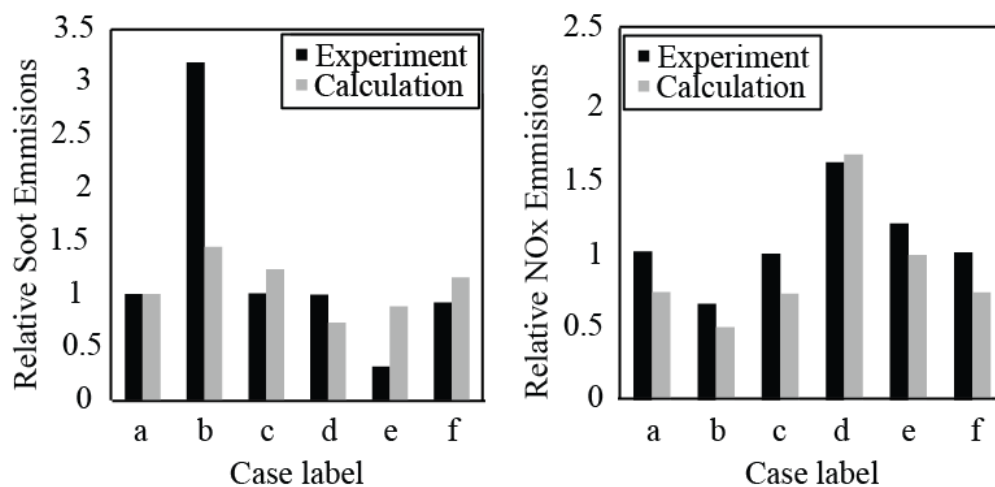


**Figure 14** Comparison of calculated and measured soot and NO<sub>x</sub> emissions relative to the case *a*

### 3.2. Euler Eulerian spray model parametric studies

After analysing the modelling results obtained by the Euler Lagrangian DDM approach presented in the previous section, the Euler Eulerian size – of – classes approach was used to model non – reactive spray processes. The main idea was to validate and parameterize the existing models and to take advantages of the Euler Eulerian spray modelling approach. Therefore, this section deals with a high pressure diesel fuel injection into the pressurized combustion chamber. Several fuel injection cases were modelled by employing the Euler Eulerian size – of – classes approach. Precisely, six diesel – like injection cases were computationally modelled, in which liquid fuel was injected into a pressurised non – reactive environment (100 % N<sub>2</sub>) through a 205 μm nozzle hole. The analysis was focused on the liquid jet and vapour penetrations, describing the spatial and temporal evolution of the sprays. For this purpose, an existing Eulerian multiphase model was employed, variations of the sub – model coefficients were performed, and their impact on the spray formation was investigated. The

final set of sub – model coefficients was applied to all operating points. The liquid fuel was injected with 50, 80, and 120 MPa, combined with different chamber pressures of 5.4 and 7.2 MPa. The modelled results were compared to the available experimental data. The produced results share a similar spray cloud shape for all operation conditions but with different vapour and liquid penetration lengths. The liquid penetration is shortened with the increase of the chamber pressure, whilst the vapour penetration is more pronounced by elevating the injection pressure. Finally, the CFD results show a good agreement with the measurements, and they yield the correct trends for both the liquid and vapour penetrations under different operating conditions.

### 3.2.1. Experimental data and numerical setup

The experimental investigations were performed at Daimler – Chrysler Research Centre within the framework of the European funded I – LEVEL project. The liquid diesel fuel was injected into a high pressure chamber through a single hole nozzle with an orifice diameter of 205  $\mu\text{m}$  into 100 %  $\text{N}_2$  environment. The flow within the nozzle was controlled by the fast opening and closing of the needle valve, and it was shaped by the nozzle itself. Figure 15 shows the experimental data of the selected fuel injection cases.

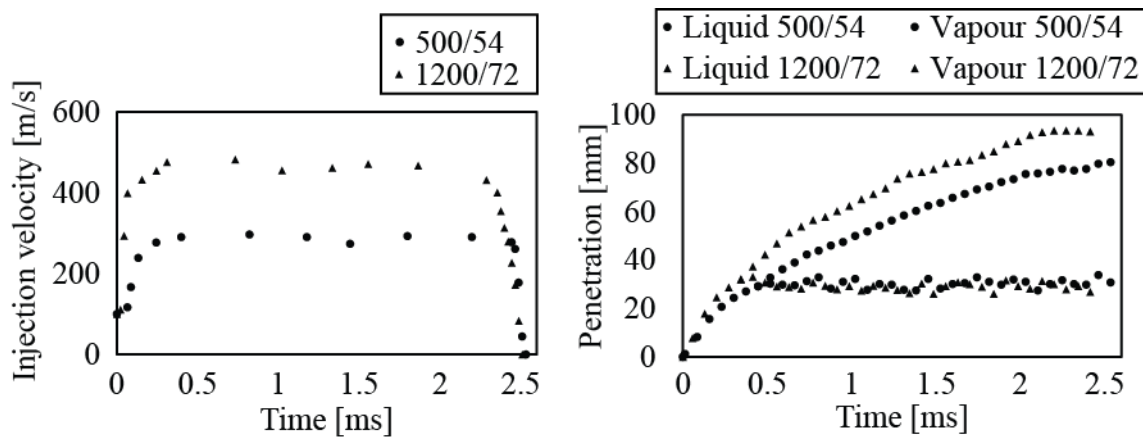


**Figure 15** Experimental data of injection velocity and fuel tip penetration

On the one hand Figure 15 shows that higher injection pressures result in more intensive penetrations of the vapour phase, whilst the liquid fuel penetrations stay at similar levels. On the other hand, the fuel jet velocity is dependent on the injection pressure, which is visible on the left – hand side of Figure 15. The maximum fuel injection velocities are in the range from 300 to 500 m/s, depending on the injection pressure. The inlet velocities were imposed according to the experimental data of the measured injection rates, which were normalised in

order to eliminate the measured velocity fluctuations. The liquid fuel was defined with a temperature of 373 K, density of 755 kg/m<sup>3</sup>, specific heat capacity of 2394 J/kg/K, and a molecular viscosity of 5.123x10<sup>-4</sup> kg/m/s.

The numerical simulations of fuel injection were performed by using the Euler Eulerian size – of – classes approach where six different operating points were investigated, and the specific conditions for each operating point are shown in Table 10.

**Table 10 Operating conditions for model parameterization**

Case	a	b	c	d	e	f
Injection pressure [MPa]	50	50	80	80	120	120
Chamber pressure [MPa]	5.4	7.2	5.4	7.2	5.4	7.2

In order to achieve mesh independency, three different computational meshes were generated and examined. They were generated with 1400, 2880 and 5860 control volumes. As a result of mesh dependency study and by observing the flow field and droplet size distribution, the mesh with 1400 control volumes was selected for further research, as shown in Figure 16. The computational mesh was generated as a two – dimensional static grid, extending from 0 to 120 mm in the axial direction, and from 0 to 25 mm in the radial direction. Such a mesh was used to reduce the CPU time necessary to perform a high number of CFD simulations for model parameterization. Using two – dimensional computational meshes is reasonable for symmetric injectors creating symmetric sprays. The defined boundary selections are shown in Figure 16 where the symmetry boundary condition (1) was applied in the tangential direction, and the mesh was refined towards the spray inlet (3) and the spray axis (4) selections. At the outlet of the domain, a static pressure boundary condition was applied (2). The injector surface was defined as impermeable wall boundary condition with constant temperature of 900 K.

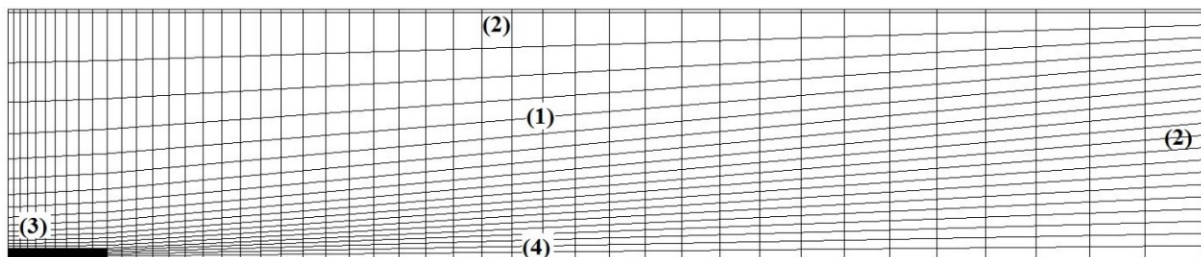


**Figure 16 Computational mesh for Euler Eulerian spray model parameterization**

Nine Eulerian classes were defined and applied for all spray simulations – one for the gas phase, seven droplet classes and one class for the bulk liquid emerging from the nozzle hole. The corresponding diameters were defined with 5, 10, 20, 40, 70, 95, 140  $\mu\text{m}$  (droplet classes), and a diameter of 205  $\mu\text{m}$  was assigned to the bulk liquid class. For turbulence, volume fraction and energy transport equations a first order UPWIND differencing scheme was applied, whilst for the continuity equation the CDS was employed. A combination of CDS and UPWIND scheme was proposed for the momentum equations by introducing the blending factor of 0.5 [56]. For all simulations the first order Euler implicit time integration was employed ensuring solution stability, whilst the accuracy was achieved by employing sufficiently small simulation time steps. The influence of the false diffusion on the penetration results was minimized by performing a mesh dependency analysis as discussed above. The advanced  $k-\zeta-f$  turbulence model was used for turbulence modelling. The solution convergence criterion was achieved when the momentum, pressure, energy and volume fraction residuals decrease under the value of  $1 \times 10^{-4}$ . The pressure – velocity coupling of the momentum and continuity equations was obtained by using the SIMPLE algorithm. The time discretisation varied with simulation time. Small time steps were used due to the fact that gradients in the mass exchange models can be very high. Therefore, at the beginning of injection process the time steps were small ( $3 \times 10^{-8}$  s), and they were continuously increased throughout the injection time (up to  $5 \times 10^{-7}$  s).

### 3.2.2. Results and discussion

Operating point  $d$  with the injection conditions described in Table 10 was used as referent case for model parameterization. As discussed in section 2.6.1, the primary break – up model coefficient  $B_{p1}$  influences the turbulent time scale,  $B_{p2}$  dictates the turbulent length scale, whilst the coefficient  $B_{p3}$  defines the influence of the aerodynamic length scale on the spray penetration. In this section of the thesis the overall atomization time scale is defined as the harmonic combination of the turbulent and aerodynamic time scale which ensures that the faster mechanism dominates. Higher values of coefficient  $B_{p1}$  result in weaker liquid jet disintegration causing intensive higher spray tip penetration, as shown in Figure 17. This can be addressed to the prevalence of bigger droplets possessing higher momentum and reduced influence of the drag force on the droplet penetration. The same conclusion may be drawn for the influence of the  $B_{p3}$  coefficient, and therefore, the parameterization results for this

coefficient are not shown. The change in the coefficient  $B_{P2}$ , which influences the mass exchange rate, has the opposite effect on the spray temporal distribution, compared to  $B_{P1}$  and  $B_{P3}$ . The increase in the mass exchange rate results in a decrease of the liquid jet penetration due to the higher diameter change rate and the creation of smaller droplets which are more influenced by the drag force.

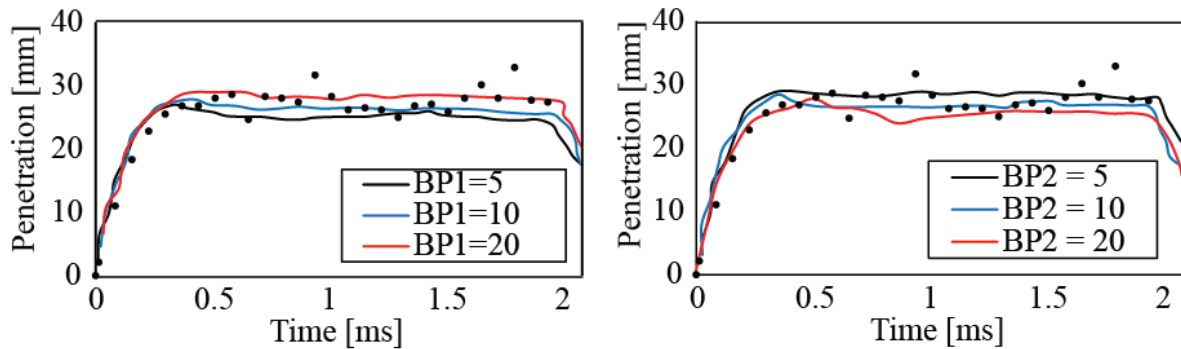
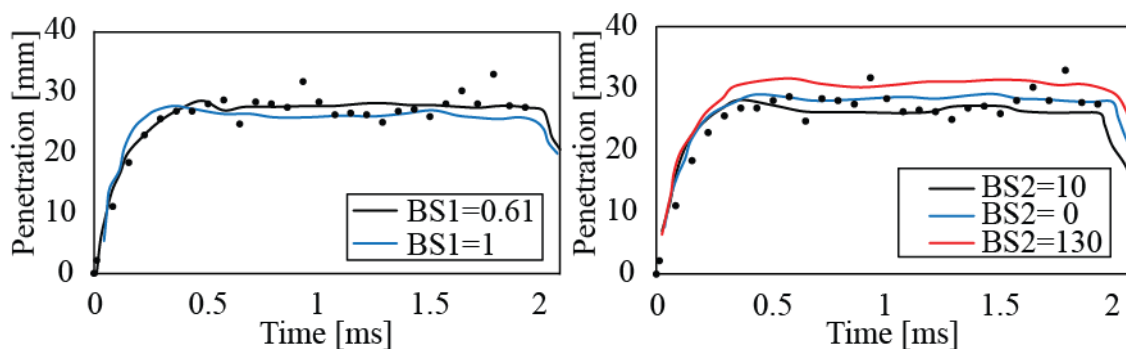


Figure 17 Parameterization of the primary atomization model for operating point d

The model used for describing the secondary atomization process takes into account the occurrences of surface instabilities caused by both the aerodynamic and turbulent forces. The diameter of the created droplet is correlated to the wavelength of the fastest growing surface wave. Correlation between the diameter and the wavelength is defined by the atomization coefficient  $B_{S1}$ , as discussed in section 2.6.2. Higher values of this coefficient result in the creation of bigger droplets. The recommended values for  $B_{S1}$  are in the boundaries of 0.61 and 1. To take into account the influence of the nozzle flow on the secondary atomization process, the coefficient  $B_{S2}$  is introduced. With increasing the value of this coefficient the atomization time is prolonged and liquid spray tip penetration is enlarged. The influence of the secondary atomization model coefficients is shown in Figure 18.



**Figure 18 Parameterization of the secondary atomization model for operating point d**

Figure 19 shows the comparison of the simulated and measured liquid and vapour spray tip penetrations for all investigated cases. The black solid line represents the calculated results, where primary atomization, secondary atomization, and evaporation models were considered, whilst the results of the experimental research are represented with black dots. At the initial stage, the liquid fuel penetrates rapidly. The normal velocity condition was applied for the inlet boundary. For a detailed investigation of the spray characteristics and the combustion process, a more detailed inlet boundary description by resolving the nozzle flow field should be used. Such a condition, which is discussed in section 3.3, will resolve the flow effects caused by the needle movement and the nozzle hole geometrical imperfections. Therefore, a more accurate and reliable approach would measure the needle lift movement by including the axial and radial displacement as first step, and calculate fuel flow through the nozzle channel as second step. In this way, a more realistic conditions at the nozzle hole exit, which takes into account the turbulent fluid flow and the cavitation process, would be considered.

The liquid fuel evaporates due to the elevated temperature conditions, and a certain amount of mass and momentum is transferred to the gas phase, leading the similar penetration velocities for both phases. At this point it is important to mention that the detection of the spray contour in the Euler Eulerian spray simulation was more difficult than for the Lagrangian spray model. Here, the spray contours were determined by scanning the flow fields for the threshold values of liquid volume and vapour mass fractions, respectively. In this section of the thesis, the liquid spray tip penetration was defined as the furthest distance of the liquid phase where the total liquid volume fraction accounts for 0.1 % of the observed control volume. With regard to the vapour penetration, a threshold value of 1 % was defined. At a certain time after start of injection, approximately at 0.4 ms, the liquid droplets located at the jet tip are completely evaporated, and the liquid volume fraction drops below the defined threshold value. Complete evaporation for the defined injection parameters was achieved at approximately 30 mm from the nozzle hole in the spray axis direction. The given results imply that the vapour penetration is reduced with increase in the ambient density due to the higher momentum dissipation. Furthermore, the vapour cloud penetrated further into the domain owing to increased injection pressure and higher liquid jet velocity.



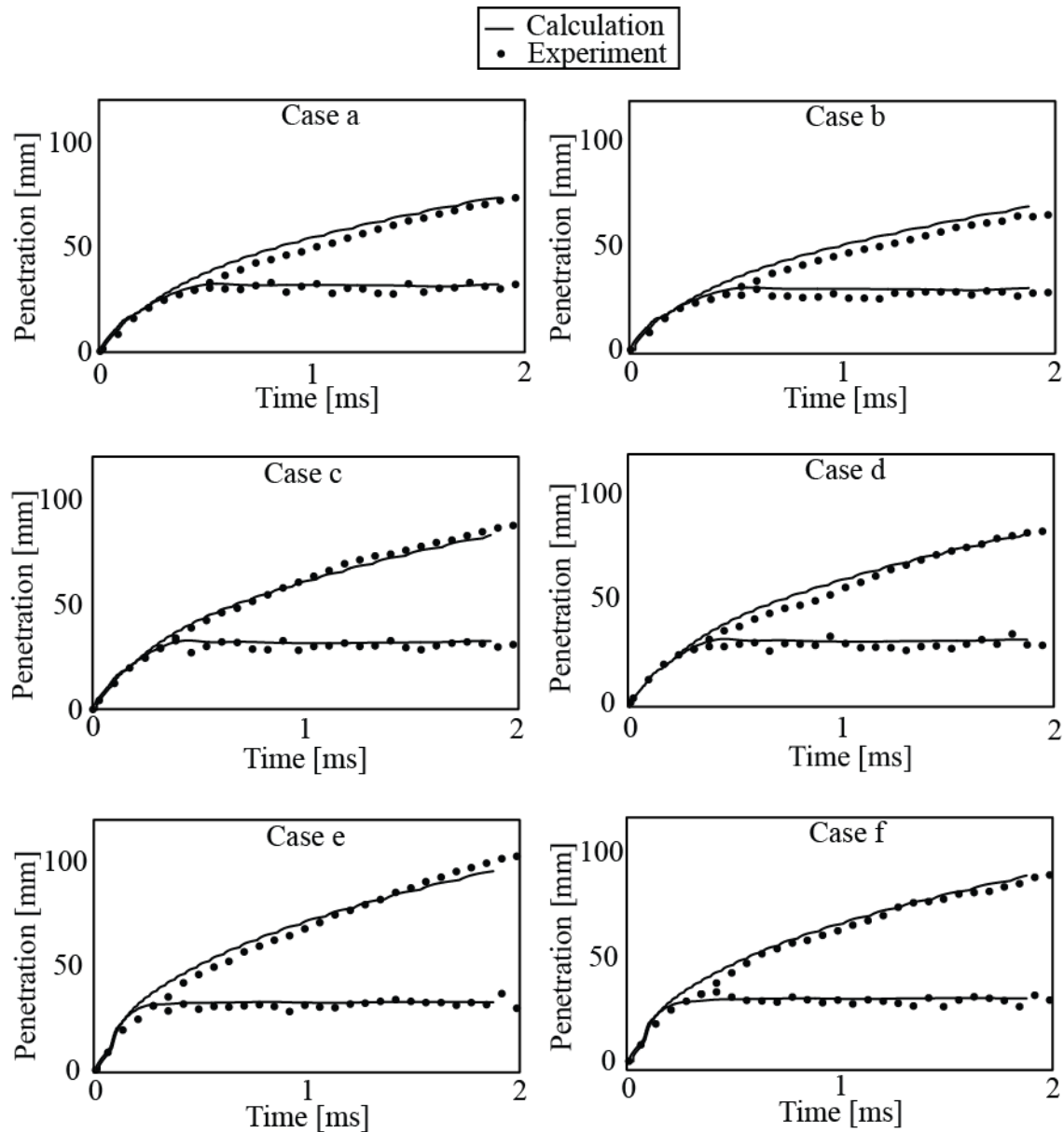


**Figure 19 Comparison of calculated and experimental liquid and vapour spray tip penetration**

Figure 20 shows the results of calculated fuel injection process at 50 MPa rail pressure and 5.4 MPa chamber pressure. It is visible that the predicted penetration is in a good agreement with the measurements, indicating that the number of droplet classes and the sub – models accounting for the appropriate spray physics were defined correctly. On the upper side of Figure 20, the calculated liquid and vapour spray tip penetrations are compared to the experimental data. It can be seen that the developed spray penetrates approximately 30 mm along the spray axis. The total liquid volume fraction (left), and the vapour mass fraction (right) are shown at the bottom of Figure 20. At a time of 0.25 ms after start of injection, the spray was still in the transitional period. The evaporated fuel followed the liquid core penetration and the penetration

curves overlapped. After reaching the developed spray state, where all liquid fuel is evaporated, the liquid penetration diminishes and oscillate around the developed penetration length. At the times of 1 ms and 2 ms after start of injection, the fuel vapour penetrates further due to the momentum transferred from the liquid fuel. In addition, the vapour mass is shifted from the spray axis in the radial direction, which is a result of turbulent dispersion forces and gas entrainment. In Figure 20, the colour bar is set to the maximum values of 1 % for the total liquid volume fraction and to 0.1 % for the vapour mass fraction, respectively. Therefore, the black area represents the control volumes at which the volume and mass fractions of the observed phases exceed the threshold values corresponding to the previously defined penetration lengths.

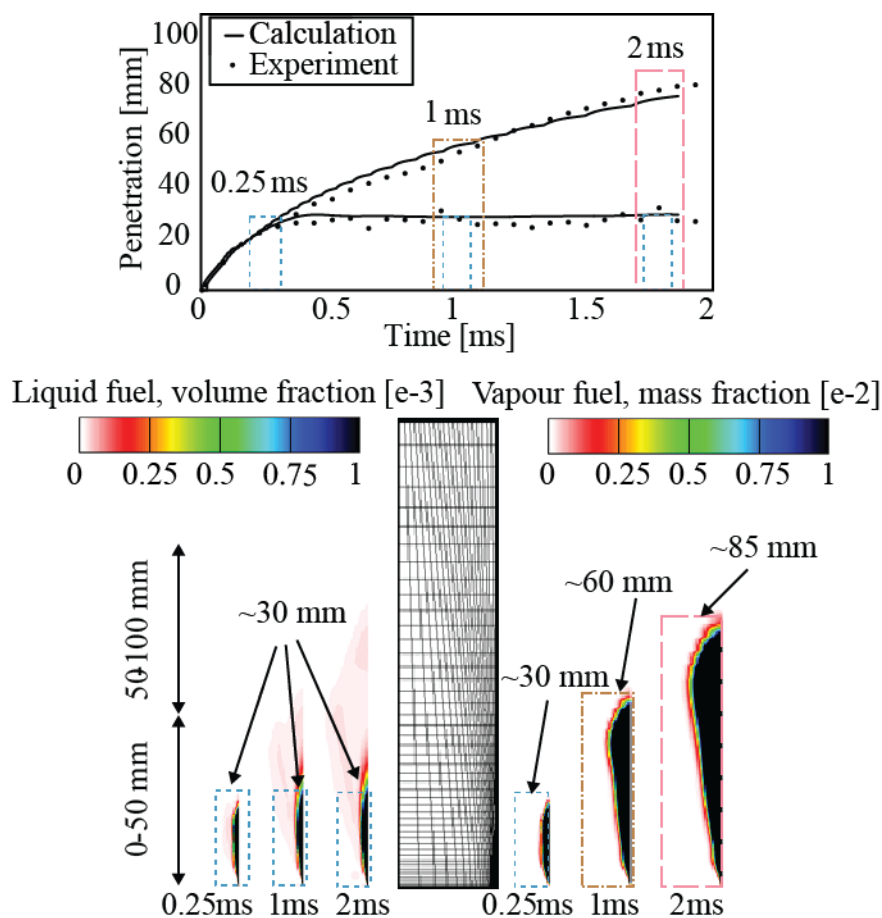


**Figure 20** Comparison of calculated and measured liquid and vapour penetration (top), and distribution (bottom) for case d

### 3.3. Nozzle – flow spray coupling

After validation of the Euler Eulerian spray code implemented within the used CFD tool, a more detailed investigation was performed regarding the modelling of fuel injection process. As it was mentioned in the introduction and in the section 3.2, the fuel injection can be modelled with a high level of details considering the in – nozzle flow (through the nozzle file interface), or it can be simplified to a velocity boundary condition. In this section of the thesis the verification results of the enhanced interface are shown. The nozzle file interface is used to couple nozzle – flow and spray CFD simulations by using the generated nozzle file as inlet boundary condition in spray simulations. Consequently, such an interface improves the predictions of spray simulations, since it takes into account the cavitation process and inhomogeneous turbulence and velocity fields at the nozzle orifice.

#### Nozzle file interface enhancement and verification

The nozzle file interface, implemented within the used CFD tool, was further enhanced with MPI option and flexible nozzle file ability. These enhancements ensured that the inlet selection of spray simulation can be divided on different processors making it more efficient in terms of overall CPU time. Furthermore, the code was modified to remove the mesh dependency disadvantage and now, the nozzle file feature can be used on any desired spray mesh. The verification of the enhanced nozzle file interface was performed by running a vast number of CFD simulations on a simplified computational domains, as shown in Figure 21. To check the feature functionality, the nozzle outlet and spray inlet selections were generated similar in size and with different number of faces. Three different meshes were used to cover all possibilities of the nozzle – spray interface, where the spray inlet selection can be generated as selection identical to the nozzle outflow selection, considering the same number of selection faces. Furthermore, the spray inlet selection can contain different number of faces which is also covered with the modified interface. The next section of this thesis shows a short introduction in the mapping procedure, and the quantities that are being mapped through the nozzle – spray interface.

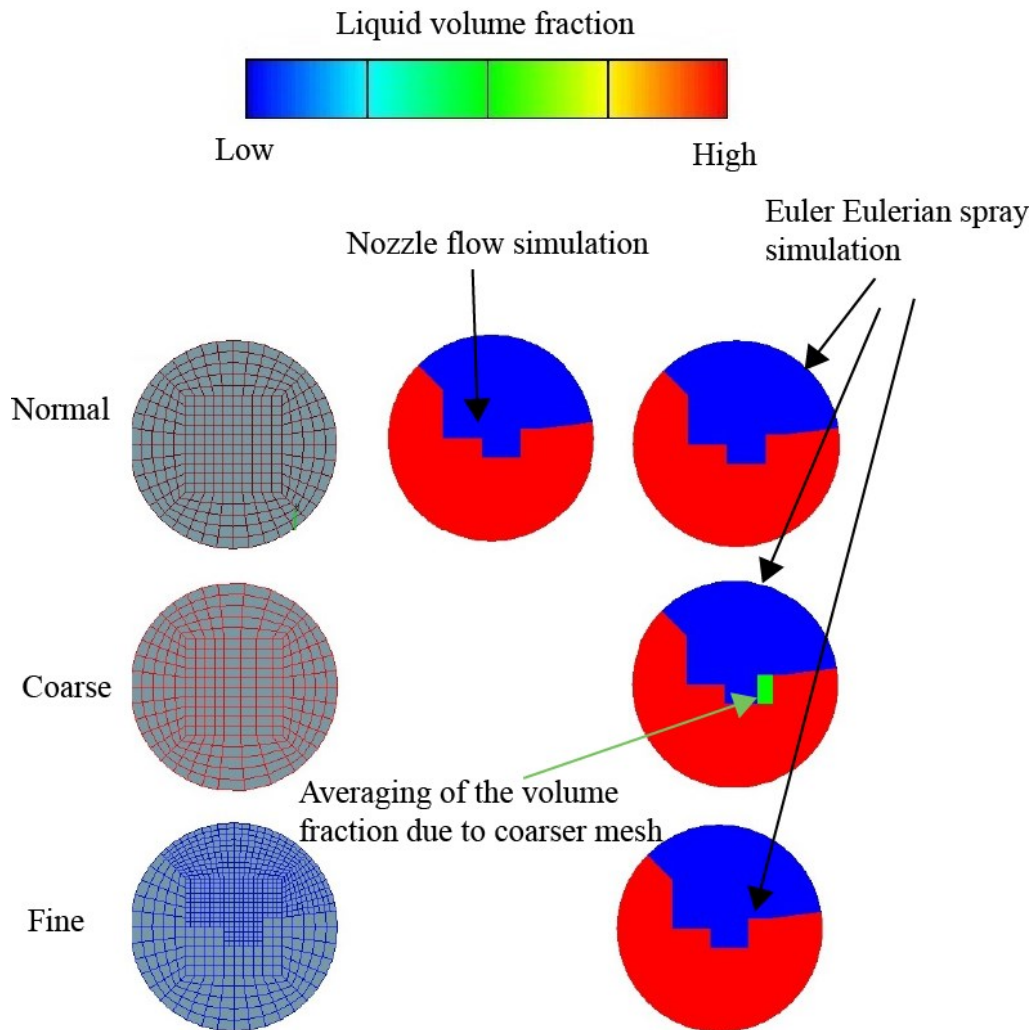


**Figure 21 Results of nozzle file mapping for the liquid volume fraction**

Figure 21 shows the results of liquid volume fraction mapping for the three possible mapping cases; (a) when nozzle outlet and spray inlet selections are the same, (b) refined or (c) coarsened. It is visible that the liquid volume fraction is adequately mapped from the nozzle to the spray simulation. The green arrow points to computational faces where averaging of the volume fraction is noticeable. In the mapping procedure the conservation principle is done over the surface area. Figure 22 shows results of the mapping procedure for the gas phase temperature, TKE, TED, and the gas phase velocity. The results are shown for mapping case when nozzle outlet selection and spray inlet selections are identical. The nozzle flow simulation results are numerated with 1, whilst results with number 2 show the inlet boundary condition in the Eulerian spray simulation.

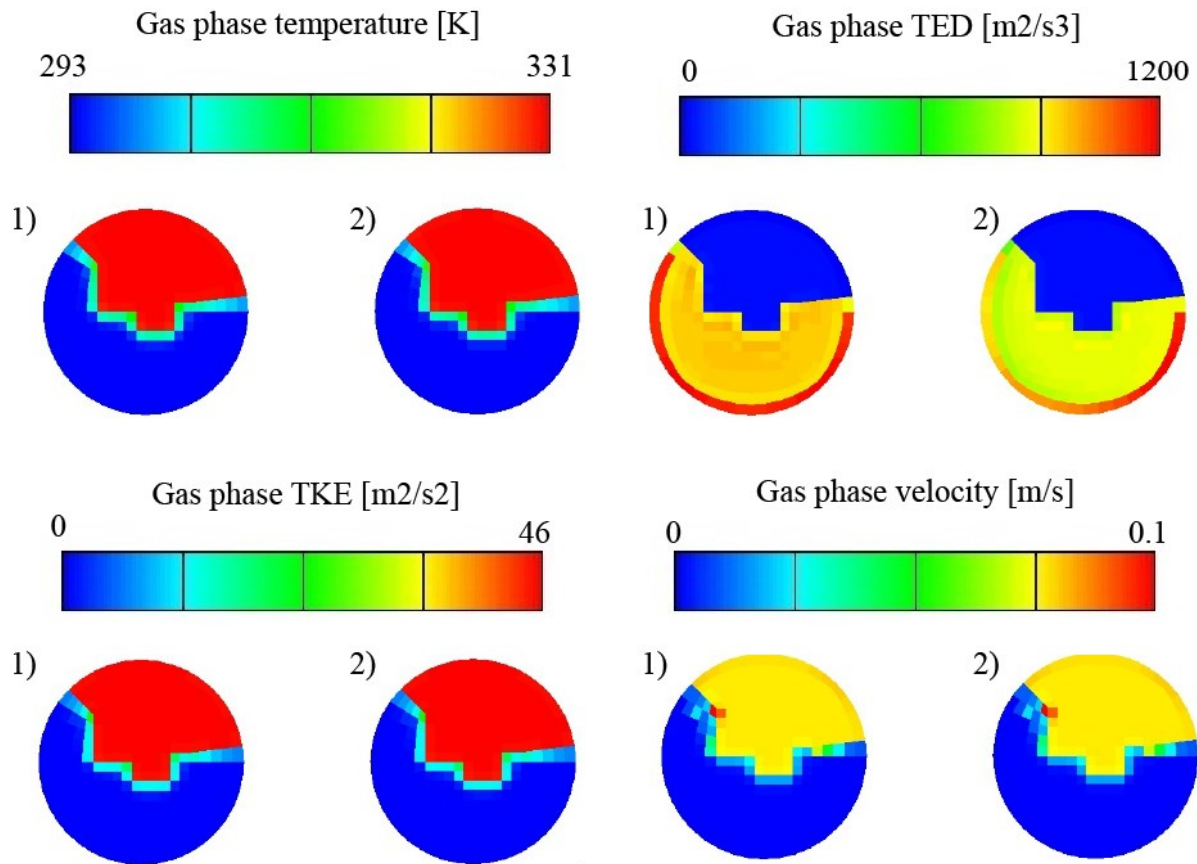


Figure 22 Results of nozzle file mapping for various quantities

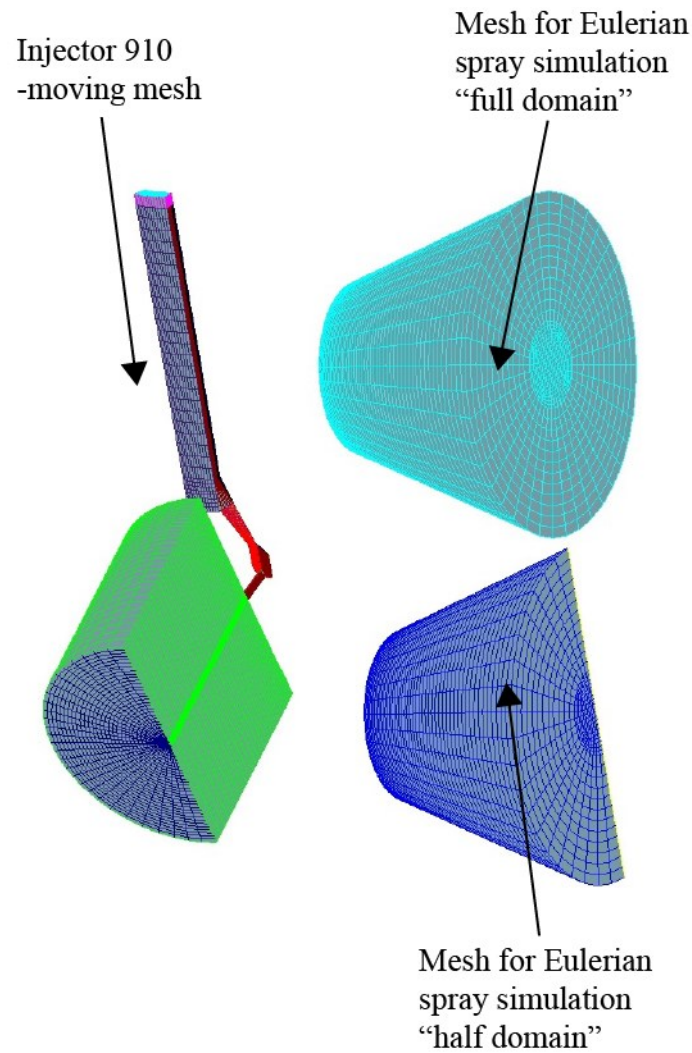
### Validation of the nozzle file interface

For validation of the nozzle file interface the injector simulation was performed [56]. The liquid fuel was injected with 50 MPa injection pressure into the chamber pressurized up to 0.5 MPa. The mapping procedure was thoroughly tested for several cases, as shown in Table 11.

Table 11 Nozzle flow – spray interface validation cases

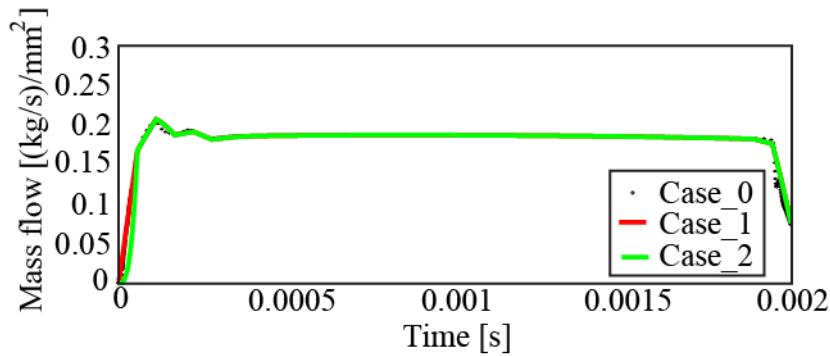
Case_0	Injector simulation
Case_1	Euler Eulerian simulation – Full geometry
Case_2	Euler Eulerian simulation – Half geometry

The nozzle files were generated by performing a separate injector flow simulation on a geometry covering half of the nozzle design (domain entitled Injector 910 moving mesh), as seen in Figure 23. For the validation process, two different geometries were created. One geometry was used to simulate the half geometry corresponding to the 910 injector case, and a full 360° geometry that was used to test the nozzle file mirroring capabilities.



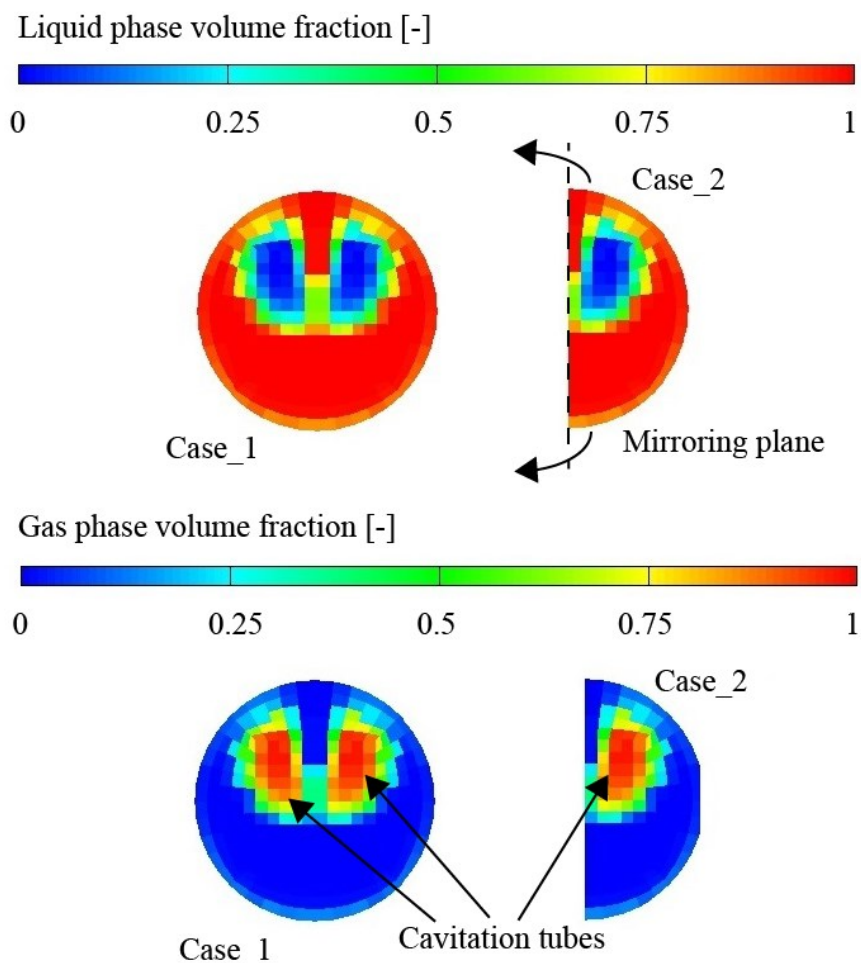
**Figure 23** Computational meshes used for validation of the nozzle file interface

Figure 24 shows the mass flow rate normalized by the inlet selection surface area in the Euler Eulerian spray simulation. For the injector simulation, Case\_0, the liquid mass flow is normalized by the surface area of the outlet selection. This selection was used for generating the nozzle files. A slight differences between the injector simulation Case\_0 and the Eulerian spray cases is noticeable, which can be addressed to the interpolation procedure of the nozzle file data, and to larger computational time steps defined within the injector simulation. The observed parameter for the validation of the nozzle – spray interface was the total injected mass, which was successfully captured in all performed validation simulations.



**Figure 24** Calculated mass flow profile

Figure 25 shows the volume fraction fields on the inlet selection of the Eulerian spray simulation cases. The results are shown for the simulation time 1 ms after start of injection. This figure shows the importance of the nozzle file boundary condition in the spray simulations. During the fluid flow through the nozzle channels, the liquid fuel is being accelerated at the flow passage with reduced cross – section.



**Figure 25** Cavitation influence on the spray inlet boundary selection captured with the mapping procedure

As a consequence, the local pressure decreases. If the local pressure is lower than the saturation pressure, the liquid fuel changes its state and cavitation occurs. The vapour bubbles accumulate, and if they are not collapsing, they are transported towards the nozzle hole outlet. On the one hand, the cavitation process enhances the liquid jet atomization processes, but on the other hand it decreases the effective nozzle cross section, and has a destructive influence on the nozzle channel walls when cavitation erosion takes place. Figure 25 shows the occurrence of the “vapour tubes” as a result of the in – nozzle cavitation process, which can have important influence on the spray formation, evaporation, and subsequently on the overall combustion process.

### 3.4. Primary atomization modelling

After enhancing the nozzle flow – spray interface, special attention was given to understanding of the liquid jet primary atomization process occurring in the nozzle vicinity. Therefore, in this section of the thesis the results of primary atomization process numerical modelling, focusing on the processes occurring in the near nozzle region, are shown. It is known that in IC diesel engines the liquid fuel is injected into the combustion chamber with high velocities through a nozzle holes characterized with small diameter. Accordingly, turbulent and aerodynamic forces act on the fuel jet surface resulting in a rapid liquid jet atomization causing a huge number of unstable ligaments and droplets. Taking into account that the experimental investigation of the optically dense spray region (close to the nozzle) is highly complex, the computational simulation results were compared to the available DNS data of the fuel jet break – up process. The axial and radial mixture volume fraction were compared to the DNS studies [48][102]. From the literature review it was concluded that the Euler Eulerian size – of – classes approach has not been extensively tested on its ability to capture the highly turbulent diesel spray primary atomization process. The main objective of this section was to validate the used primary atomization model, and to find the appropriate model setup for accurate and numerically efficient computational simulations.

#### 3.4.1. DNS data and numerical setup

To validate the primary atomization model, a DNS numerical simulation results of near nozzle region were used. In the DNS study the liquid jet disintegration was calculated, whilst other processes have been suppressed. The computational results obtained with the Eulerian size – of – classes spray approach were compared to the available DNS simulation results obtained through the coupled level set/VOF/ghost fluid method. The generated computational



domain represents a small region next to the nozzle orifice where the primary break – up process occurs. It was created as two dimensional axisymmetric static computational domain, consisting of 54250 control volumes extending from 0 to 2.1 mm in the axial direction, and from 0 to 0.15 mm in the radial direction. It is worth to note that such a domain was used to reduce the CPU time necessary to perform a number of CFD simulations intended for the model parametrization. The cell size with  $2.4\ \mu\text{m}$  was uniform in the radial direction, whilst a refinement towards the inlet selection was performed to fulfil the Courant number requirements, considering the magnitude of the velocity and grid dimensions. The number of computational cells in the radial direction was 62, whilst in the axial direction it counted 875. The inlet of the liquid fuel jet was refined with 21 computational faces. Use of two dimensional computational meshes is reasonable when a symmetric spray can be assumed and, therefore, in the tangential direction the symmetry boundary condition was applied. At the domain inlet, a normal velocity boundary condition was applied, which corresponds to the DNS studies. The injector surface was defined with the constant temperature wall boundary condition with 293.15 K. The calculation domain represents the area of the primary break – up process, and therefore on the outlet selection a pressure boundary condition was set. The generated computational domain with defined boundary conditions is shown in Figure 26.

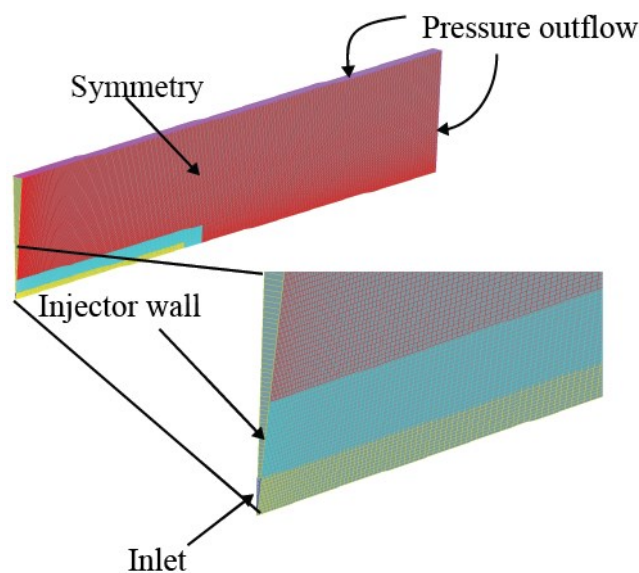


**Figure 26 Computational mesh used for validation of the primary break – up model**

Six Eulerian classes were defined for the numerical modelling of the primary break – up process – one for the gas phase, four droplet classes, and one class for the liquid jet. The corresponding class diameters were defined with 2.4, 10, 20, 40  $\mu\text{m}$  (droplet classes), and

100  $\mu\text{m}$  was assigned to the bulk liquid class. The fuel injection velocity was held constant with 100 m/s throughout the whole simulation process. Fuel temperature was set to 293.15 K, density to 696  $\text{kg}/\text{m}^3$ , surface tension to 0.06  $\text{kg}/\text{s}^2$ , and liquid dynamic viscosity was set to  $1.2 \times 10^{-3}$   $\text{kg}/\text{m}\cdot\text{s}$ . The environmental gas density was set to 50  $\text{kg}/\text{m}^3$ . For the turbulence, volume fraction and energy transport equations the first order UPWIND differencing scheme was applied, whilst for the continuity equation the CDS scheme was employed. For the momentum equation a combination of CDS and UPWIND was proposed with blending factor of 0.5. For all calculations the Euler implicit time integration was employed ensuring solution stability whilst the accuracy was achieved by employing sufficiently small time step. The influence of the false diffusion on the penetration results was minimised by a performing mesh dependency analysis before. The turbulence was modelled using the advanced  $k - \zeta - f$  turbulence model, with the initial fluctuation intensity of 5 % and the initialized turbulent length scale 10  $\mu\text{m}$ . The solution convergence criterion was achieved when the residual for momentum, pressure, energy and volume fraction decrease below the value of  $1 \times 10^{-4}$ . The pressure – velocity coupling was obtained by using the SIMPLE algorithm. The time discretisation of the simulation varied with simulation time, where small time steps were used due to the fact that gradients in the mass exchange models can be very high. Therefore, at the beginning of injection the time step was very small ( $3 \times 10^{-8}$  s), but later it was continuously increased throughout the injection time (up to  $5 \times 10^{-7}$  s).

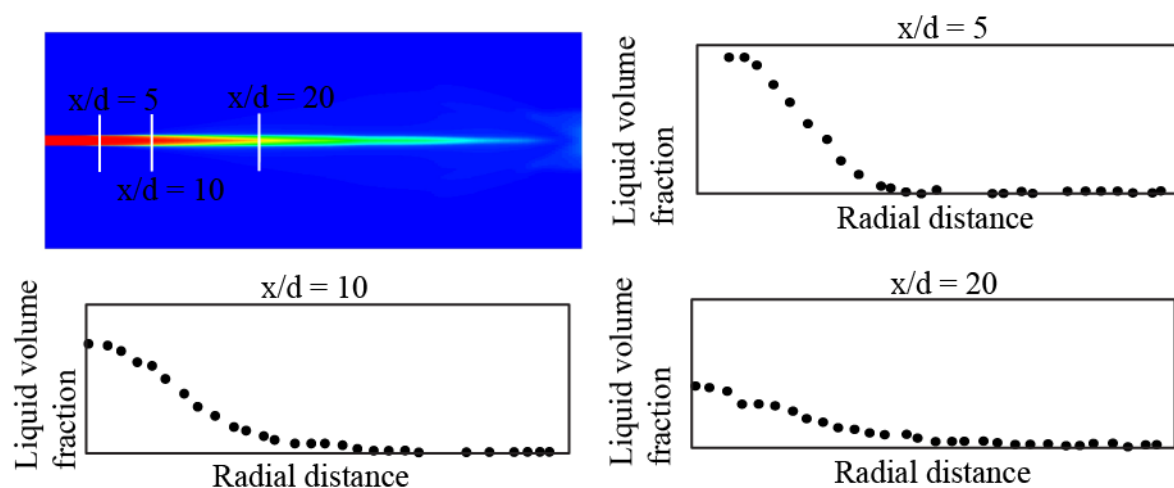


**Figure 27** 2D Euler Eulerian simulation results and DNS diagrams of volume fraction distribution

The results from the DNS studies have been time averaged so that they can be compared with the present RANS simulations. Figure 27 shows a 2D cut of the Eulerian simulation in the spray axis, and the DNS results [102] of the radial volume fraction profiles recorded at different axial positions. From the DNS results it is visible that the liquid jet emerging from the nozzle disintegrates, and the jet tip reaches its steady state at certain position downstream of the nozzle. At the distance  $x/d=5$  the liquid core is unattached in the spray axis. Further downstream, at the distance  $x/d=10$  and  $x/d=20$ , the droplets and unstable ligaments are created and the bulk liquid class volume fraction is reduced.

### 3.4.2. Results and discussion

The calculated liquid volume fraction distribution in the radial direction, at the distance 0.5 mm from the injecting point is compared to the available DNS data [102], as shown in Figure 28. At this distance, the calculated volume fraction profile corresponds well to the results of the DNS study. A smooth decrease in liquid volume fraction is noticeable in the DNS simulations, whilst the Euler Eulerian spray modelling provides a steeper decrease in the radial direction. Such behaviour is also visible in results shown in Figure 32, and could be addressed to a slightly underestimated primary break – up process.

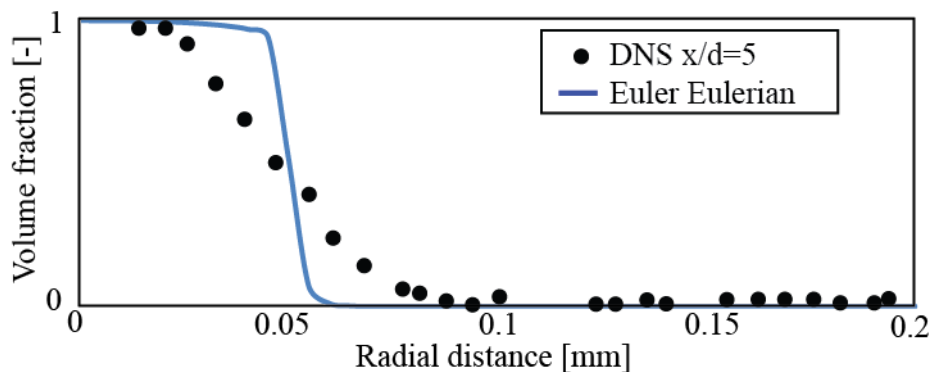


**Figure 28 Comparison of calculated and DNS radial mixture distribution at  $x/d=5$**

The liquid volume fraction distribution in the radial direction, at the distance 1 mm from the injecting point, is shown in Figure 29. At this point both, the DNS and the Euler Eulerian simulation results are in a good agreement. A smoother decrease in the radial volume fraction is noticeable for both modelling approaches, but a slight differences are noticed. The volume fraction predicted with the Eulerian approach is higher near the spray axis which could be addressed to an underestimated radial velocity modelled by the break – up process.

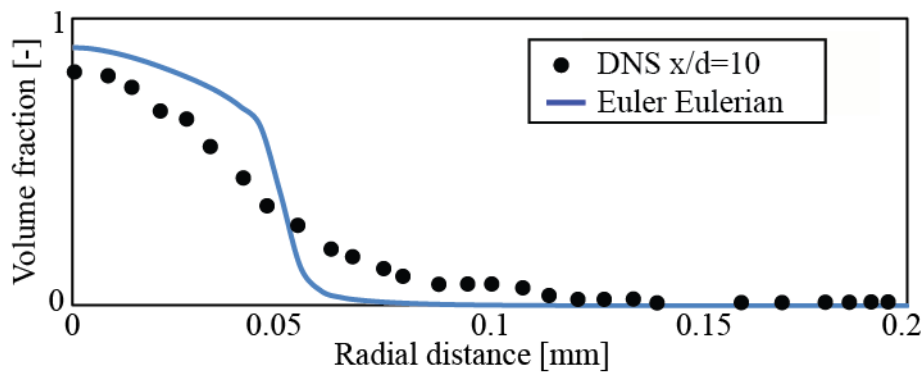


**Figure 29 Comparison of calculated and DNS radial mixture distribution at  $x/d=10$**

The liquid volume fraction distribution in the radial direction, at the distance 2 mm from the injecting point, is shown in Figure 30. At this distance the radial liquid volume fraction corresponds well to the DNS data. A smooth decrease in volume fraction is noticeable for both simulations. However, as noticed at the distance of 1 mm, the volume fraction near the spray axis is over – predicted, whilst it is under – predicted at the radial distance bigger than 0.05 mm. Such behaviour could be a consequence of an underestimated radial break – up velocity modelled with the used turbulent dispersion model.

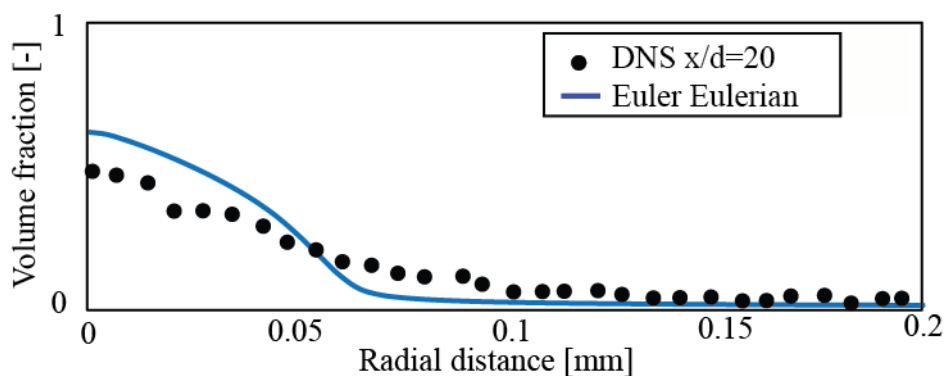


**Figure 30 Comparison of calculated and DNS radial mixture distribution at  $x/d=20$**

The axial liquid volume fraction distribution in spray axis direction is shown in Figure 31. The volume fraction is averaged for all computational cells covering the nozzle hole. The Euler Eulerian simulation results follow the DNS simulation results, where the volume fraction decrease in the axial direction is adequately captured. The volume fraction continuously decreases as consequence of the liquid jet atomization process. The liquid mass is detached from the liquid core, and unstable ligaments and droplets are formed.

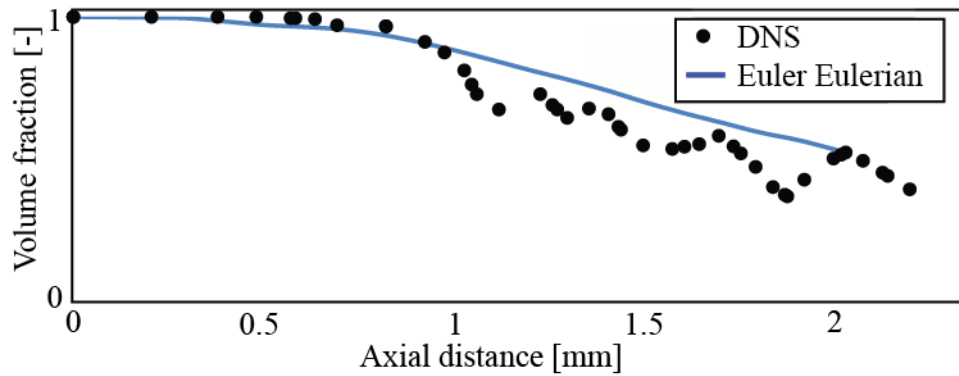


**Figure 31 Comparison of calculated and DNS axial mixture distribution**

The liquid volume fraction 2D cut comparison of the DNS and Euler Eulerian computational results is shown in Figure 32. The results are shown for the cut extending 2.2 mm in the axial direction and 0.15 mm in the radial direction. The generated domain is 2D axisymmetric in design, as described in previous section, and therefore, the results were mirrored along the injector axis. A good agreement to the DNS results is noticeable, but a slightly overestimated liquid jet penetration in both, the axial and radial direction, can be observed. Such behaviour is reasonable, since in previous figures an underestimation of the primary atomization process was noticed.

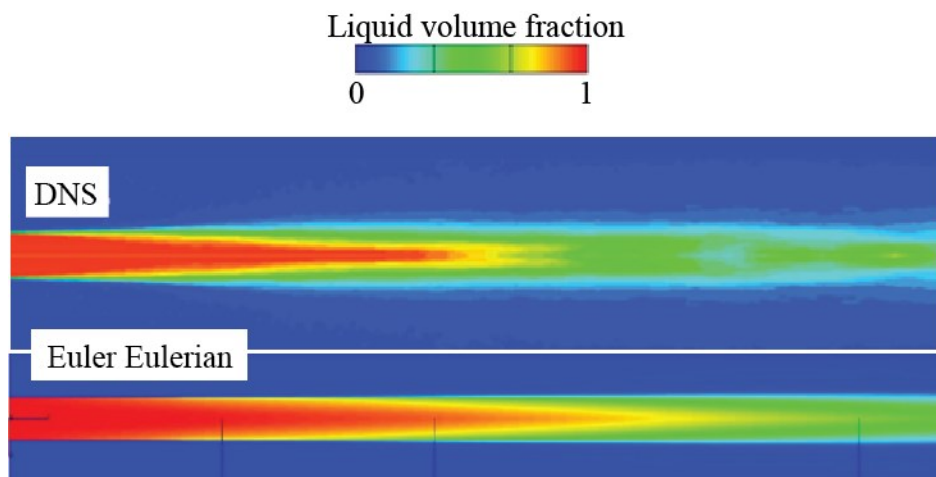


**Figure 32 Comparison of calculated and DNS liquid volume fraction field**

As it was aforementioned, the processes occurring in the near nozzle region are hard to capture in the experimental research. Therefore, in order to validate the existing primary atomization model, the calculated results were compared to the DNS study [102]. The presented results show a good behaviour of the used atomization model where a slight underestimation of mass transfer from the liquid jet towards the droplet classes can be observed. However, fuel

radial and axial distribution was correctly modelled, and it can be concluded that the used model could be used in a various real engineering applications.

### 3.5. Secondary atomization modelling

After the liquid fuel is injected through the small diameter nozzle and disintegrated due to the primary atomization process, the created ligaments and fuel droplets are subject to further disintegration – process referred as the secondary break – up. In this section the modelling results of such process is shown, and its influence on the fuel spray spatial and temporal development is discussed.

#### 3.5.1. Experimental data and numerical setup

The experimental measurements of high pressure diesel fuel injection into the non – reactive environment have been performed at Toyota Motor Corporation and Toyota Central Research and Development laboratories [103]. The liquid fuel was injected through a small diameter nozzle into the constant volume vessel CVV filled with CO<sub>2</sub> and pressurized to the defined level. The main goal of the conducted experiments was to investigate the microscopic and macroscopic characteristics of the spray. In the experimental research the Mia – Scattering measuring technique [104] was employed to capture the spatial and temporal spray development. The measured liquid spray tip penetration curves for four different nozzle configurations are shown in Figure 33, where  $d$  denotes the nozzle hole diameter and  $L$  stands for the nozzle channel length.

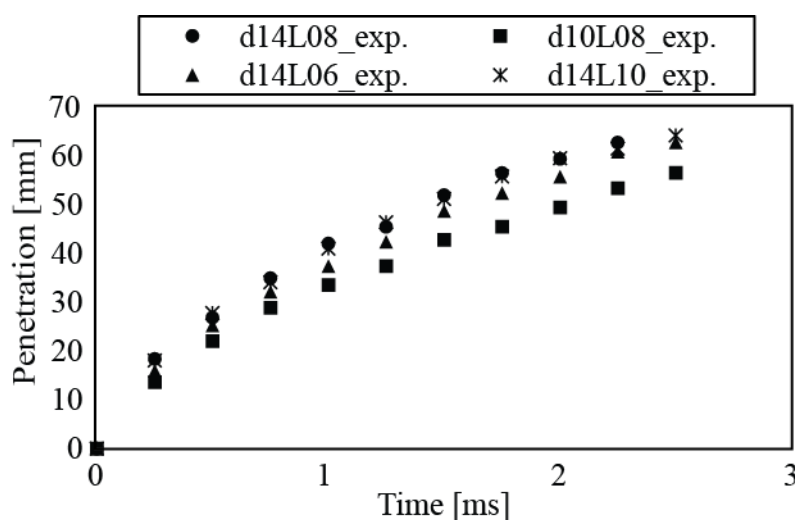


Figure 33 Measured spray tip penetration

In the experimental work, several spray microscopic characteristics such as SMD and droplet distribution were measured. The SMD was recorded from the global spray droplet population measured in the time frame of 8 ms, starting with SOI. It was measured with the Phase Doppler Particle Analyser (PDPA) measurement technique [20] with the lower measurability limit of 1  $\mu\text{m}$ . The SMD measurements were performed at several locations downstream in the axial direction covering a round measurement area of 1 mm in diameter. The measured data are shown in Table 12. The microscopic spray characteristics that are discussed in this section are the droplet number and volume distributions, where droplets smaller than 1  $\mu\text{m}$  in diameter were not taken into account. In addition, next table shows the spray angle measurement results, where the spray angle is defined as the droplet cloud spreading angle recorded 2 ms after SOI at the axial distance of 70 % of liquid spray penetration.

**Table 12 Measured spray characteristics for the examined nozzle designs**

	<b>Bore Length [mm]</b>	<b>Bore diameter [mm]</b>	<b>Spray angle [°]</b>	<b>SMD [<math>\mu\text{m}</math>]</b>	<b>Measuring location [mm]</b>
Nr1	0.8	0.14	18.9	23.2	72
Nr2	0.8	0.1	18.9	21.9	62
Nr3	0.6	0.14	21.6	23.3	69
Nr4	1	0.14	16.8	23	73

For the numerical modelling of the spray processes, the cylindrical computational domains with approximately 50000 hexahedron cells were generated, as shown in Figure 34. Initially, the mesh was generated for modelling the fuel injection through the nozzle hole with diameter 140  $\mu\text{m}$ , and then it was scaled for the other nozzle diameters retaining the same cell distribution in both the axial and radial directions. The computational meshes were refined towards the nozzle hole in the radial and in the axial direction to better capture the processes occurring in the injector vicinity.

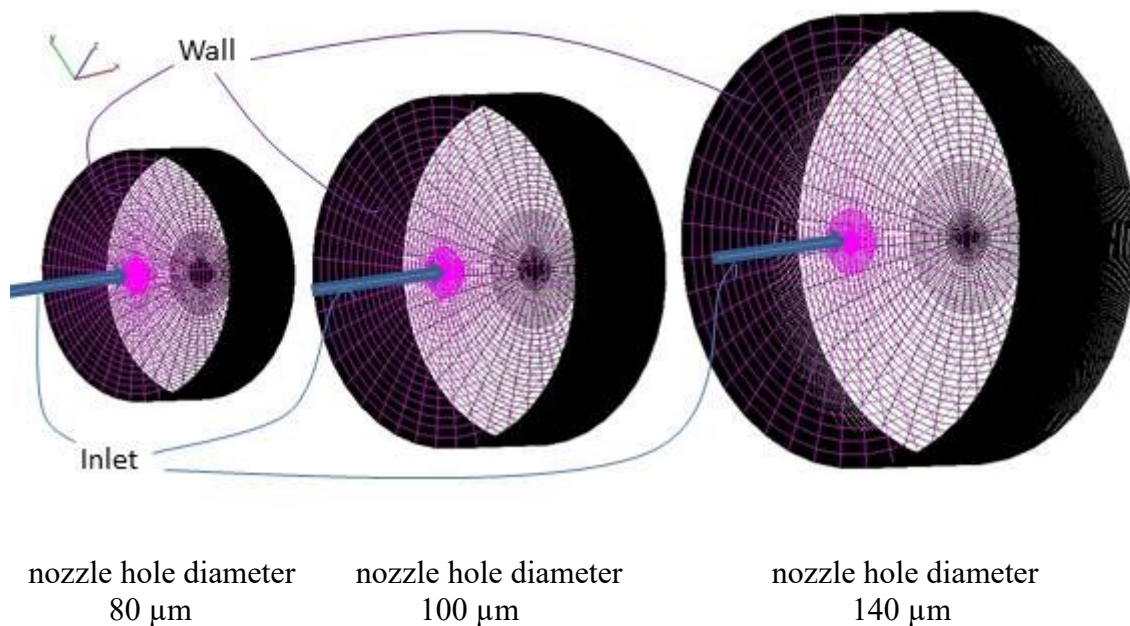


**Figure 34** Computational meshes used for validation of secondary break – up model

To take into account the influence of the nozzle flow on the spray characteristics, the inlet boundary condition was defined through the nozzle – file interface. Around the nozzle hole, on the same plane as the inlet selection, the constant temperature wall boundary condition was applied. The diameter of the cylindrical meshes was large enough to minimize the influence of the outer boundary conditions and therefore it was not necessary to model the whole CVV geometry. On all other domain surfaces, the static pressure boundary condition was imposed. The pressure – velocity coupling was obtained through the SIMPLE algorithm. The CDS was used for the convective terms in the continuity equation, whilst a hybrid between the CDS and the upwind scheme with a blending factor of 0.5 was used for the convective terms in momentum equations. The turbulence was modelled using the advanced  $k-\zeta-f$  model described in the previous sections.

The injected fuel had a dynamic viscosity of 0.00338 Pas and a surface tension of 0.0270 N/m. The fuel density was 810 kg/m<sup>3</sup>, whilst the injection pressure was set to 87.5 MPa. The liquid fuel was injected into the constant volume vessel filled with CO<sub>2</sub> pressurized up to 2.1 MPa, which corresponds to the gas density of 38.6 kg/m<sup>3</sup>. The environment temperature was set to 293 K, and therefore the droplet vaporization rate was minimized. The simulation time was set to 8 ms, and the simulation time step size was defined through the time step table. At the beginning of simulation the time step was 6x10<sup>-7</sup> s and it was steeply increased up to 3x10<sup>-5</sup> s. A total number of ten Eulerian classes were defined in all simulations, one for the gas



phase, one for the bulk liquid class emerging from the nozzle, and eight classes denoting the fuel droplets. The initial diameters assigned to the droplet classes were 0.5, 1.5, 15, 25, 35, 45, 55, 90 and 100, 140 or 180  $\mu\text{m}$  for the bulk liquid class, which depends on the nozzle hole diameter.

### *3.5.2. Results and discussion*

In the following section the CFD simulation results of the non – reactive liquid fuel injection are shown. One of the most important properties of sprays, but unfortunately not enough for full spray characterization, is the distance of the spray tip in the axial direction measured from the injection point. As previously mentioned, this characteristic is called the liquid tip penetration. In the simulated cases due to the low surrounding gas temperature the vaporization was minimized and therefore, the vapour penetration curve is not shown. Figure 35 shows the calculated penetration curves for four different nozzle designs. The liquid fuel enters the domain with high velocity, disintegrates into smaller droplets and penetrates over time into the vessel. A slight decrease of the penetration speed, which is visible for all four cases, is addressed to the higher influence of drag force on the spray droplet population. The smaller the droplet diameter, the higher is the influence of the drag force due to reduced momentum/drag ratio. The liquid penetration is shown only for the period from SOI until 2.5 ms, but a good agreement was observed during the whole simulation time.

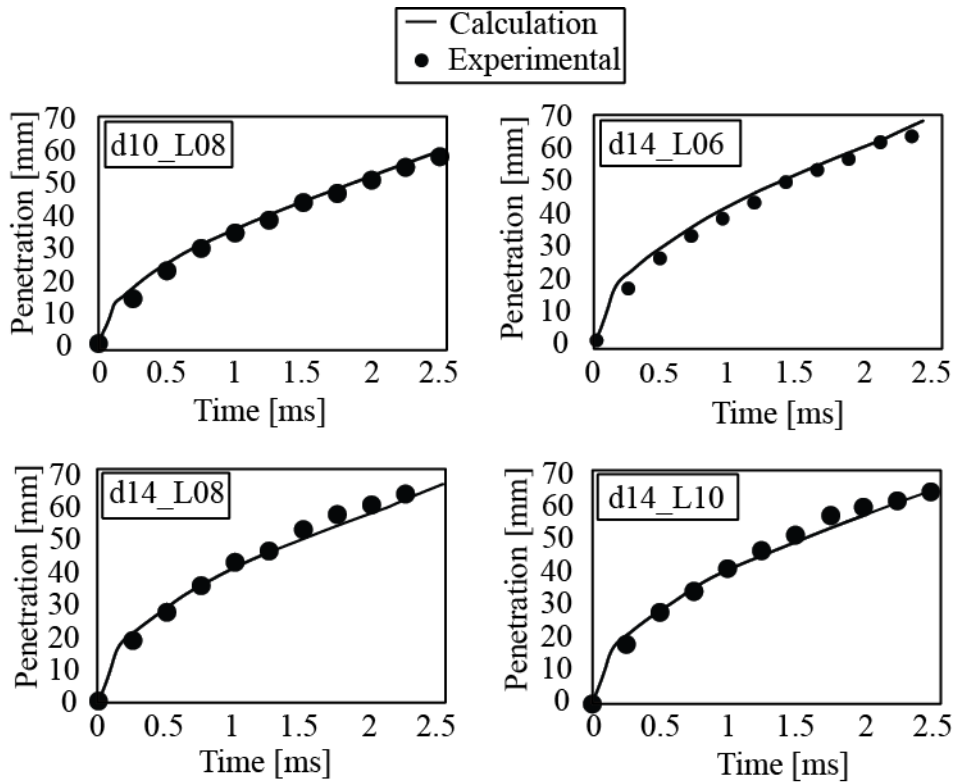


**Figure 35 Comparison of calculated and measured spray tip penetration**

The comparison between the modelled and measured spray angle data are shown in Figure 36. The results obtained in this thesis, denoted as “Eulerian”, are in excellent agreement with the measured data, and also close to calculation results from the Lagrangian spray simulations [103]. It can be concluded that the a slight change in nozzle hole diameter and nozzle hole channel length, retaining the injection and chamber pressure on the same level, have a low influence on the spray angle.

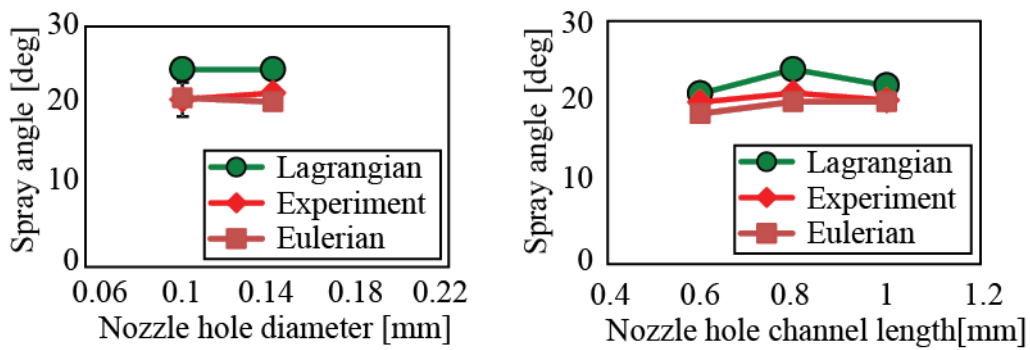


**Figure 36 Comparison of calculated and measured spray angle**

Figure 37 shows the calculated droplet number and volume distributions in comparison with the available experimental data. For the analysis of the droplet distributions the droplets smaller than  $1 \mu\text{m}$  were not considered, according to the PDPA measurement data. The data is collected from the overall spray population on the certain distance from the injector, as shown in Table 12. For all observed injecting points, the distributions have similar shape but a slight differences can be noticed. A smaller population of bigger diameter is produced from the small diameter nozzle, which corresponds well to the measured data.

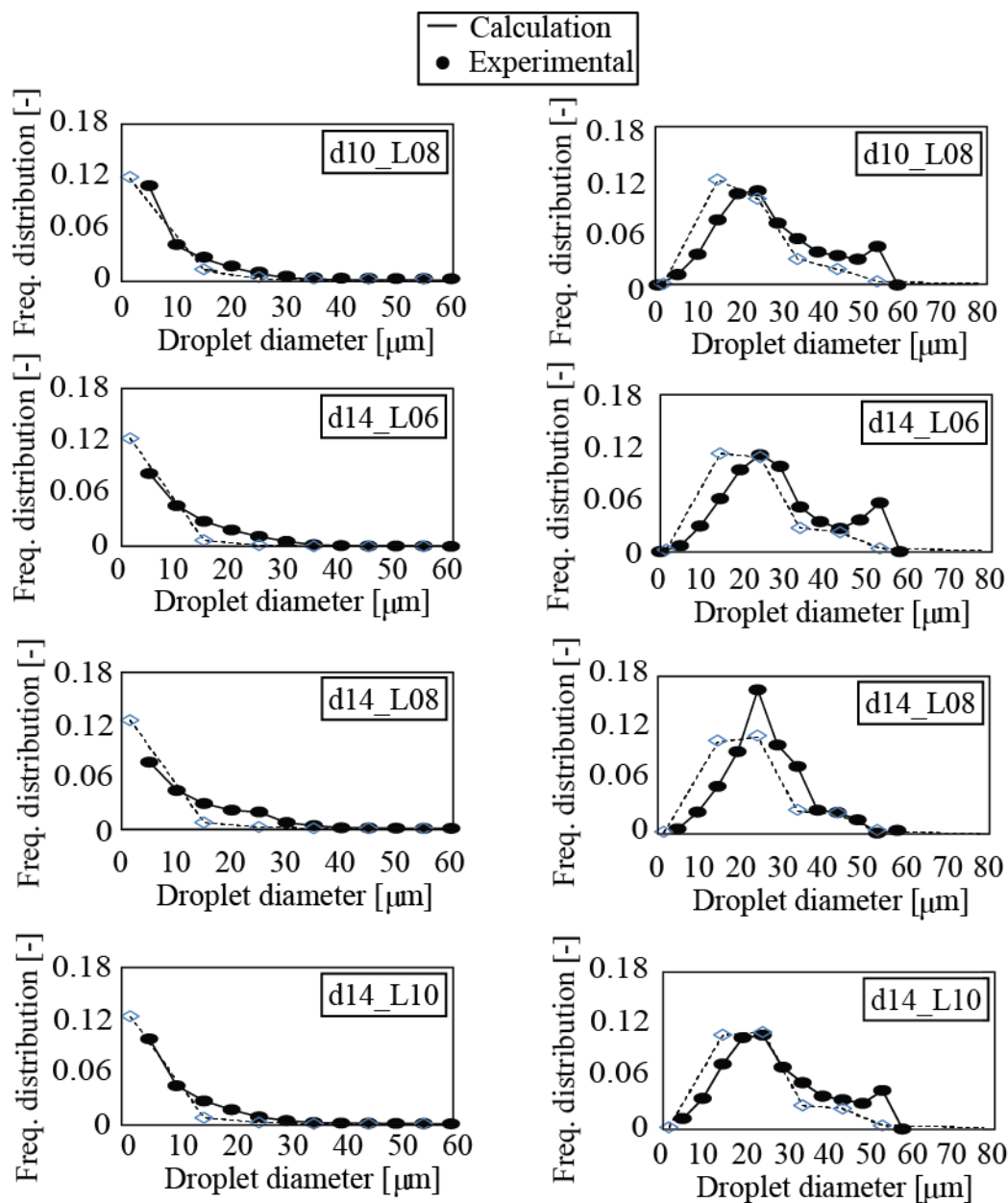
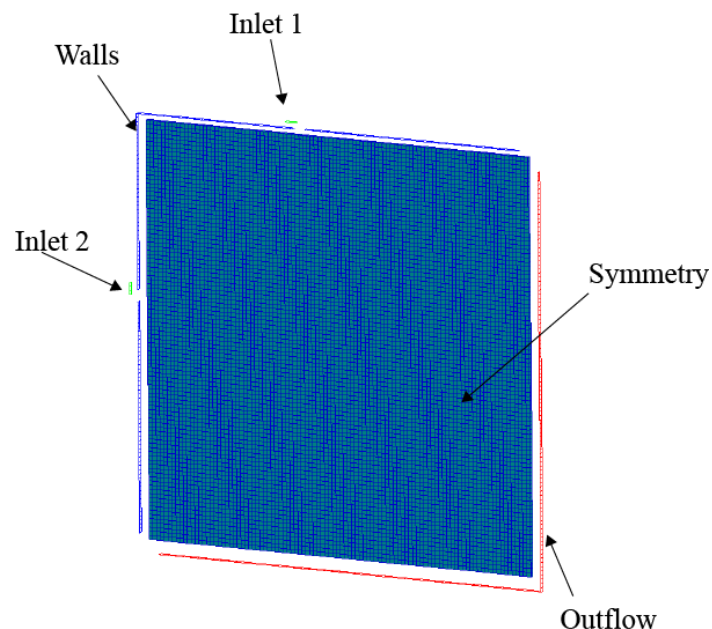


**Figure 37 Comparison of calculated and measured droplet number distribution (left) and droplet volume distribution (right)**

To summarize, the spray models are usually compared solely to the spray tip penetration curves and/or to the volume fraction distributions. In this research, a validation of the model was performed including more details such as: spray angle, droplet volume and droplet number distributions. Experimental research of such data is costly, and therefore the droplet distribution data is rarely available. The WAVE model used for secondary atomization process was modified with the child droplet option, and it was validated against distribution curves. A good agreement to the experimental data was achieved, which implies that such model could be used in a real engineering applications.

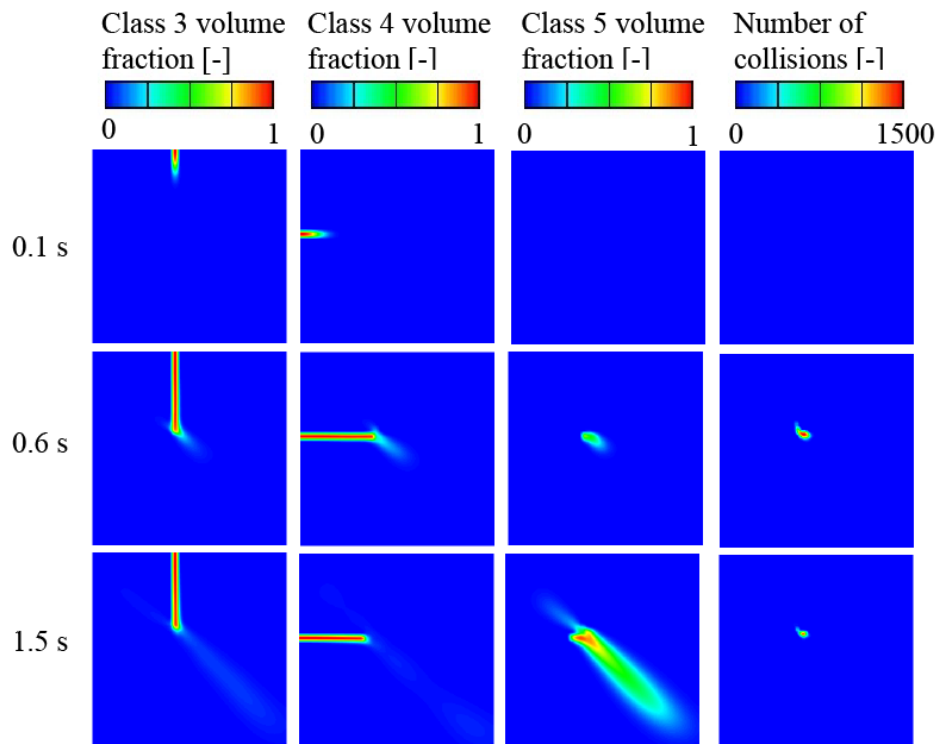
### 3.6. O'Rourke collision model

In this section the verification of the implemented O'Rourke collision model is discussed. The implementation of such model into the commercial CFD code was an important step for improving the modelling accuracy of the Eulerian size – of – classes model. The computational domain, shown in Figure 38, was created as two dimensional square shaped domain consisting of 10000 hexahedral cells. The domain characteristic dimension is set to 100 mm. Symmetry boundary conditions were applied to the sides of the domain, whilst the outflow from the domain was defined as the static pressure boundary condition.



**Figure 38** Computational mesh used for verification of the collision model

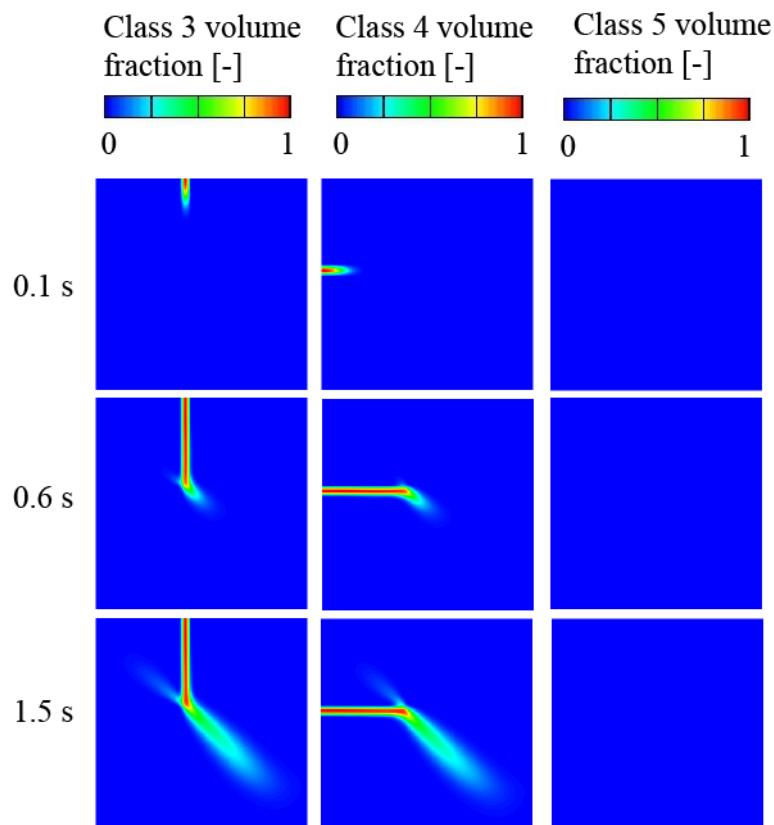
The computational simulation was performed for 1.5 s with the constant time step of 0.01 s. For the verification of the implemented model six Eulerian classes were defined, five droplet classes and one gas class. The droplet classes were defined with droplet diameters of 10, 20, 40, 60 and 160  $\mu\text{m}$ . The liquid fuel was injected into the domain through two inlet selections which are resolved with three faces and are rotated for  $90^\circ$ , one relative to other. At the inlet selections a normal velocity boundary conditions were applied, where at selection *Inlet 1* the droplets with diameter 20  $\mu\text{m}$  and velocity 0.1 m/s were released into the domain. The 40  $\mu\text{m}$  droplets were released from another inlet selection with the same injection velocity. The initial gas temperature and the temperature of the injected liquid fuel were set to room temperature of 20  $^\circ\text{C}$ . The liquid fuel used for verification of the implemented model is referred as DIESEL 1 with a corresponding density of 810  $\text{kg}/\text{m}^3$ . The CDS was used for the convective terms in the continuity equation, whilst a hybrid between the CDS and the upwind scheme with a blending factor of 0.5 was used for the convective terms in momentum equations. The upwind discretization scheme was used for the convective terms in the scalar equations. Figure 39 shows the modelled volume fraction and collision frequency for the observed verification collision conditions.



**Figure 39** Calculated volume fraction field, and the number of droplet collisions with implemented collision model

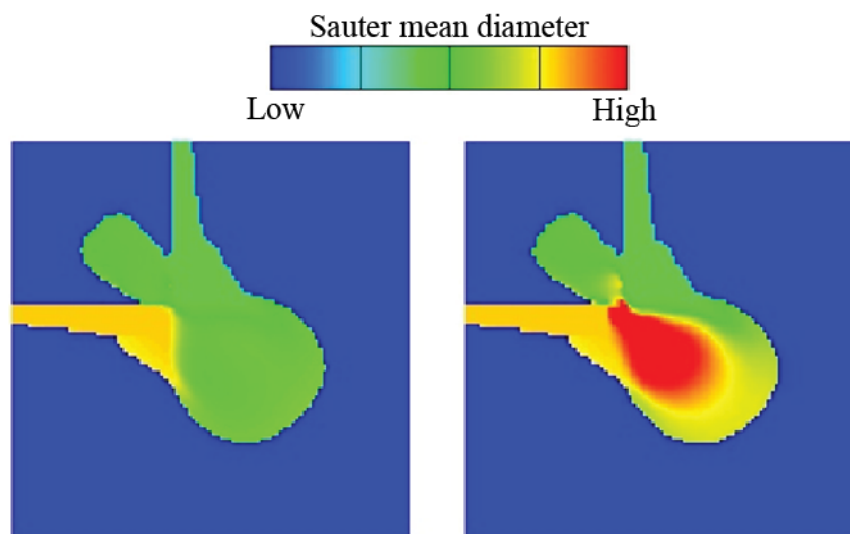
The results are shown in three rows for time instances 0.1, 0.6 and 1.5 s after start of injection, respectively. In the first and second column the droplet free stream is shown. After a certain time the liquid jets collide, and the mass of droplet classes 3 and 4 is used for creation of new droplets placed within droplet class 5 characterized by a larger droplet diameter, as seen in column 3. The droplet jet direction is changed as a result of momentum conservation, noticeable in the next figure. The last column shows the number of calculated collisions between colliding droplet classes 3 and 4.

Figure 40 shows the calculated results of the jet collision without implemented collision model. The droplet classes introduced at the inlet selections penetrate through the domain and collide after a certain time. However, without collision model the bigger droplets are not created. Furthermore, it can be seen that the droplet jets change the penetration direction due to the momentum conservation between classes.



**Figure 40** Calculated volume fraction field without implemented collision model

The modelled results of the spray SMD, with implemented collision model, are significantly different to the simulation results without collision model. When the conditions for collision are achieved, the formation of new bigger droplets takes place. This leads to an increased SMD, as it is visible in Figure 41. The computational results are shown for 0.6 s after start of injection when two jets are already colliding. On the left – hand side of Figure 41, the SMD is shown for the case with disabled collision model, whilst on the right – hand side the SMD is shown for the case with enabled collision model.



**Figure 41** Calculated sauter mean diameter field without (left) and with implemented collision model (right)

### 3.7. Reactive multiphase spray modelling

In the previous sections, the details regarding nozzle flow influence on the spray process, liquid jet break – up and subsequent droplet atomization have been discussed. The importance of the nozzle flow was shown by introducing the nozzle file option and enhancing it with the MPI capability. The primary atomization model was validated against DNS data where liquid volume fraction distributions were compared with the simulation data. Afterwards, the child droplet option was developed to correctly describe the secondary atomization process, where the liquid tip penetration, droplet distributions, and spray angle were compared to the available experimental data. All mentioned tasks were performed to show the influence of various modelling parameters on the spray temporal and spatial development, which is of great importance since the atomization process and the fuel – air mixing have a significant influence on the spray combustion process.

This section deals with modelling of the non – reactive and reactive spray processes. The spray process was modelled by using the Euler Eulerian size – of – classes approach where the discrete phase is considered as continuum, and is further divided into classes sorted according their ascending droplet diameter. The combustion process was modelled by taking into account chemical kinetics and by solving the general gas phase reactions. The combustion model was implemented into a commercial CFD code, and it was used in combination with the previously implemented and validated spray sub – models. Initially, the method was tested on an artificial combustion reactor case. Furthermore, two separate non – reactive spray cases with n – dodecane and n – heptane fuel were modelled to tune the spray model parameters for the observed injection system. A fuel – air mixing process was validated by comparing the liquid jet and fuel vapour development with the available experimental data. The results show excellent agreement in terms of penetrations and radial mixture distribution at different distances from the nozzle hole. After acquiring the best model parameters, the developed method was validated by performing the computational simulations of a CVV and by comparing the modelled results to the ECN experimental data [19]. The CVV conditions correspond well to the IC engine diesel – like conditions in terms of gas residuals, pressure and temperature. The ECN is a worldwide group of institutions that perform both, experimental and numerical research. Their ultimate goal is to enrich the knowledge of spray and combustion processes at engine relevant conditions. As a result of their work a large public set of experimental data and numerical recommendations at low temperature combustion conditions relevant for engines that use moderate EGR has been generated. The provided results imply a good agreement of the lift off length and the ignition delay trends concluding that the developed method is suitable for modelling sprays and combustion processes.

### *3.7.1. Euler Eulerian reactive spray method verification*

For the plausibility of the developed method a 3D computational mesh consisting of 2050 hexahedral control volumes was used, as shown in Figure 42. The reactor surfaces were defined as impermeable wall with constant temperature boundary condition.



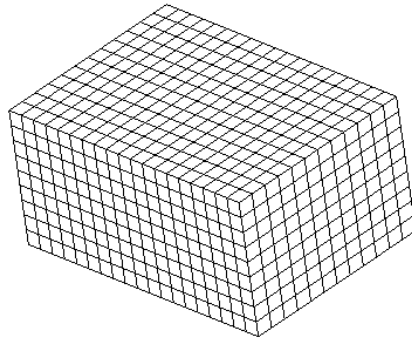


**Figure 42 Computational mesh used for verification of the Euler Eulerian reactive spray method**

The domain interior was filled with a gas mixture (99.95 % *vol.*) consisting of 24 % O<sub>2</sub> and 76 % N<sub>2</sub> (*mass*), whilst the rest of the volume was occupied by n – heptane fuel in liquid form. The initial gas temperature and pressure conditions were set to 1200 K and 2 MPa respectively, the fuel temperature was initialised with 323 K, and a quiescent environment was assumed. For the plausibility tests three Eulerian classes were defined, one for the gas phase and two droplet classes with diameters equal to 10 and 20 μm. The Abramzon – Sirignano evaporation model was used to model the droplet evaporation process. It should be mentioned that the exact evaporation rate, species concentration or temperature values were not of primary interest in this section of research. Instead, the overall system behaviour was observed. The CDS scheme was used for the continuity equations, while a combination of CDS and UDS scheme with blending factor 0.5 was used for the momentum equation. The UDS was also applied for turbulence, volume fraction and energy transport equations. The turbulence was modelled by the standard  $k - \varepsilon$  turbulence model and the convergence criterion was achieved when the normalized residuals for momentum, pressure, energy and volume fraction reached values lower than  $10^{-4}$ . The pressure – velocity coupling was obtained by using the SIMPLE algorithm and the simulation time step was set to  $10^{-5}$  s.

The fuel droplets placed within the reactor are enforced to evaporate due to the elevated temperature conditions. The concentration of fuel vapour arises according to the evaporation model, and the reactor mean temperature decreases, as seen in Figure 43.

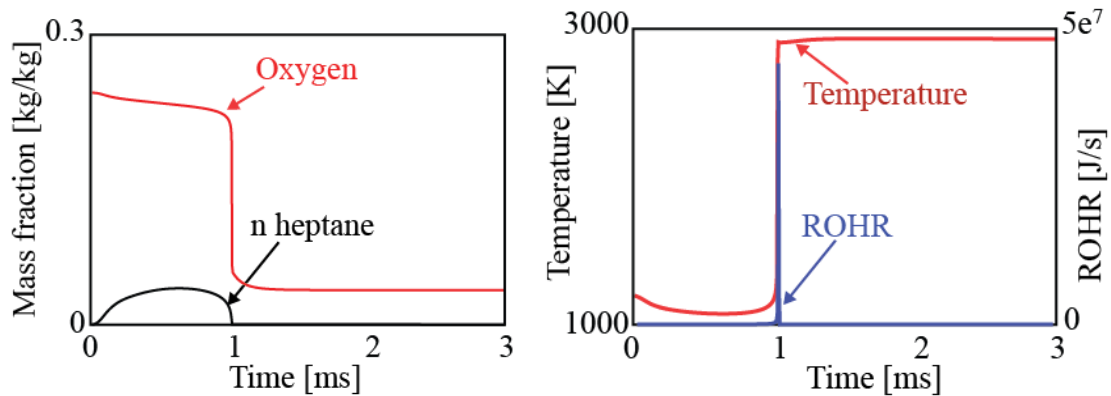


**Figure 43** Calculated profiles of fuel mass fraction, oxygen mass fraction, temperature and ROHR

The vaporized fuel reacts with the surrounding oxygen leading to combustion and elevation of the mixture temperature, as seen on the right – hand side in Figure 43. On the same figure it can be seen that the combustion process leads to decrease in fuel vapour concentration, oxygen depletion and significant heat release. When all reactant species are consumed the combustion process stops, mixture temperature reaches a “stationary” value, and the heat release from the chemical reactions is finished. The plausibility tests confirmed the correct implementation and the physical behaviour of the developed method.

### 3.7.2. Experimental data and numerical setup

For the validation process several operating points from the ECN database were computationally modelled. The modelled ECN CVV is made in a cubical shape and the characteristic dimension of the sapphire windows equals 108 mm. At the initial stage, the vessel was filled with a combustible gas mixture ignited by spark plugs located within the CVV. Through the premixed combustion the desired diesel engine conditions were achieved in terms of temperature, pressure and EGR. These conditions were used as initial conditions in this modelling work. Next, the liquid fuel was injected with approximately 150 MPa pressure through a SAC type [105] fuel injector located in the centre of one vessel side area. For the n – dodecane injection, a nozzle with diameter of 84  $\mu\text{m}$ , discharge coefficient of  $Cd = 0.9/0.89$  (0 %  $\text{O}_2$ / 15 %  $\text{O}_2$ ), and the area contraction coefficient of  $Ca = 0.98$  was applied. For the n – heptane fuel injection, a 100  $\mu\text{m}$  nozzle hole characterized with  $Cd = 0.8$  and  $Ca = 0.86$  was used. The operation conditions of the modelled non – reactive and reactive cases are listed in Table 13. A more detailed description on the experimental apparatus can be found at the ECN website and in published articles [19].

**Table 13 Operation conditions for the non-reactive and the reactive spray cases**

Case	Fuel type	CVV temp. [K]	CVV pressure [MPa]	Mixture composition [% vol]	Injection duration [ms]
Case_h	n-heptane	1000	4.33	3.77 H <sub>2</sub> O, 6.52	6.8
Case_d1	n-dodecane	900	6.05	CO <sub>2</sub> , 89.71 N <sub>2</sub> ,	6
Case_d2	n-dodecane	1100	4.96	0 O <sub>2</sub>	
Case_h_r1	n-heptane		4.28	3.67 H <sub>2</sub> O, 6.32	6.9
				CO <sub>2</sub> , 80.01 N <sub>2</sub> , 10 O <sub>2</sub>	
Case_h_r2	n-heptane	1000	4.25	3.62 H <sub>2</sub> O, 6.23	6.8
				CO <sub>2</sub> , 75.15 N <sub>2</sub> , 15 O <sub>2</sub>	
Case_h_r3	n-heptane		4.21	3.56 H <sub>2</sub> O, 6.11	6.8
				CO <sub>2</sub> , 69.33 N <sub>2</sub> , 21 O <sub>2</sub>	
Case_d_r	n-dodecane	1200	7.94	3.62 H <sub>2</sub> O, 6.23	6.1
				CO <sub>2</sub> , 75.15 N <sub>2</sub> , 15 O <sub>2</sub>	

Following the experimental matrix, seven high pressure spray operating points were computationally modelled. In the first column of Table 13 the case titles are given, where index *h* stands for n – heptane, index *d* for the n – dodecane fuel, whilst index *r* denotes the reactive cases. The n – heptane fuel was injected into the computational domain with temperature of 373K, whilst the n – dodecane fuel was injected with 363K. A mesh dependency study was performed, and the adequate computational meshes were chosen. For injecting the liquid n – heptane fuel a computational mesh consisting of 11000 control volumes was chosen, and for the n – dodecane cases a mesh with 8900 volumes was used. The difference in the control volume number is a consequence of the different nozzle hole diameters. Both computational meshes were generated as two dimensional (2D) and axisymmetric domains extending from 0 to 108 mm in the axial and from 0 to 54 mm in the radial direction. By using a 2D computational mesh the computational time was significantly reduced. It is known that nozzle effects like cavitation, nozzle geometry and injector needle motion have direct impact the spray development. However, in this research, nozzle cavitation have been suppressed by the nozzle design and a normal velocity boundary condition was applied at the inlet selection. The turbulence generated within the injector was taken into account by defining the mean values of *k* and *ε* at the nozzle orifice selection. For both computational meshes, the nozzle inlet hole was resolved by 5 faces over the nozzle radius, which yielded a smallest cell size of 10 μm for the

n – heptane cases. The symmetry boundary condition was applied on the lateral surfaces, and the meshes were refined towards the spray inlet and along the spray axis direction. The walls of the CVV and the nozzle walls were defined as the non – permeable walls with constant temperature recorded in the experimental research. In Figure 44 the defined boundaries for the n – heptane injection case are presented, and the same definition was applied for the n – dodecane modelling cases.

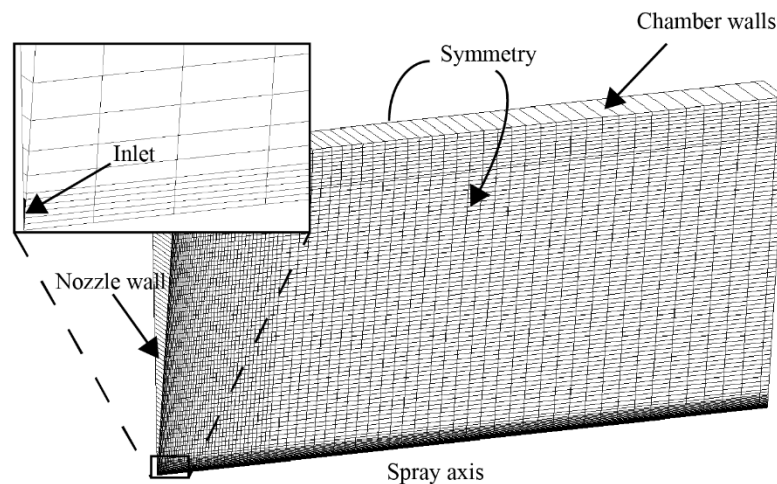


**Figure 44 Computational mesh used for the n – heptane spray simulation**

The next section describes the numerical setup for both, the non – reactive and the reactive spray simulations. A seven Eulerian classes were defined for the spray simulations – one class for the gas phase and six classes for the liquid phase. The liquid phase was sorted into five droplet and one bulk liquid class according to the droplet diameter. The droplet classes were defined with diameters of 1.5, 5, 10, 15, and 40  $\mu\text{m}$ , whilst a diameter of 100  $\mu\text{m}$  was assigned to the bulk liquid class for n – heptane, and 84  $\mu\text{m}$  for the n – dodecane injection cases. For turbulence, energy and volume fraction transport equations the first order UDS was applied, whilst for the continuity equation the CDS was employed. For the momentum equation a combination of CDS and UPWIND was proposed by introducing the blending factor of 0.5, and the turbulence was modelled by using the advanced turbulence model. The convergence was achieved when the normalized momentum, pressure and volume fraction residuals reached values lower than  $2 \times 10^{-4}$ , and  $10^{-4}$  for the energy residual. The pressure – velocity coupling was performed by using the SIMPLE algorithm. The time discretization was varied over the simulation time, where the maximum time step size was limited with the reaction rates of the used mechanisms. At the beginning of the injection process the computational time step was

set to  $5 \times 10^{-8}$  s and it was continuously increased throughout the injection time up to the maximum value of  $10^{-6}$  s.

### 3.7.3. Results and Discussion

#### Non-reactive spray simulations

In this section a modelling results of the developed method for the non – reactive sprays is discussed [106]. In most of the IC diesel engines diffusion driven combustion is present, meaning that the spray characteristics have a significant influence on the fuel energy conversion and on the formation of harmful substances [107][108][109]. Therefore, for reliable modelling of combustion process, it is important to correctly predict the spray temporal and spatial development. In the first validation step, the liquid spatial and temporal penetrations were compared to the available experimental data. To define the suitable spray model parameters, several spray cases where liquid fuel was injected into non – reactive environment were modelled, as shown in Table 13. The fuel penetration was defined by setting the same threshold values for the spray mass fraction as recommended by the ECN researchers. Accordingly, the liquid tip penetration was defined as the furthest distance of the liquid phase where the total spray mass accounts for 90 % of the whole liquid mass in the domain, whilst a value of 95 % was defined for defining the vapour phase penetration.

#### N-heptane fuel injection into non – reactive environment

The comparison between calculated and experimental data [110][111] of the liquid and vapour spray tip penetration is shown on the left – hand side in Figure 45. A good agreement between the results can be observed with slightly underestimated vapour penetration at later stage of injection. After SOI, the liquid fuel disintegrates into smaller diameter droplets and ligaments where this effect is caused by the high liquid momentum arising from the injector – CVV pressure differences. The created droplets tend to evaporate due to the elevated temperature condition, and the fuel vapour penetrates into the CVV together with the spray jet. After the liquid jet has reached its developed state, the vapour cloud continues to penetrate further into the domain. On the right – hand side in Figure 45 the radial mixture fraction profiles at developed state (2.5 ms) for four axial locations are shown. The experimental data [112][113] are shown with symbols whilst different styles of continuous lines are used to present the calculated data. The liquid evaporation is a result of the heat exchange between the gas mixture and the liquid fuel. In the early stage of the injection process, liquid fuel jet penetrates along

the spray axis and later, due to the turbulent dispersion forces, some droplets and vaporized fuel are transferred in the radial direction forming a conical spray cloud. Such behaviour reduces the jet penetration, and it influences the local combustion process within the reactive environment. In the nozzle vicinity approximately 20 mm from the injection point, the liquid jet is more concentrated along the spray axis whilst far downstream a wider mixture distribution can be observed (on the distance of 40 – 50 mm from the injection point).

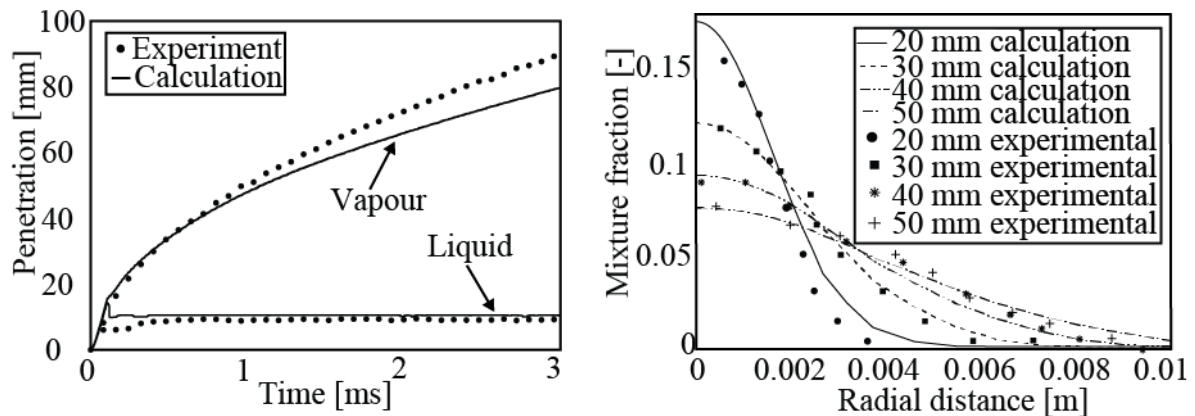


**Figure 45 Comparison of calculated and measured liquid and vapour penetration, and mixture radial distribution profiles (right) for Case\_h**

The experimental results of the fuel liquid – gas mixing process are averaged and compared with the modelled results, shown in Figure 46. The upper row of this figure depicts the modelled CFD results, whilst in the second row the experimental data are shown [19][112][114]. The frame of the experimental images is extending from -14.2 to 14.2 mm in the radial direction and from 16.4 to 55.8 mm in the axial direction. The centre of the nozzle outlet is defined by the coordinates 0, 0 mm.

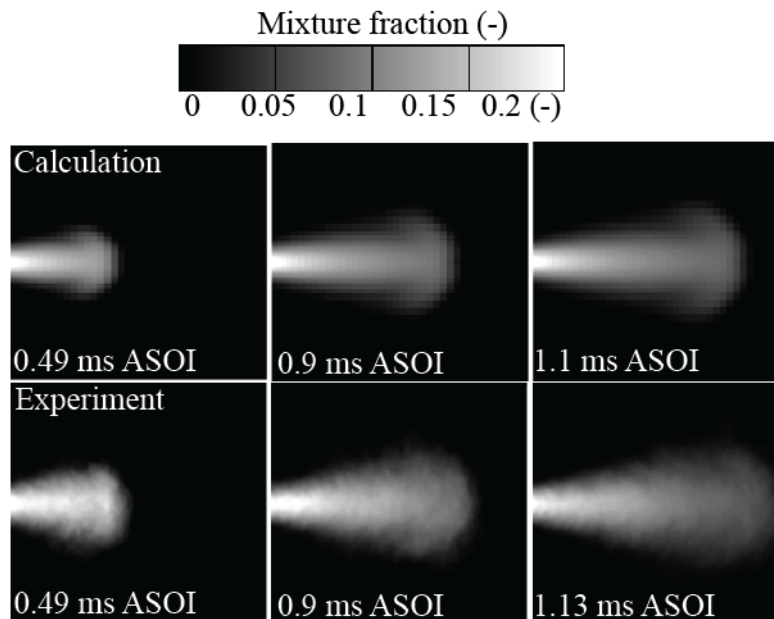


**Figure 46 Comparison of calculated and measured mixture field for Case\_h**

The calculated vapour cloud is in a good agreement with the experimental data at early stage of injection, as it is visible in the first column in Figure 46. In the later stage, a slight underestimation of vapour penetration is noticeable, both at 0.9 ms and 1.1 ms after SOI. Such behaviour corresponds well to the results shown on the left – hand side in Figure 45. The slightly under – predicted vapour penetration may be addressed to too intensive break – up of the liquid core and the droplets which result from the used break – up model constants. In the same figure, the conically shaped vapour cloud is visible, which is a result of turbulent dispersion forces acting on fuel droplets providing the momentum in the radial direction.

The averaged temperature fields for different time steps are shown in Figure 47. The temperature is shown for the range from 700 K – 1000 K, which corresponds to the available experimental data. The lowest temperature, caused by the temperature of the injected fuel, is noticeable in the region near the injection axis, whilst higher temperatures are visible at the periphery of the spray cloud. An increase of the vapour temperature is noticeable at later stages of injection due to the higher amount of heat transferred from the surrounding mixture. It is important to mention that the experimental images of gas mixture are recorded from the lateral position, and therefore they represent the whole spray surface, whilst the simulation results are shown for the planar cut in the middle of the spray cloud.

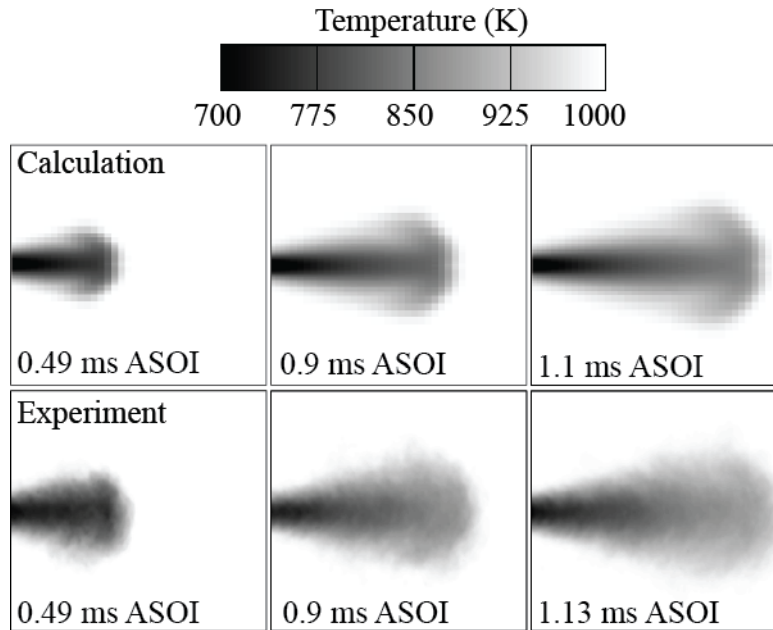


**Figure 47 Comparison of calculated and measured temperature field for Case\_h**

*N – dodecane fuel injection into non – reactive environment*

For further validation of the developed method, the non – reactive n – dodecane spray process was modelled. The same model coefficients, same numerical setup and same discretisation techniques, as those for modelling the n – heptane fuel injection were used. In Figure 48 the liquid and vapour axial spray tip penetrations are shown for two non – reactive spray simulation cases.

The penetration results show a good agreement with the experimental data, especially at the initial stage of injection. However, at the later stages, the vapour penetration is slightly underestimated. The reason for such behaviour, also noticed in the n-heptane cases, may be addressed to the too intensive break – up process and the overrated dispersion of the fuel vapour in the radial direction. This underestimation could be avoided by using different turbulence models.



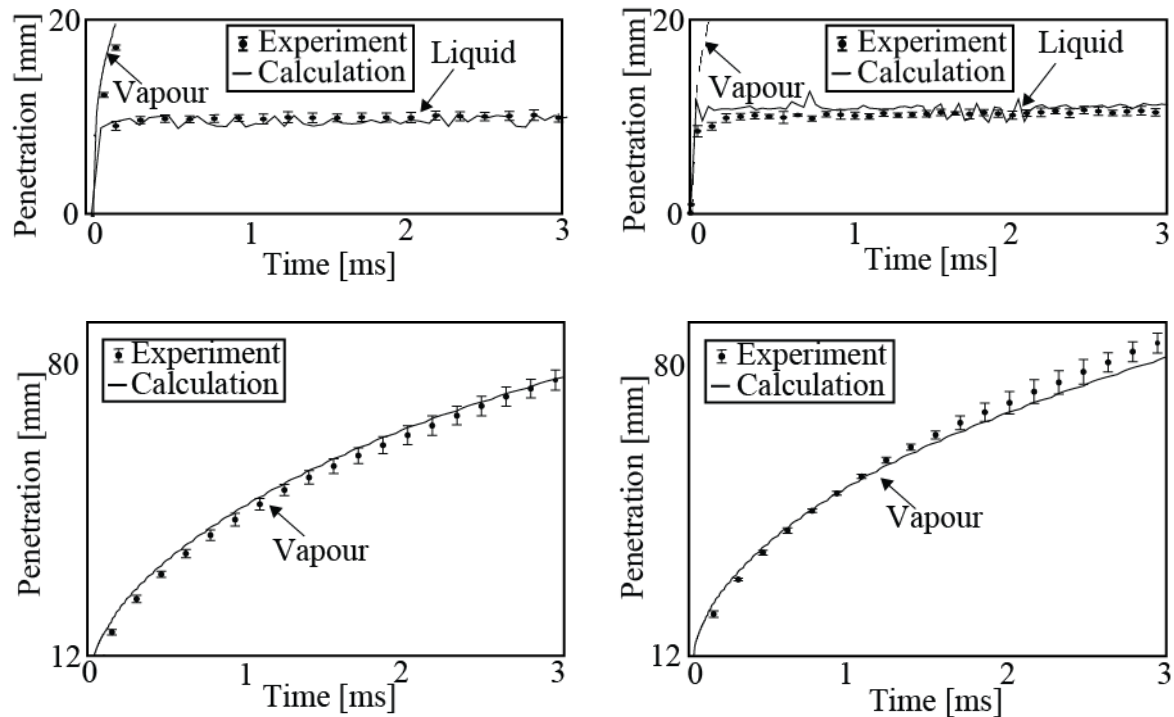


**Figure 48** Comparison of calculated and measured liquid and vapour penetration for Case\_d1 and Case\_d2

Mie – scattered light images were acquired during the quasi – steady period of the spray development. More details on the measurement techniques and experimental research can be found in [115][116]. The first row in Figure 49 shows the comparison of the radial mixture fraction distribution recorded at developed spray state. The injection Case\_d2 shows a higher concentration of the mixture compared to Case\_d1, for the given time step. This can be addressed to the lower CVV pressure and the higher CVV gas temperature. In both cases the mixture is more concentrated in the vicinity of the injector axis. The spray spreading is clearly visible in the radial profiles (results shown at distance 45 mm from the nozzle), and it is more pronounced for Case\_d2 which can be addressed to the lower CVV pressure. The results in the second row show the comparison of the axial vapour mixture distribution at developed spray state for both n – dodecane injection cases. The experimental results were recorded in the axial direction in the range between approximately 10 to 60 mm. At the distance of approximately 10 mm downstream from the nozzle, the vaporization rate of the liquid fuel is more pronounced in Case\_d2 due to the higher CVV temperature. The decrease in the mixture fraction in the axial direction can be addressed to the spray radial movement and the mass shift towards the spray periphery.

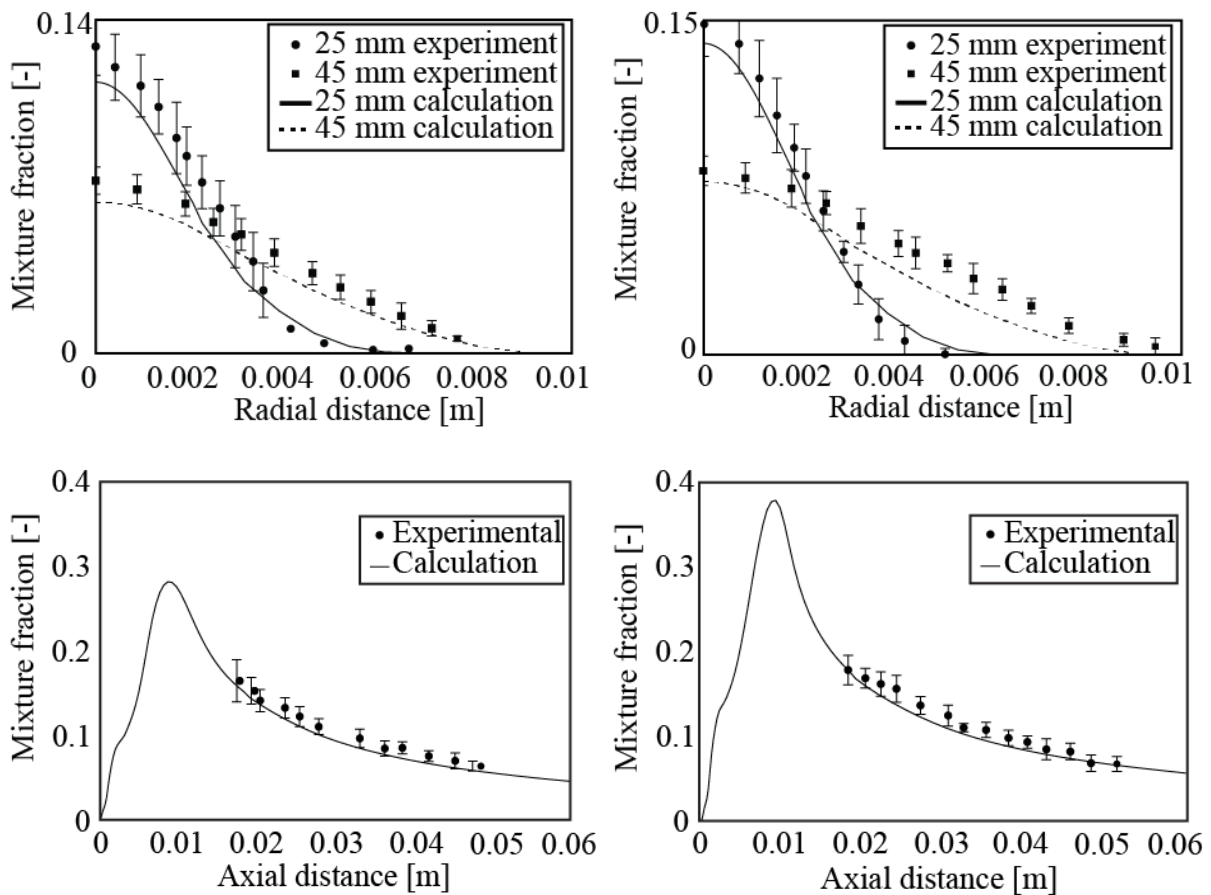


**Figure 49** Comparison of calculated and measured fuel vapour radial (top) and axial distribution (bottom) for Case\_d1 and Case\_d2

The averaged experimental images [19] for Case\_d2 are compared to the modelled results, as shown in Figure 50. The instantaneous images were recorded at developed spray state and the imaging frame is extending from 14.4 mm to 14.1 mm in the radial direction, and from 17.8 mm to 51.6 mm in the axial direction. On the left – hand side a transport of vaporised fuel in the radial direction is noticeable, which is a result of the gas entrainment and dispersion forces. The comparison of the temperature fields shows slightly underestimated modelled gas mixture temperatures which can be addressed to the underestimated penetration of the liquid fuel. This may be a result, either of a slightly underestimated evaporation or of a too strong gas entrainment. A further reason for the differences may arise from different “views” of the experimental and the simulation results (surface vs. planar cut in spray axis).

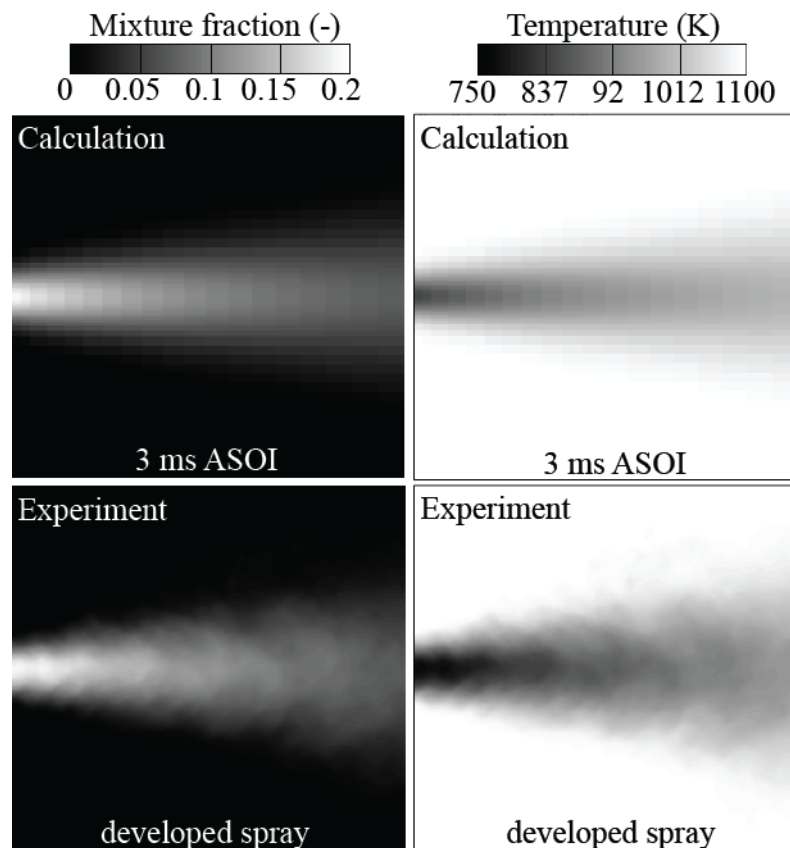


Figure 50 Comparison of calculated mixture and temperature field for Case\_d2

### Reactive spray simulations

After discussing the non – reactive spray cases, the modelling results of the reactive spray cases are presented and compared to the available experimental data. Based on the calibrated spray sub – model coefficients, the combustion process was researched for different oxygen concentrations, fuels, nozzle geometries and CVV conditions. The validation of the reactive spray cases was performed by investigating the LOL, ID and pressure rise. The LOL is defined as the closest distance from the injector with temperature of 1600 K and, in some cases, as a certain threshold value for the OH species concentration. The ID is defined as the time after SOI when the mean ROHR has the maximum positive gradient.

#### *N – heptane fuel injection into reactive environment*

Computational simulation results of reactive n – heptane spray cases are presented within this section. The main difference between the reactive and non – reactive spray cases is the presence of the oxygen species in the surrounding gas environment, as seen in Table 13. On the left – hand side of Figure 51, the calculated and measured LOL results are compared. Due to the mixing of evaporated fuel and hot environment, the vapour temperature increases and the

combustion process starts. This leads to a rapid temperature rise, and production of chemical species that further react following the rules of the used chemistry mechanism. The comparison to the experimental data shows a good agreement but a slight underestimation of the LOL for all three modelled injection cases can be observed. This may be addressed to the overrated atomization process, discrepancies in the initial conditions or to the used chemistry mechanism. The LOL under prediction was expected, since in the non – reactive spray modelling the penetration of the vapour phase was slightly underestimated. However, the LOL trend is correctly described where a higher oxygen concentrations led to lower LOL values, corresponding well to the experimental data. The ID for the examined cases is shown on the right – hand side of Figure 51. A good agreement to the experimental data is achieved with a slight ID overestimation for cases with 15 % and 21 % oxygen concentration. However, the decreasing trend was correctly captured. The used method and the defined numerical setup shows the correct chemical and physical behaviour, where the earlier occurrence of the combustion process can be addressed to the higher oxygen concentration.

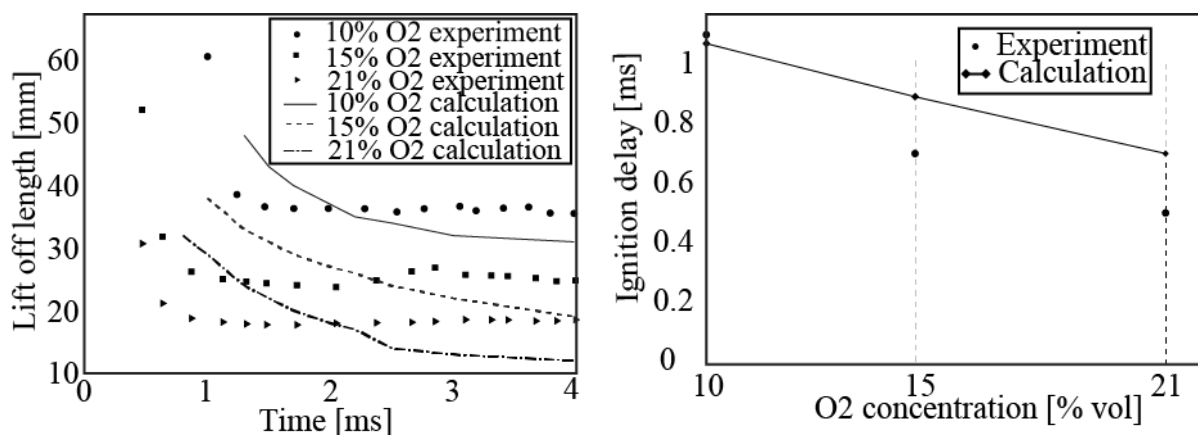


**Figure 51 Comparison of calculated and measured lift off length and ignition delay for n – heptane spray cases**

#### N – dodecane fuel injection into reactive environment

In this section, the developed method was employed for modelling reactive spray processes where liquid n – dodecane fuel was injected into the pressurized CVV. The liquid fuel was injected through a smaller nozzle under different CVV/injector conditions, as seen in Table 13. Figure 52 shows penetration of the vapour fuel mixture for the reactive spray Case\_d\_r. The black solid line represents the calculated penetration of vaporized fuel, whilst the black dots represent the available experimental data. Initially, the modelled vaporised fuel

follows the measured penetration curve. At approximately 20 mm in the axial direction and 0.35 ms after SOI the fuel vapour is completely consumed. At this point another species must be tracked to record the vapour cloud development. For that reason, the OH radical species was tracked. The OH species penetration is shown for three different time frames (1, 2 and 3 ms after SOI) and a very good agreement to the experimental data can be observed.

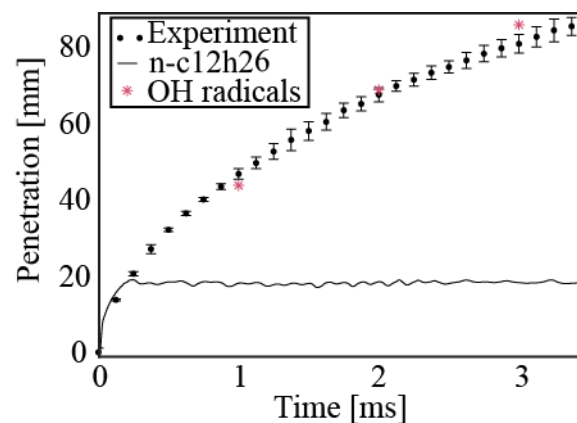


**Figure 52 Comparison of calculated and measured vapour penetration for Case\_d\_r**

The left-hand side of Figure 53 represents a qualitative comparison between the calculated and measured combustion progress for Case\_d\_r. In shown planar cuts, the OH radical concentration is shown at four different calculation time steps: 0.2, 0.3, 0.5 and 1 ms after SOI. The maximum colour bar value is chosen as 2 % of OH concentration that was recorded at the developed spray state. Below the red dashed lines the available chemiluminescence experimental data are shown. The modelled results are obtained from a 2D computational domain with symmetry boundary conditions where a 5° sector of the whole domain was calculated. The benefit of the developed method for describing the spray and combustion processes should be noticeable in cases where the combustion process takes place near the nozzle hole. The modelled LOL for the observed case is 10, 8 and 7 mm at 0.3, 0.5 ms and at developed state, respectively. This corresponds well to the experimental LOL value which is given with approximately 7.6 mm for the developed spray state. The calculated ID time is slightly over – predicted. In the calculation, the combustion process starts around 0.2 ms after SOI, whilst in the measurements the combustion process was recorded around 0.11 ms. Such behaviour was expected based on the observations and conclusions from the previous sections. It is worth to mention that the same spray model parameters, obtained from the calibration of the non – reactive Case\_h, have been used for all simulation cases.

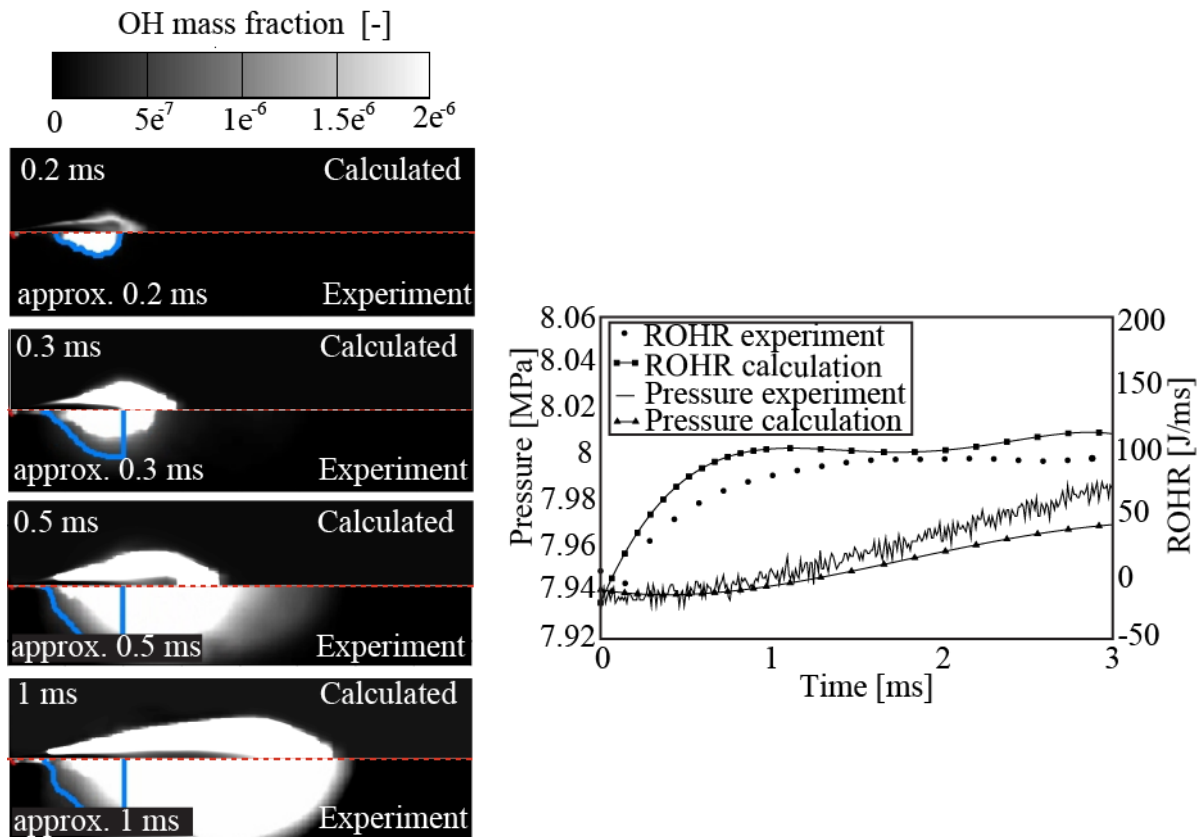


**Figure 53 Comparison of calculated and measured OH results of mass fraction field (left), pressure rise and rate of heat release profiles**

On the right – hand side of Figure 53 the pressure rise and ROHR is shown. An almost linear pressure trend is noticeable with a slight inclination at 0.2 ms after SOI which can be addressed to start of the combustion process. The oscillatory behaviour of the ROHR was averaged for better visibility, and a good comparison to the experimental data can be observed. The ROHR steeply increases in the early stage of the combustion process, and the highest slope is noticeable around 0.2 ms after SOI. However, the ROHR stays at the same level from around 1 ms after SOI when the flame reaches the developed state.

### 3.8. Euler Eulerian engine modelling

This section illustrates the capabilities of the developed method for simulating complex engineering applications such as IC diesel engines. The spray process was modelled with the Euler Eulerian size – of – classes approach which has advantages in description of the physical processes occurring in the near nozzle region. The combustion process was modelled by solving the chemical reactions within the gas phase by using reaction mechanisms. In the vicinity of the nozzle it is considered that the Eulerian spray approach is fairly efficient. This approach is extended to the multi – continuum approach when the discrete phase is divided into droplet classes, where for each class a set of conservation equations is solved. By increasing the number of classes the resolution of the droplet size distribution is enhanced, but also the computational effort is increased. Even though such approach is considered suitable for modelling the dense spray region, it can be used for the whole spray domain as it is shown in the results of this section. The calculated results are compared to the available experimental data, and to the results obtained with Euler Lagrangian DDM approach.

#### 3.8.1. *Experimental data and numerical setup*

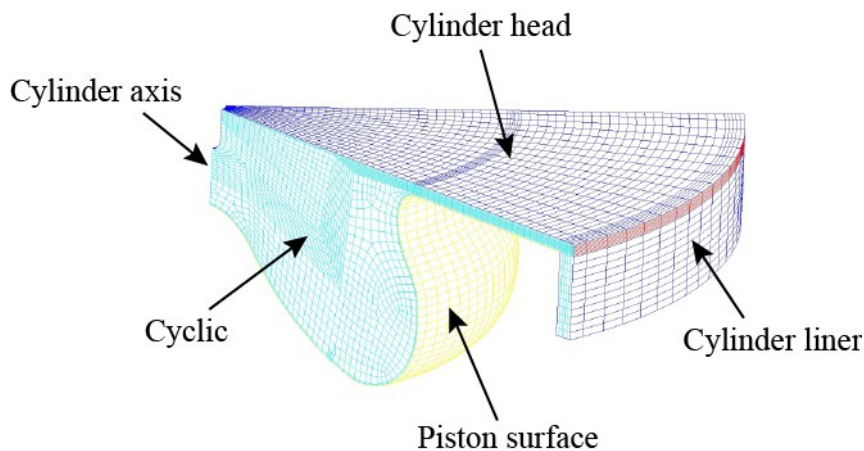
A new method was used for modelling a real IC engine configuration, where the validated spray approach was used together with the chemistry mechanism to adequately describe the dense spray region and combustion processes. The geometry of the IC engine combustion chamber and the 7 – hole injector are symmetrical in design. Therefore, the engine calculation domain was constructed as 1/7 of the total engine geometry considering the fuel flow from a single nozzle hole and the computational effort was significantly reduced. The engine computational mesh contains approximately 37400 control volumes at the TDC, and approximately 112000 control volumes in the BDC. During the piston movement, the mesh is rezoned due to the deformation and high aspect ratio of some computational cells. The rezone procedure is a mesh replacement at defined crankshaft position, where the mesh has the same outer shape but a different number of control volumes, used to avoid undesirable cell distortions. To provide an adequate wall treatment on the modelled results, a 2 – cell boundary layer was created in the vicinity of the defined wall boundary selections.

The stroke, bore, compression ratio and the engine speed of the investigated engine configuration are 93.15 mm, 81 mm, 15.6:1, and 2000 rpm, respectively, as shown in Table 14.

**Table 14 Engine specifications**

<b>Stroke</b>	93.15 [mm]
<b>Bore</b>	81 [mm]
<b>Spray angle</b>	17.5 [°]
<b>Compression ratio</b>	15.6 [-]
<b>Number of injection holes</b>	7
<b>Engine speed</b>	2000 [rpm]

The defined boundary selections and the generated computational mesh at position of 720 °CA are presented in Figure 54. The cylinder geometry is assumed to be symmetric around the cylinder axis and therefore, the periodic conditions are applied on the cyclic boundary selections. A moving, constant temperature wall boundary condition is applied to the piston surface, whilst a constant temperature condition is prescribed for the fixed cylinder head selection.

**Figure 54 Computational mesh used for engine calculation**

More details on the used computational mesh are shown in Figure 55. The inlet selection is a real representation of the nozzle orifice discretized with 60 faces. This yields the minimum cell size on the inlet selection of approximately  $6 \times 30 \mu\text{m}$ . The centre of the inlet selection is located at 0.000, 0, -0.0016 m, whilst the spray angle was set to 17.5 deg. The liquid fuel was injected into the cylinder through the nozzle orifice with diameter of 125  $\mu\text{m}$ .



Introducing the European biofuels directive (2003/30/EC) in 2003, an obligation to ensure a minimum level of used biofuels is enforced to all member states of the European Union. In the last decade the maximum permitted amount of bio – content was 5 %, but, according to the EU directive, the proportion of biofuel for road transport use must increase over the coming years. To ensure that fuels available for road transport are fit for this purpose, the European Standards Committee (CEN) developed the EN 590 diesel standard. Recently, CEN updated the maximum amount of bio – content up to 7 %, compared to the 5 % previously allowed. To research the influence of the biofuel addition, the EN 590 B7 mixture was modelled with new method developed in this thesis. The reaction mechanism used to describe the EN 590 B7 combustion process consists of 45 species and approximately 180 chemical reactions.

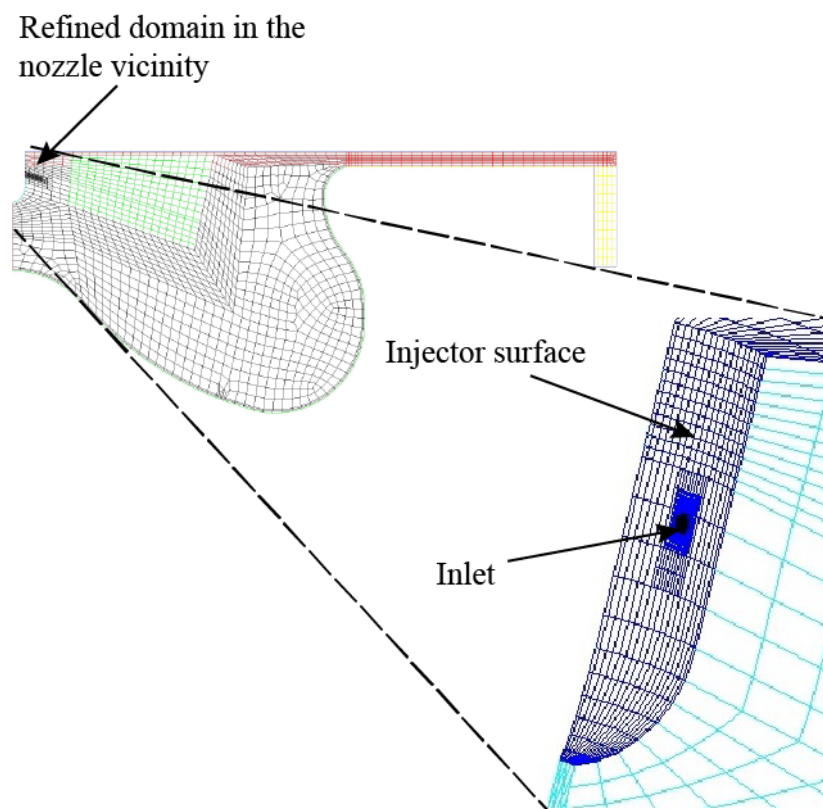


**Figure 55** Details of the computational mesh used for engine modelling

The combustion characteristics of the modelled IC engine are shown in Table 15. The engine simulations are performed from 585 °CA until 840 °CA covering the engine compression and the expansion stroke period.

**Table 15 Combustion characteristics of the simulated operating point**

<b>Engine speed (min<sup>-1</sup>)</b>	2000	<b>Swirl (min<sup>-1</sup>)</b>	4740
<b>SOI (°)</b>	718.2	<b>Fuel temperature (K)</b>	317.11
<b>EOI (°)</b>	731.3	<b>Injected mass (mg)</b>	4.121
<b>EGR composition (kg/kg)</b>			
O <sub>2</sub>	0.22797	CO <sub>2</sub>	0.00331
N <sub>2</sub>	0.76718	H <sub>2</sub> O	0.00155

For all CFD simulation performed in this section, five Eulerian classes were defined. One class was defined as the gas phase, four as droplet classes and one class as the bulk liquid entering into the domain from the nozzle orifice. Fuel droplets are sorted into classes according to their diameter in ascending manner with assigned diameters of 5, 20 and 40  $\mu\text{m}$  for the droplet classes and 125  $\mu\text{m}$  for the bulk liquid class. The number of classes and their diameters were chosen from the experience made in previous research studies [117][118][60], and the available CPU power. The primary break – up process was modelled according to the DCI break – up model, whilst the secondary break – up process was modelled according to WAVE break – up model. The fuel evaporation was modelled according to the Abramzon – Sirignano evaporation model. The influence of droplet distortion on the drag coefficient is taken into consideration, and also the droplet dispersion due to the turbulent forces.

At the inlet boundary condition, the injection velocity was calculated from the measured rate of injection curve and the used velocity profile is shown in Figure 56. The inlet selection is defined with volume fraction of the bulk liquid phase equal to 0.72. The rest of the inlet is defined as gas phase with velocity of 0 m/s. The inlet selection surface on the computational mesh is approximately 39 % bigger than the real orifice effective cross section and therefore, to match the inlet mass flux, the volume fraction of the bulk liquid phase was reduced.

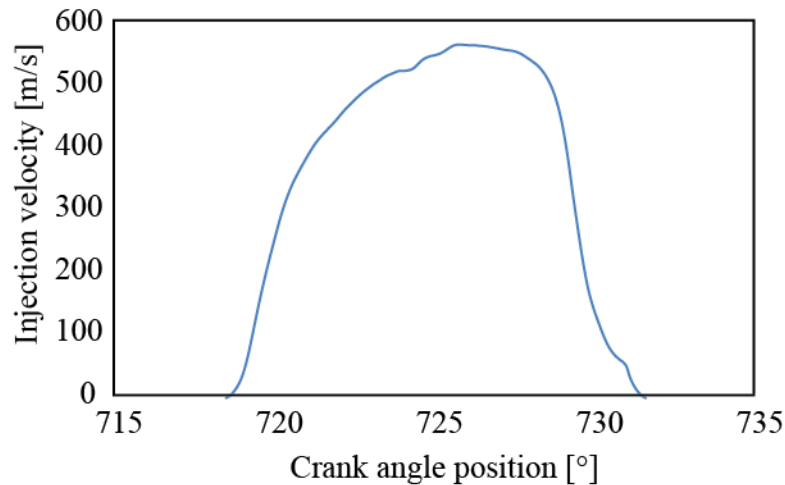


**Figure 56 Injection velocity profile**

The in – cylinder thermodynamic state and flow distribution prior to the injection of liquid fuel were obtained through the simulation of the compression stroke, period from 585 – 718.2 °CA. The initial conditions used for the IC engine calculation defined at 585 °CA are summarized in Table 6.4.

**Table 16 Initial conditions for engine simulation**

<b>Pressure</b>	216687 [Pa]
<b>Temperature</b>	363 [K]
<b>Gas composition</b>	EGR
<b>Turbulent kinetic energy</b>	10 [m <sup>2</sup> / s <sup>2</sup> ]
<b>Turbulent length scale</b>	0.002 [m]
<b>Number of injection holes</b>	1

Modelling the IC engine configuration differs from the validation cases discussed in previous section. In the validation cases, a 2D axisymmetric stationary computational domains were used. The control volume size near the orifice in spray axis direction was approximately 30 μm, and the overall domain was refined with small computational cells with fixed domain boundaries. On the other hand, in modelling of a real engineering application such fine discretisation would result in unreasonably high number of control volumes and unaffordable, long computational time. In this section the same time discretisation, which was used for the

Lagrangian DDM approach, is used for Euler Eulerian CFD simulation of the IC diesel engine. The used time discretisation settings are shown in Table 17. The smallest time step size was used at the crank angle positions where the injection and combustion process occurred.

**Table 17 Time discretization for engine simulation**

Up to	Crank-angle [°]	$\Delta\alpha/s$
up to	700	$1/8 \times 10^{-5}$
up to	760	$0.2/1.67 \times 10^{-5}$
up to	800	$0.5/0.42 \times 10^{-5}$
up to	840	$10^{-5}$

The CDS scheme was used for the convective term in the continuity equation, whilst a hybrid between the CDS and the upwind scheme with a blending factor of 0.5 was used for the convective terms in the momentum equations. The upwind discretization scheme was used for the convective terms in the scalar equations. The convergence of the solution is achieved with a proper set of under-relaxation factors and sufficiently small time steps to fully account the dynamic spray behaviour. The turbulence was modelled using the advanced  $k-\zeta-f$  turbulence model. Of particular advantage is that this model is sufficiently robust to be used for computations involving grids with moving boundaries, and highly compressed and swirl flows as occurring in IC diesel engines.

### 3.8.2. Results and discussion

AVL AST, GmbH provided the measured data of mean pressure, calculated temperature and rate of heat release for the engine compression and expansion strokes, as shown in Figure 57.

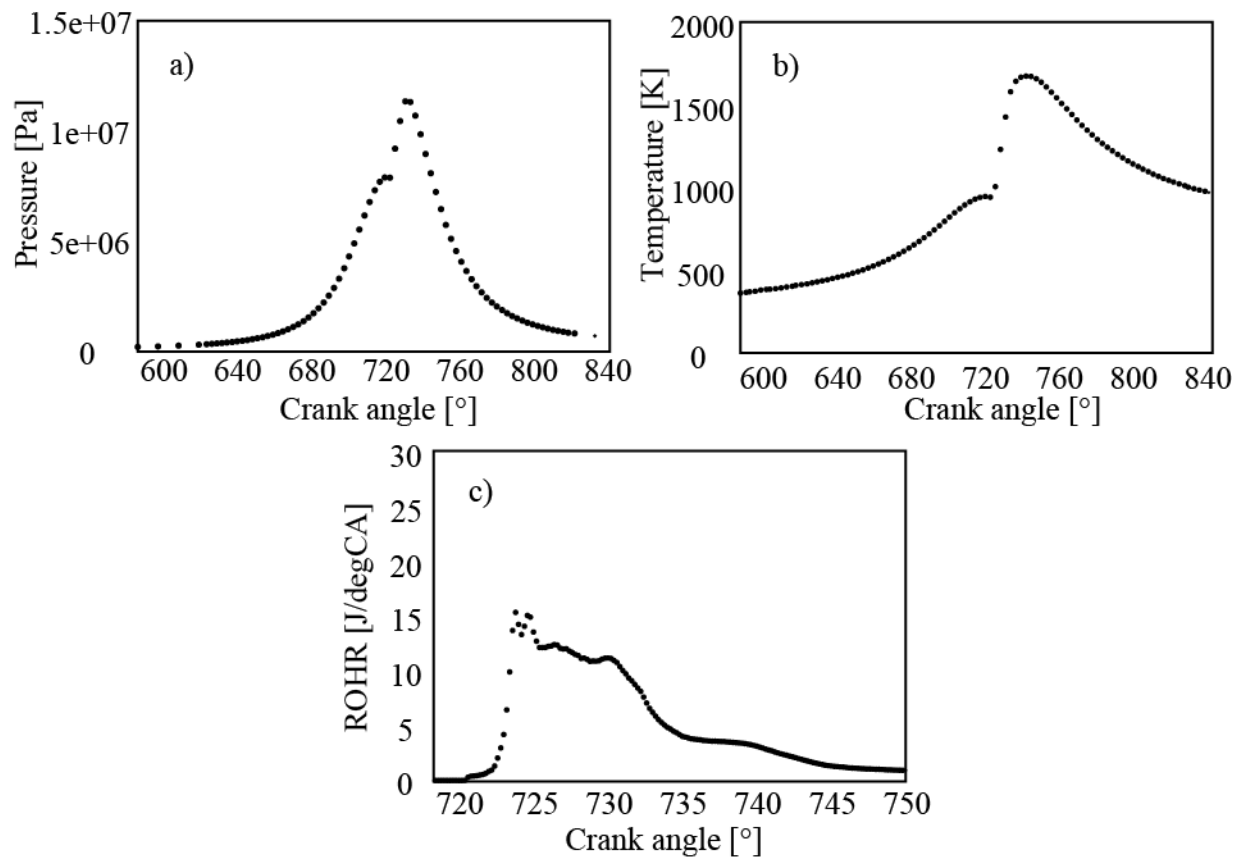


**Figure 57** Experimental results of mean pressure a), mean temperature traces b) and rate of heat release c)

After the fuel injection, due to the elevated temperature conditions enforced by the compression stroke, the atomized fuel starts to evaporate and a certain liquid mass is transferred to the gas phase. After reaching the ignition temperature, the vaporized fuel ignites and starts to combust leading to a rapid rise of the in – cylinder pressure and temperature. This behaviour is shown in Figure 58 and Figure 59, where a rapid rise of temperature and pressure is visible around 720 °CA. After the fuel is ignited, the flame front propagates through the combustion chamber and consumes the evaporated fuel. At later crank angle positions, when the flame is in a completely developed state, the mean temperature reaches maximum values around 1700 K. Afterwards, at the TDC, the expansion stroke starts and the piston moves in the opposite direction towards the BDC. With the piston motion the cylinder working volume is enlarged, which results in the in – cylinder pressure and temperature decrease. For both modelling approaches a similar development of pressure and temperature was noticed and a good comparison to the experimental data was achieved.

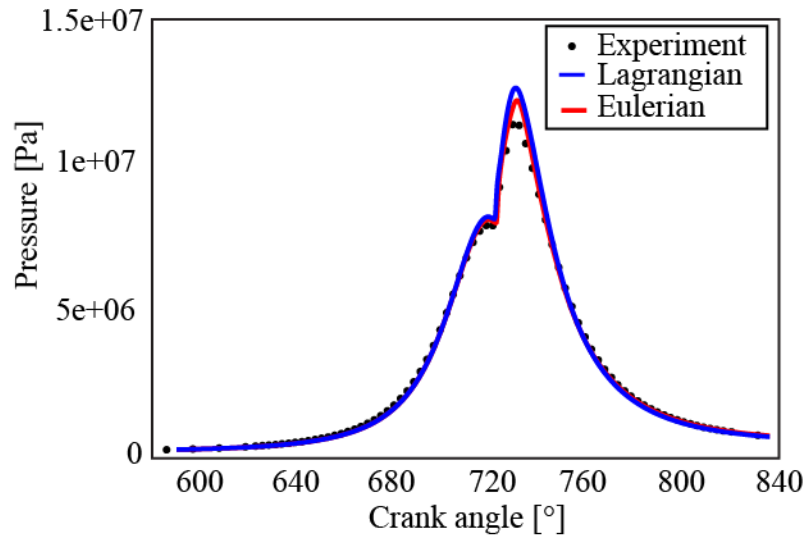


**Figure 58 Comparison of calculated and measured in – cylinder mean pressure**

In Figure 59 one can observe a rise in the mean in – cylinder temperature traces due to the compression stroke where the cylinder working volume is reduced, and the temperature is increased from the initial state of 363 K up to approximately 900 K. Such a high temperature is necessary to promote the evaporation of the fuel droplets. At the crankshaft position around 722.5 °CA, the vaporized fuel starts to combust and the temperature increase is more pronounced. The temperature peak can be observed at 735 °CA, several crank angles after the end of injection. Afterwards, the mean in – cylinder temperature is decreased which can be addressed to the increase of the cylinder working volume during the expansion stroke and the heat exchange through the engine cylinder walls.

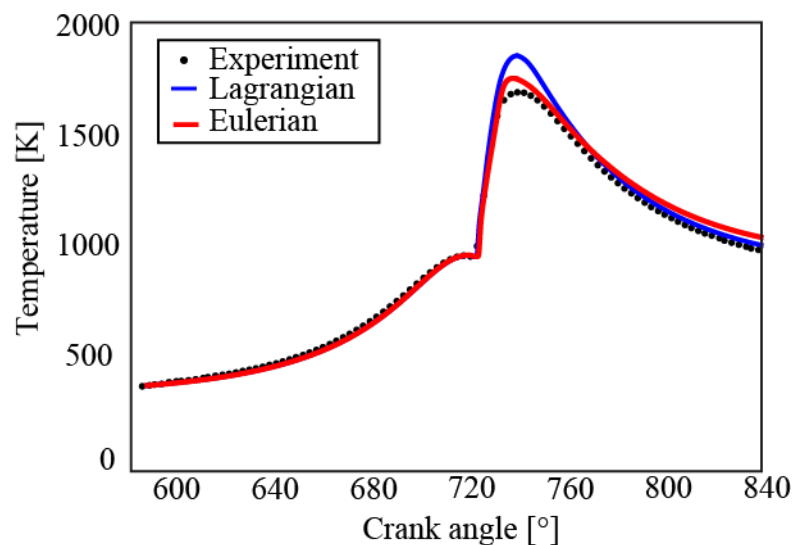


**Figure 59 Comparison of calculated and measured in – cylinder mean temperature**

The heat release due to the combustion process is shown in Figure 60. It is expressed in energy unit per crank angle, where a good comparison to the measured data can be observed for both modelling approaches. The heat is released after the fuel jet atomization when fuel vapour is produced and combusted. The highest increase in heat release is noticeable around 722.5 °CA which is addressed to occurrence of the combustion process. The heat release decreases during the expansion stroke when the reactive species are converted to product species according to the used chemistry mechanism.

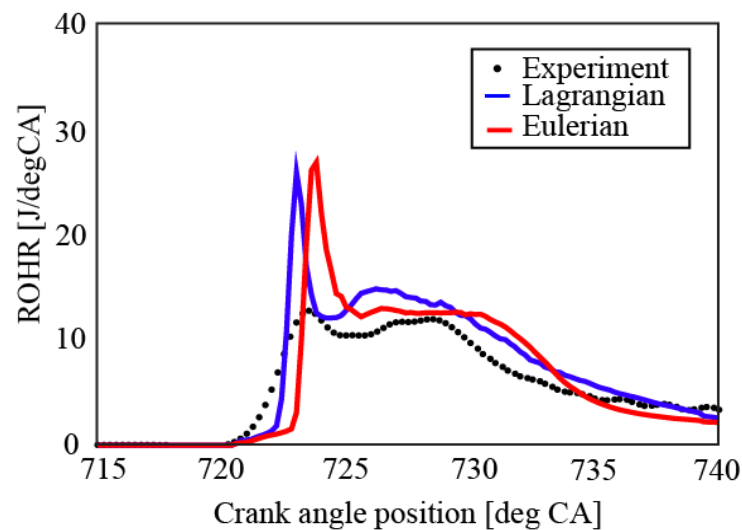


**Figure 60 Comparison of calculated and measured rate of heat release**

The cutting plane used to discuss the modelled results is defined in the middle of the spray axis and computational domain, as shown in Figure 61.

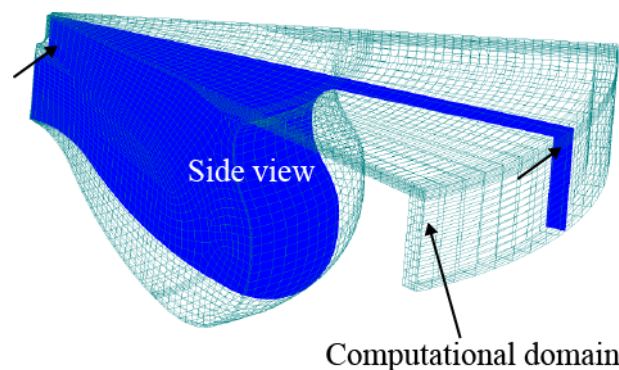


**Figure 61 Cutting plane used for analysing the calculated results**

The cutting plane is located in the spray axis and therefore, quantities such as atomization rates, vaporized fuel concentration, and temperature field can be visualized and discussed. The gas phase velocity field for three different crank angle positions is shown in Figure 62. The highest gas phase velocity is noticed in the nozzle vicinity where the liquid fuel is injected into the computational domain. The gas phase is accelerated due to the liquid – gas mixing to approximately 250 m/s and 60 m/s for the crank angle positions at 720 and 730 °CA, respectively. This corresponds well to the velocity of the injected liquid fuel, shown in Figure 56. The accurate description of the gas velocity field can be addressed to the fine mesh resolution, adequate description of the liquid – gas relative velocity and therefore, reliable interphase momentum exchange. A good description of the interphase interaction is one of the main benefits of the Euler Eulerian size – of – classes spray modelling approach. Lower momentum transfer is predicted with the Euler Lagrangian DDM approach, as shown in the upper – side of Figure 62. Throughout the simulation, the mass of the liquid fuel is reduced as a result of the evaporation process which is a consequence of heat transfer from the surrounding gas by conduction and convection processes. The produced fuel vapour constantly mixes with the hot surrounding gas phase. The main mechanisms responsible for gas mixing within the IC engine chamber are convection and diffusion [36][107][108][109].

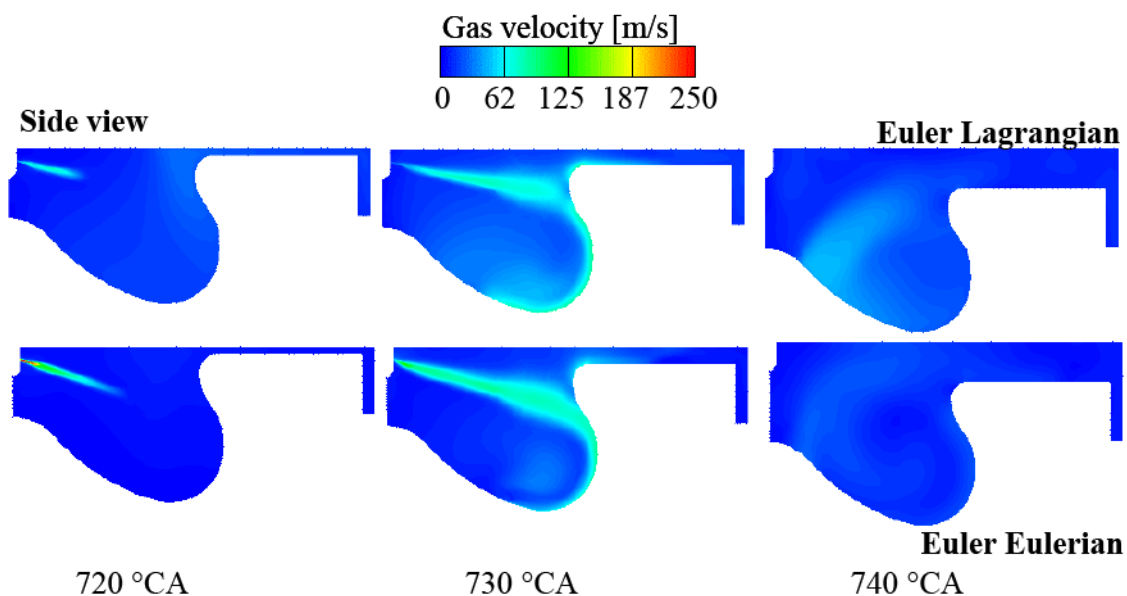


**Figure 62** Calculated gas velocity field at different crank angle positions



Figure 63 shows gas phase temperature distribution recorded at three different crank angle positions, for two aforementioned modelling approaches. At the initial stage, the liquid fuel with temperature of 317.11 K is injected into the computational domain. It disintegrates into smaller diameter droplets which increases the surface available for the evaporation process. Cooling of the gas phase with the liquid core is visible for the crank angle position at 720 °CA. As it was stated, the liquid fuel evaporates, the vaporized fuel is further compressed and the mean cylinder temperature is increased. At the crank angle position at approximately 722.5 °CA, as it is visible in Figure 60, the conditions in the combustion chamber are such that the combustion process is triggered. The combustion starts in the high temperature region at the periphery of the vaporized cloud. The flame front develops through the combustion chamber and the heat is released from the chemical reactions until the reactant species are consumed. The peak in in-cylinder pressure and temperature is found around 735 °CA, slightly after the end of injection.

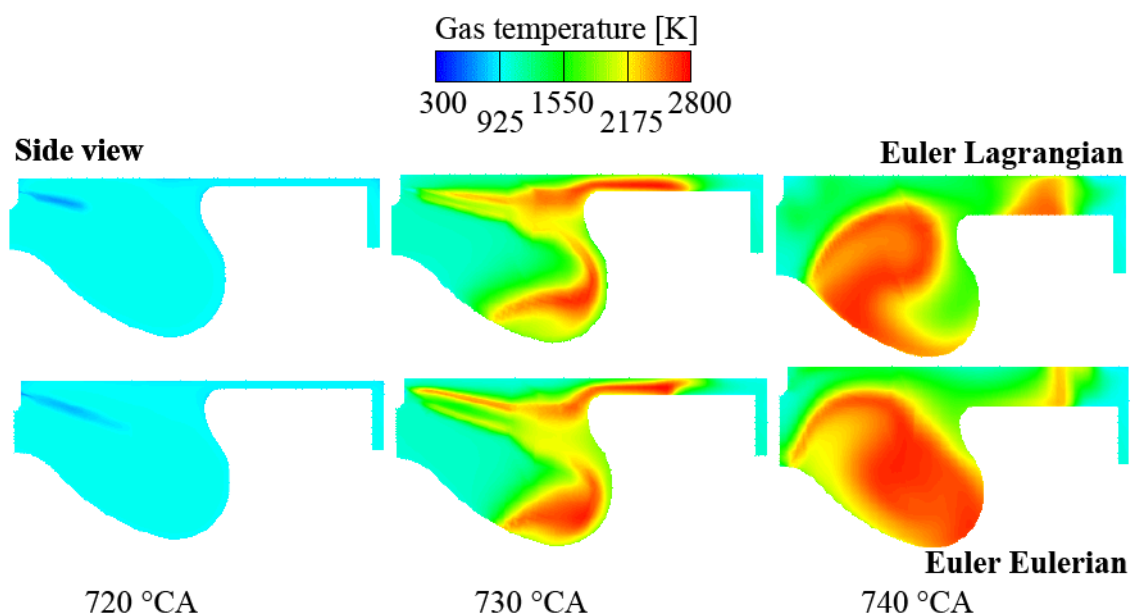


**Figure 63** Calculated gas temperature field at different crank angle positions

It could be stated that by using the Euler Eulerian spray modelling approach a good description of all spray regions is achieved, including the dense spray region. This leads to a reliable description of fuel evaporation and fuel – air mixing processes. Consequently, with a good prediction of the spray process, a reliable combustion processes was achieved.

## 4. CONCLUDING REMARKS, CONTRIBUTION AND FUTURE WORK RECOMMENDATIONS

### 4.1. Thesis conclusion

Numerous reliable and validated methods have to be used to model turbulent reacting multiphase flows in a real combustion applications. In this thesis, an advanced modelling method was developed for the computational simulation of highly turbulent reactive multiphase flows. The method was developed by combining the Euler Eulerian size – of – classes approach that is suitable for modelling the dense and diluted spray regions, together with the chemistry mechanism that was used for modelling the combustion process. Such a method was validated on various spray cases, both simplified and real engineering applications. The main aim of the developed method is a good description of the fuel – air mixing process, focusing on the near nozzle region, and therefore achieving a reliable modelling of multiphase combustion processes. In the following part the conclusions derived for each thesis section, defined in the chapter 1.3 Objective and hypothesis of research, are shown.

#### 4.1.1. Eulerian Lagrangian modelling

In this section of the thesis the spray process was modelled by employing the Euler Lagrangian DDM model. The combustion was modelled by using the common ECFM 3Z combustion model, whilst the soot and the NO<sub>x</sub> emissions were modelled by using the kinetic and extended Zeldovich models, respectively. The aim of this section was to gain insight into advantages and disadvantages of the Euler Lagrangian DDM spray model.

Concluding remarks are:

- The investigation of in – cylinder fluid flows and chemical reactions was performed and the mathematical models for prediction of the in – cylinder processes were presented.
- The mathematical models of spray and pollutant emission formation previously implemented into a commercial CFD code FIRE® were validated.
- Combustion parameters such as start and end of injection, swirl number, injected mass and exhaust gas mass fraction were varied, and their influence on the emission was investigated.
- Modelled results show the influence of the combustion system parameter variations on in – cylinder pressure, NO<sub>x</sub> and soot formation trends.
- Pressure and temperature traces, heat release and pollutant formation show a good agreement with the experimental data.

- The disadvantages of the Lagrangian DDM model were noticed. Such model suffers from poor description of the interfacial momentum transfer in the near nozzle region, lower statistical convergence, it is mesh dependant, and it suffers from several disadvantages related to the MPI performance.

#### 4.1.2. Parametric study of spray sub – models

The validation of the Euler Eulerian size – of – classes approach was conducted by comparing the modelling results against the available experimental data. Overall, it can be stated that the used approach adequately describes the liquid and fuel vapour penetrations in comparison with all observed experimental cases, covering a wide range of high pressure injection conditions. The Euler Eulerian multiphase spray approach showed the capability of predicting the impact of the rail pressure on the vapour and liquid spray tip penetrations. Furthermore, it was shown that the used approach is capable to adequately describe the highly turbulent liquid fuel injection, and it can serve as valuable tool in the development process of modern fuel injection systems.

Concluding remarks are:

- An Eulerian multiphase spray modelling concept, applying the method with constant size class diameters assigned to each of the liquid droplet phases, was presented.
- The primary break – up, secondary break – up, and evaporation models were utilised to model the fuel spray injection with different injection and chamber pressure combinations.
- The increase of the injection pressure results in the increase of the fuel vapour penetration, but it has only minor influences on the liquid fuel penetration.
- The increase of the chamber pressure had the opposite effect. Due to the higher surrounding gas mixture pressure and increased density, a larger spray angle with lower tip penetration was observed.
- The final set of model coefficients was derived by performing the model parameterization on the reference case, where the influence of individual model coefficients was examined.
- Changing the model coefficients influences the droplet size and atomization rate. This results in different temporal and spatial droplet-vapour distributions.

Concluding remarks from modelling the primary atomization model:

In this section of the thesis computational simulations of liquid fuel atomization focusing on the processes in the near nozzle region were performed. The atomization process was modelled by employing the Euler Eulerian size – of – classes approach. The simulation results were compared to available DNS results where the axial and radial mixture volume fractions were researched.

- At small distances, in the near nozzle region (in the observed case at 5 x nozzle diameter distance in the axial direction) the liquid core is unattached. Further downstream, the liquid mass detachment due to the primary atomization is visible.
- The calculated volume fraction is higher near the spray axis, comparing to the DNS data. This could be addressed to underestimated modelled radial velocity arising from the droplet detachment from the liquid core.
- Further downstream the radial liquid volume fraction corresponds better to the DNS data.
- The liquid volume fraction decreases along the axial direction, which is a consequence of the primary atomization of the liquid jet. The liquid mass is detached from the liquid core and an unstable ligaments and droplets are formed.

*4.1.3. Validation of the WAVE secondary atomization model*

In this section of the thesis a high-pressure diesel fuel injection into a pressurized CVV filled with non – reactive gases was modelled. The influence of the nozzle hole diameter and the nozzle channel length on the spray characteristics was examined. The spray penetration, spray angle, droplet distributions and the SMD were thoroughly analysed and compared to the available experimental data. The common WAVE model was modified where the target droplet diameter was taken as the arithmetic mean value between parent and original target droplet diameter.

Concluding remarks are:

- Four non – reactive spray operating points were simulated.
- A small influence of the nozzle channel length on the liquid penetration was observed.
- A small influence of the nozzle hole length and nozzle diameter on the spray angle was observed. This corresponds well to the data found in the literature. A stronger influence on the spray angle could be achieved by variations in chamber and injection pressures.

- The WAVE model in the Euler Eulerian size – of – classes approach, is found to be sensitive to the mesh resolution and the number of Eulerian droplet classes. Therefore, a modification of the model was performed.
- The global SMD is found to be similar for all modelling cases were a small influence of the bore length and diameter was observed.
- For the observed cases the spray droplet cloud was consisting of droplets with diameters between 1 and 20  $\mu\text{m}$ .

A good agreement between modelled and measured volume and number based droplet size distributions was achieved.

#### 4.1.4. *O'Rourke collision model*

The aim of this section was to modify and to implement the O'Rourke collision model within the Euler Eulerian size – of – classes approach framework. As a results, the collision process can be calculated for defined collision interfaces. The implemented model was verified on a simplified case with two colliding droplet jets.

Concluding remarks are:

- The O'Rourke collision model was adjusted for the Euler Eulerian approach and it was verified on a 2D domain.
- The influence of the collision model on the SMD distribution was discussed, and the introduced constraints regarding mass exchange were presented. These constraints allow collision process calculations for defined Eulerian collision interfaces.
- The mass exchange from the collisions process results in a change of the droplet size and droplet number distributions.
- A clear influence of the collision model on the colliding jets was noticed in terms of SMD increase.

#### 4.1.5. *Verification of the developed multiphase combustion method*

The reactive spray process was modelled by using the Euler Eulerian size – of – classes approach, and the combustion process was modelled through chemical kinetics by solving general gas phase reaction equations. The method was initially verified on the simplified combustion case.

Concluding remarks are:

- The concentration of fuel vapour arises due to the evaporation process and the reactor mean temperature decreases.

- The combustion process leads to decrease in fuel vapour concentration, oxygen depletion and a rise of the heat release.
- After the reactant species have been completely consumed, the combustion process is finished and the mixture temperature reaches a stationary value; the heat is not released by the reactions anymore.
- The specific multiphase combustion cases provided the same results as the single phase combustion approach, which was considered as a verification proof of the implemented method.
- The method was implemented into the commercial CFD software and can be used on MPI simulations for both the stationary and moving meshes including the rezone and restart options.

#### 4.1.6. *Validation of the developed multiphase combustion method*

Several non – reactive and reactive spray cases with n-dodecane and n-heptane fuel were modelled to acquire the best set of spray model parameters for the observed injection system. The fuel – air mixing process was validated by comparing liquid jet and vapour development to the available experimental data from the ECN database.

#### Concluding remarks regarding the non – reactive spray modelling:

- The radial/axial mixture distributions, and the liquid/vapour penetrations were compared to the available experimental data.
- The method successfully captured the influence of the nozzle diameter, fuel inlet conditions and CVV thermodynamic state on the overall spray development.
- Due to the turbulent dispersion force, fuel droplets and vapour tend to move in a radial direction and form a conically shaped spray cloud. Radial movement reduces the liquid jet penetration.
- In the nozzle vicinity, the liquid jet is more concentrated around the spray axis, whilst further downstream a wider mixture distribution was noticed.
- The lower vapour penetration may be addressed to a slightly overrated break – up of the liquid core and liquid droplets which is a result of the used model constants.
- Higher CVV pressure leads to higher spray spreading and to decreased vapour axial penetrations. The decrease of the mixture fraction in the axial direction can be addressed to the mass shift to the spray periphery due to the radial forces.

Concluding remarks regarding the reactive spray modelling:

- An increase in the ambient oxygen concentrations leads to lower LOL and ID values. This behaviour corresponds well to the experimental data.
- A slight underestimation of the LOL and slight overestimation of the ID was observed. This may be addressed to the overrated atomization process, discrepancies in the initial conditions or to the used reaction mechanism.
- The overall spray characteristics, LOL and ID trends were described correctly.
- The ROHR and pressure change due to the combustion process were found to be in good agreement with the experimental data.

**4.2. Thesis contributions**

The thesis expected contributions are:

- The validation of the Euler Lagrangian DDM model was performed on a real engineering combustion systems. The previously implemented spray and emission models were used to show the ability of the used CFD code to predict the pollutant emissions. The CFD modelling was performed on a computational domain with moving boundaries with included rezone procedure.
- The validation of the primary and secondary atomization models within the Euler Eulerian multiphase spray module was performed. The Diesel Core Injection (DCI) primary atomization model was thoroughly compared to DNS simulation results from the literature. The secondary atomization model was modified to match the global SMD, and global number and volume distributions. A deeper insight into the primary and secondary atomization processes was provided, and a recommended set of model coefficients was found.
- The nozzle file interface, used for coupling nozzle flow and spray simulations, was enhanced for full MPI and flexible nozzle format capability. The enhancement was done in AVL FIRE® for the Euler Eulerian spray model, and the same methodology was used for coupling the nozzle flow and ELSA spray simulations.
- To accurately model near nozzle processes that occurs in a high pressure liquid fuel injection systems, a droplet collision process should be considered. Due to that fact, the O'Rourke collision model was modified and implemented into the Euler Eulerian spray code.

- A new method for solving the reactive multiphase processes was developed by combining the Euler Eulerian size – of – classes approach together with the chemical kinetics. The method was initially developed on a simplified combustion case and it was later thoroughly validated taking into account various combustion parameters.
- The newly developed method was used for modelling real engineering combustion systems. To the authors knowledge such an approach has never been reported in the literature.
- All the performed work within this thesis directly contributed to the industrial sector where all model modifications were implemented into the commercial CFD code.
- The developed method can be used to extend the usage of the Eulerian multi-continuum approach to various applications with reactive multiphase flows.

### 4.3. Recommendations for future research

The work performed in this thesis produced new ideas for further development of CFD models. The work was based on some assumptions and simplification which can be further improved. Also, the numerical efficiency of the overall method could be increased. Some of the recommendations for future work are described in the following part:

- The nozzle flow – spray interface could be further enhanced. In the current approach, the mapping is performed by searching nearest neighbour faces between the overlapping selections. This way, a  $n^2$  loop was introduced which is found to be computationally ineffective ( $n$  is number of nozzle outlet faces). It could be enhanced by developing the spline surface from the nozzle outlet selection data (for all necessary quantities). Such surface can be mirrored and placed in a certain direction and position to cover the inlet selection in the spray simulation. The inlet boundary data can then be interpolated from the spline surface, which is considered to be efficient and mesh independent.
- The primary break – up model within the Euler Eulerian framework could be further modified to take into account creation of unstable fuel ligament structures. The question is how the solver should be changed, and if this could be done only by modification of the drag coefficient for certain droplet classes. Such an enhancement would lead to some changes in the modelled results, but it would introduce more physics in the overall modelling process.
- The secondary break-up WAVE model could be further modified. Instead of the modification shown in this thesis, the mass shift from the parent class could be



transferred to all child classes through desired distribution function. For this, a validation case which neglects all other physical models should be used. Therefore, instead of injection of a bulk jet, injection of droplets from a droplet generator should be applied. The evaporation process can be suppressed by injection at low temperature environments.

- The O'Rourke collision model implemented within the Euler Eulerian size – of – classes approach could be further improved. In the current approach, the collision between droplets of same Eulerian class is not calculated due to the absence of the droplet relative velocity which is needed to calculate droplet collision frequency. The implemented model considers only the coalescence collision regime. This could be enhanced with other collision outcomes, as there are separation and bouncing described in the literature.
- The Euler Eulerian size – of – classes approach could be further enhanced with a wall interaction model.
- The developed method for modelling the multiphase combustion process could be modified by several enhancements:
  - In a real combustion applications where the combustion is described through chemistry mechanisms, a common way is to use the multi – zone model. This model groups computational cells according to certain rules and significantly reduces the computational time necessary for DVODE solver. In the current approach, the multi – zone model cannot be used together with the turbulence chemistry interaction model. Therefore, the development of the multi – zone model to take into account the turbulence influence should be developed [56].
  - The developed method should be tested on more chemistry mechanisms to found the reasons for the overestimated ID discussed in this thesis in sections 3.7 and 3.8.
  - Some user – friendly GUI modification should be performed. As it was stated in the thesis, the ID and LOL are quantities used for spray characterization. In the literature both of them are defined in various ways, and therefore it is not straight forward how to define them within the commercial CFD code.
- The Euler Eulerian size – of – classes approach could be further enhanced with the soot model.

- The Euler Eulerian spray size – of – classes approach could be further enhanced with the NO<sub>x</sub> model.
- The numerical efficiency of the Euler Eulerian size – of – classes approach could be further improved. In the engine working cycle, the multiphase flow is only reasonable in the period from SOI until the EOI. This implies, that before and after this points the flow could be considered as a single phase flow which could reduce the necessary CPU time.

**LITERATURE**

- [1] Reşitoğlu IA, Altinişik K, Keskin A. The pollutant emissions from diesel-engine vehicles and exhaust aftertreatment systems. *Clean Technol Environ Policy* 2014;17:15–27. doi:10.1007/s10098-014-0793-9.
- [2] Som S, Ramirez AI, Longman DE, Aggarwal SK. Effect of nozzle orifice geometry on spray, combustion, and emission characteristics under diesel engine conditions. *Fuel* 2011;90:1267–76. doi:10.1016/j.fuel.2010.10.048.
- [3] Payri R, García JM, Salvador FJ, Gimeno J. Using spray momentum flux measurements to understand the influence of diesel nozzle geometry on spray characteristics. *Fuel* 2005;84:551–61. doi:10.1016/j.fuel.2004.10.009.
- [4] Payri F, Bermúdez V, Payri R, Salvador FJ. The influence of cavitation on the internal flow and the spray characteristics in diesel injection nozzles. *Fuel* 2004;83:419–31. doi:10.1016/j.fuel.2003.09.010.
- [5] Faeth G., Hsiang L-P, Wu P-K. Structure and breakup properties of sprays. *Int J Multiph Flow* 1995;21:99–127. doi:10.1016/0301-9322(95)00059-7.
- [6] Reitz RD. Mechanism of atomization of a liquid jet. *Phys Fluids* 1982;25:1730. doi:10.1063/1.863650.
- [7] Arcoumanis C, Gavaises M, French B. Effect of Fuel Injection Processes on the Structure of Diesel Sprays, 1997. doi:10.4271/970799.
- [8] Gavaises M, Arcoumanis C, Theodorakakos A, Bergeles G. Structure of high-pressure diesel sprays, 2001. doi:10.4271/2001-24-0009.
- [9] Reitz RD. Modeling atomization processes in high-pressure vaporizing sprays. *At Spray Technol* 1987;3:309–37.
- [10] Reitz RD. Atomization and other breakup regimes of a liquid jet. PhD Thesis Princet Univ, NJ 1978.
- [11] In EU zur S, Transparenten verdampfenden und nicht verdampfenden B unter, Hochdruck. Experimentelle Untersuchung zur Spraystruktur in transparenten, verdampfenden und nicht verdampfenden Brennstoffstrahlen unter Hochdruck. Experimentelle Untersuchung zur Spraystruktur in transparenten, verdampfenden und

- nicht verdampfenden Brennstoffstrahlen unter Hochdruck, 2003.
- [12] Rotondi R, Bella G, Grimaldi C, Postriotti L. Atomization of High-Pressure Diesel Spray: Experimental Validation of a New Breakup Model, 2001. doi:10.4271/2001-01-1070.
- [13] Pilch M, Erdman CA. Use of breakup time data and velocity history data to predict the maximum size of stable fragments for acceleration-induced breakup of a liquid drop. *Int J Multiph Flow* 1987;13:741–57. doi:10.1016/0301-9322(87)90063-2.
- [14] Bower G, Chang SK, Corradini ML, El-Beshbeeshy M, Martin JK, Krueger J. Physical Mechanisms for Atomization of a Jet Spray: A Comparison of Models and Experiments, 1988. doi:10.4271/881318.
- [15] Hiroyasu H, Arai M. Structures of Fuel Sprays in Diesel Engines. 1990. doi:10.4271/900475.
- [16] Dent JC. A Basis for the Comparison of Various Experimental Methods for Studying Spray Penetration. 1971. doi:10.4271/710571.
- [17] Delacourt E, Desmet B, Besson B. Characterisation of very high pressure diesel sprays using digital imaging techniques. *Fuel* 2005;84:859–67. doi:10.1016/j.fuel.2004.12.003.
- [18] Sovani S., Chou E, Sojka P., Gore J., Eckerle W., Crofts J. High pressure effervescent atomization: effect of ambient pressure on spray cone angle. *Fuel* 2001;80:427–35. doi:10.1016/S0016-2361(00)00105-8.
- [19] Pickett L. Engine Combustion Network 2014. <http://www.sandia.gov/ecn/>.
- [20] Semião V, Andrade P, Carvalho M da G. Spray characterization: Numerical prediction of Sauter mean diameter and droplet size distribution. *Fuel* 1996;75:1707–14. doi:10.1016/S0016-2361(96)00163-9.
- [21] Luo Y, Zhu L, Fang J, Zhuang Z, Guan C, Xia C, et al. Size distribution, chemical composition and oxidation reactivity of particulate matter from gasoline direct injection (GDI) engine fueled with ethanol-gasoline fuel. *Appl Therm Eng* 2015;89:647–55. doi:10.1016/j.applthermaleng.2015.06.060.
- [22] Chen P-C, Wang W-C, Roberts WL, Fang T. Spray and atomization of diesel fuel and its alternatives from a single-hole injector using a common rail fuel injection system. *Fuel* 2013;103:850–61. doi:10.1016/j.fuel.2012.08.013.

- [23] Suh HK, Lee CS. Effect of cavitation in nozzle orifice on the diesel fuel atomization characteristics. *Int J Heat Fluid Flow* 2008;29:1001–9. doi:10.1016/j.ijheatfluidflow.2008.03.014.
- [24] Suh HK, Roh HG, Lee CS. Spray and Combustion Characteristics of Biodiesel/Diesel Blended Fuel in a Direct Injection Common-Rail Diesel Engine. *J Eng Gas Turbines Power* 2008;130:32807. doi:10.1115/1.2835354.
- [25] Labs J, Parker T. Two-dimensional droplet size and volume fraction distributions from the near-injector region of high-pressure diesel sprays. *At Sprays* 2006;16:843–56. doi:10.1615/AtomizSpr.v16.i7.90.
- [26] Faeth GM. Current status of droplet and liquid combustion 1977;3. doi:10.1016/0360-1285(77)90012-0.
- [27] Taseska V, Markovska N, Causevski A, Bosevski T, Pop-Jordanov J. Greenhouse gases (GHG) emissions reduction in a power system predominantly based on lignite. *Energy* 2011;36:2266–70. doi:10.1016/j.energy.2010.04.010.
- [28] Mathiesen BV, Lund H, Karlsson K. 100% Renewable energy systems, climate mitigation and economic growth. *Appl Energy* 2011;88:488–501. doi:10.1016/j.apenergy.2010.03.001.
- [29] International Energy Agency. CO2 Emissions from fuel Combustion. vol. S/V. 2012. doi:10.1787/co2-table-2011-1-en.
- [30] Khair KM, Majewski WA. Diesel Emissions and Their Control. SAE International; 2006.
- [31] Correa SM, Smooke MD. Nox in parametrically varied methane flames. *Symp Combust* 1991;23:289–95. doi:10.1016/S0082-0784(06)80272-9.
- [32] Vujanović M. Numerical Modelling of Multiphase Flow in Combustion of Liquid Fuel, Doctoral Thesis. Zagreb: 2010.
- [33] Zeldovich YB, Sadovnikov YP, Frank-Kamenetskii D. a. Oxidation of nitrogen in combustion. Academy of Sciences of USSR, Institute of Chemical Physics, Moscow-Leningrad.; 1947.
- [34] Matti Maricq M. Chemical characterization of particulate emissions from diesel engines:

- A review. *J Aerosol Sci* 2007;38:1079–118. doi:10.1016/j.jaerosci.2007.08.001.
- [35] Burtscher H. Physical characterization of particulate emissions from diesel engines: a review. *J Aerosol Sci* 2005;36:896–932. doi:10.1016/j.jaerosci.2004.12.001.
- [36] Choi CY, Reitz RD. An experimental study on the effects of oxygenated fuel blends and multiple injection strategies on DI diesel engine emissions. *Fuel* 1999;78:1303–17. doi:10.1016/S0016-2361(99)00058-7.
- [37] Kong S-C, Reitz RD. Application of detailed chemistry and CFD for predicting direct injection HCCI engine combustion and emissions. *Proc Combust Inst* 2002;29:663–9. doi:10.1016/S1540-7489(02)80085-2.
- [38] SAARIO A, REBOLA A, COELHO P, COSTA M, OKSANEN A. Heavy fuel oil combustion in a cylindrical laboratory furnace: measurements and modeling. *Fuel* 2005;84:359–69. doi:10.1016/j.fuel.2004.10.002.
- [39] Sun Z-Y, Li G-X, Chen C, Yu Y-S, Gao G-X. Numerical investigation on effects of nozzle's geometric parameters on the flow and the cavitation characteristics within injector's nozzle for a high-pressure common-rail DI diesel engine. *Energy Convers Manag* 2015;89:843–61. doi:10.1016/j.enconman.2014.10.047.
- [40] Dukowicz JK. A particle-fluid numerical model for liquid sprays. *J Comput Phys* 1980;35:229–53. doi:10.1016/0021-9991(80)90087-X.
- [41] Gouesbet G, Berlemont A. Eulerian and Lagrangian approaches for predicting the behaviour of discrete particles in turbulent flows. *Prog Energy Combust Sci* 1999;25:133–59. doi:10.1016/S0360-1285(98)00018-5.
- [42] Loth E. Numerical approaches for motion of dispersed particles, droplets and bubbles. *Prog Energy Combust Sci* 2000;26:161–223. doi:10.1016/S0360-1285(99)00013-1.
- [43] Chen X-Q, Pereira JCF. Stochastic-probabilistic efficiency enhanced dispersion modeling of turbulent polydispersed sprays. *J Propuls Power* 1996;12:760–9. doi:10.2514/3.24099.
- [44] IYER V, ABRAHAM J. Penetration and Dispersion of Transient Gas Jets and Sprays. *Combust Sci Technol* 1997;130:315–34. doi:10.1080/00102209708935747.
- [45] Jiang X, Siamas GA, Jagus K, Karayiannis TG. Physical modelling and advanced

- simulations of gas–liquid two-phase jet flows in atomization and sprays. *Prog Energy Combust Sci* 2010;36:131–67. doi:10.1016/j.pecs.2009.09.002.
- [46] Hallmann M, Scheurlen M, Wittig S. Computation of Turbulent Evaporating Sprays: Eulerian Versus Lagrangian Approach. *J Eng Gas Turbines Power* 1995;117:112. doi:10.1115/1.2812758.
- [47] Subramaniam S. Lagrangian–Eulerian methods for multiphase flows. *Prog Energy Combust Sci* 2013;39:215–45. doi:10.1016/j.pecs.2012.10.003.
- [48] Ménard T, Tanguy S, Berlemont A. Coupling level set/VOF/ghost fluid methods: Validation and application to 3D simulation of the primary break-up of a liquid jet. *Int J Multiph Flow* 2007;33:510–24. doi:10.1016/j.ijmultiphaseflow.2006.11.001.
- [49] Shinjo J, Umemura A. Detailed simulation of primary atomization mechanisms in Diesel jet sprays (isolated identification of liquid jet tip effects). *Proc Combust Inst* 2011;33:2089–97. doi:10.1016/j.proci.2010.07.006.
- [50] Herrmann M. on Simulating Primary Atomization Using the Refined Level Set Grid Method. *At Sprays* 2011;21:283–301. doi:10.1615/AtomizSpr.2011002760.
- [51] Martin Sommerfeld, Berend van Wachem RO, editor. *Best Practice Guidelines for Computational Fluid Dynamics of Dispersed Multiphase Flows*. vol. 8. 2008.
- [52] Harlow FH, Amsden AA. Numerical calculation of multiphase fluid flow. *J Comput Phys* 1975;17:19–52. doi:10.1016/0021-9991(75)90061-3.
- [53] Iyer VA, Abraham J, Magi V. Exploring injected droplet size effects on steady liquid penetration in a Diesel spray with a two-fluid model. *Int J Heat Mass Transf* 2002;45:519–31. doi:10.1016/S0017-9310(01)00168-5.
- [54] Issa R., Oliveira P. Numerical prediction of phase separation in two-phase flow through T-junctions. *Comput Fluids* 1994;23:347–72. doi:10.1016/0045-7930(94)90045-0.
- [55] Behzadi A, Issa RI, Rusche H. Modelling of dispersed bubble and droplet flow at high phase fractions. *Chem Eng Sci* 2004;59:759–70. doi:10.1016/j.ces.2003.11.018.
- [56] FIRE manual 2013. Graz: 2013.
- [57] von Berg E, Edelbauer W, Alajbegovic A, Tatschl R, Volmajer M, Kegl B, et al. Coupled Simulations of Nozzle Flow, Primary Fuel Jet Breakup, and Spray Formation. *J Eng Gas*

- Turbines Power 2005;127:897. doi:10.1115/1.1914803.
- [58] Edelbauer W, Suzzi D, Sampl P, Tatschl R, Krueger C, Weigand B. New Concept for on-Line Coupling of 3D Eulerian and Lagrangian Spray Approaches in Engine Simulations. *Iclass-2006* 2006.
- [59] Edelbauer W. Coupling of 3D Eulerian and Lagrangian spray approaches in industrial combustion engine simulations. *J Energy Power Eng* 2014;8:190–200. doi:10.17265/1934-8975/2014.01.022.
- [60] Vujanović M, Petranović Z, Edelbauer W, Duić N. Modelling spray and combustion processes in diesel engine by using the coupled Eulerian–Eulerian and Eulerian–Lagrangian method. *Energy Convers Manag* 2016. doi:10.1016/j.enconman.2016.03.072.
- [61] Vallet A, Burluka AA, Borghi R. Development of a Eulerian Model for the “Atomization” of a Liquid Jet. *At Sprays* 2001;11:24. doi:10.1615/AtomizSpr.v11.i6.20.
- [62] De Luca M, Vallet A, Borghi R. Pesticide Atomization Modeling for Hollow-Cone Nozzle. *At Sprays* 2009;19:741–53. doi:10.1615/AtomizSpr.v19.i8.30.
- [63] Ning W, Reitz RD, Diwakar R, Lippert AM. An Eulerian-Lagrangian Spray and Atomization Model With Improved Turbulence Modeling. *At Sprays* 2009;19:727–39. doi:10.1615/AtomizSpr.v19.i8.20.
- [64] Collazo J, Porteiro J, Patiño D, Miguez JL, Granada E, Moran J. Simulation and experimental validation of a methanol burner. *Fuel* 2009;88:326–34. doi:10.1016/j.fuel.2008.09.003.
- [65] Gutheil E. Numerical investigation of the ignition of dilute fuel sprays including detailed chemistry. *Combust Flame* 1993;93:239–54. doi:10.1016/0010-2180(93)90106-D.
- [66] Ge H-W, Gutheil E. Simulation of a turbulent spray flame using coupled PDF gas phase and spray flamelet modeling. *Combust Flame* 2008;153:173–85. doi:10.1016/j.combustflame.2007.10.019.
- [67] Düwel I, Ge H-W, Kronemayer H, Dibble R, Gutheil E, Schulz C, et al. Experimental and numerical characterization of a turbulent spray flame. *Proc Combust Inst* 2007;31:2247–55. doi:10.1016/j.proci.2006.07.111.



- [68] Zhu S, Roekaerts D, Meer T Van Der. Numerical study of a methanol spray flame. *Seventh Mediterr. Combust. Symp.*, 2011, p. 1–8.
- [69] Shuai S, Abani N, Yoshikawa T, Reitz RD, Park SW. Evaluation of the effects of injection timing and rate-shape on diesel low temperature combustion using advanced CFD modeling. *Fuel* 2009;88:1235–44. doi:10.1016/j.fuel.2009.01.012.
- [70] Petranović Z, Vujanović M, Duić N. Towards a more sustainable transport sector by numerically simulating fuel spray and pollutant formation in diesel engines. *J Clean Prod* 2014. doi:10.1016/j.jclepro.2014.09.004.
- [71] Huang Y, Hong G, Huang R. Numerical investigation to the dual-fuel spray combustion process in an ethanol direct injection plus gasoline port injection (EDI+GPI) engine. *Energy Convers Manag* 2015;92:275–86. doi:10.1016/j.enconman.2014.12.064.
- [72] Guo Y. A pure Eulerian model for simulating dilute spray combustion. *Fuel* 2002;81:2131–44. doi:10.1016/S0016-2361(02)00140-0.
- [73] Beck JC, Watkins AP. Simulation of Water and Other Non-Fuel Sprays Using a New Spray Model. *At Sprays* 2003;13:1–26. doi:10.1615/AtomizSpr.v13.i1.10.
- [74] Dhuchakallaya I, Watkins AP. Application of spray combustion simulation in DI diesel engine. *Appl Energy* 2010;87:1427–32. doi:10.1016/j.apenergy.2009.08.029.
- [75] Martinez L, Benkenida A, Cuenot B. A model for the injection boundary conditions in the context of 3D simulation of Diesel Spray: Methodology and validation. *Fuel* 2010;89:219–28. doi:10.1016/j.fuel.2009.06.012.
- [76] Xue Q, Battistoni M, Powell CF, Longman DE, Quan SP, Pomraning E, et al. An Eulerian CFD model and X-ray radiography for coupled nozzle flow and spray in internal combustion engines. *Int J Multiph Flow* 2015;70:77–88. doi:10.1016/j.ijmultiphaseflow.2014.11.012.
- [77] Bekdemir C, Somers LMT, de Goey LPH, Tillou J, Angelberger C. Predicting diesel combustion characteristics with Large-Eddy Simulations including tabulated chemical kinetics. *Proc Combust Inst* 2013;34:3067–74. doi:10.1016/j.proci.2012.06.160.
- [78] Boileau M, Pascaud S, Riber E, Cuenot B, Gicquel LYM, Poinot TJ, et al. Investigation of Two-Fluid Methods for Large Eddy Simulation of Spray Combustion in Gas Turbines. *Flow, Turbul Combust* 2007;80:291–321. doi:10.1007/s10494-007-9123-1.

- [79] Chrigui M, Gounder J, Sadiki A, Masri AR, Janicka J. Partially premixed reacting acetone spray using LES and FGM tabulated chemistry. *Combust Flame* 2012;159:2718–41. doi:10.1016/j.combustflame.2012.03.009.
- [80] A. Kronenburg. *Spray Combustion – A Fresh Perspective*. In: University of Sydney, editor. *Proc. Aust. Combust. Symp.*, Sydney: University of Sydney; 2007.
- [81] Launder BE, Spalding DB. The numerical computation of turbulent flows. *Comput Methods Appl Mech Eng* 1974;3:269–89. doi:10.1016/0045-7825(74)90029-2.
- [82] Lee SL, Lahey RT, Jones OC. The Prediction of Two-Phase Turbulence and Phase Distribution Phenomena Using a K- $\kappa$  Model. *JAPANESE J Multiph FLOW* 1989;3:335–68. doi:10.3811/jjmf.3.335.
- [83] Hanjalić K, Popovac M, Hadžiabdić M. A robust near-wall elliptic-relaxation eddy-viscosity turbulence model for CFD. *Int J Heat Fluid Flow* 2004;25:1047–51. doi:10.1016/j.ijheatfluidflow.2004.07.005.
- [84] Popovac M, Hanjalic K. Compound Wall Treatment for RANS Computation of Complex Turbulent Flows and Heat Transfer. *Flow, Turbul Combust* 2007;78:177–202. doi:10.1007/s10494-006-9067-x.
- [85] Durbin PA. Near-wall turbulence closure modeling without “damping functions.” *Theor Comput Fluid Dyn* n.d.;3:1–13. doi:10.1007/BF00271513.
- [86] Hinze JO. Fundamentals of the hydrodynamic mechanism of splitting in dispersion processes. *AIChE J* 1955;1:289–95. doi:10.1002/aic.690010303.
- [87] Drew DA. *Mathematical Modeling of Two-Phase Flow*. 1982.
- [88] Huh, K Y and Gosman AD. A phenomenological model of Diesel spray atomisation. *Int Conf, Multiph. Flows*, Tsukuba, Japan: 1991.
- [89] Bianchi GM, Pelloni P. Modeling the Diesel Fuel Spray Breakup by Using a Hybrid Model. 1999. doi:10.4271/1999-01-0226.
- [90] O’Rourke PJ. Statistical properties and numerical implementation of a model for droplet dispersion in a turbulent gas. *J Comput Phys* 1989;83:345–60. doi:10.1016/0021-9991(89)90123-X.
- [91] Post SL, Abraham J. Modeling the outcome of drop–drop collisions in Diesel sprays. *Int*

- J Multiph Flow 2002;28:997–1019. doi:10.1016/S0301-9322(02)00007-1.
- [92] JSTOR: Proceedings of the Royal Society of London. Series A, Mathematical and Physical Sciences, Vol. 326, No. 1566 (Jan. 25, 1972), pp. 393-408 n.d. <http://www.jstor.org/discover/10.2307/78012?uid=3738200&uid=2&uid=4&sid=21104439754933> (accessed July 8, 2014).
- [93] Abramzon B, Sirignano WA. Droplet vaporization model for spray combustion calculations. *Int J Heat Mass Transf* 1989;32:1605–18. doi:10.1016/0017-9310(89)90043-4.
- [94] Clift, R., Grace, J.R., Weber ME. *Bubbles, Drops and Particles*. vol. 94. New York: New York ; London : Academic Press, 1978.; 1978. doi:10.1017/S0022112079221290.
- [95] YUEN MC, CHEN LW. On Drag of Evaporating Liquid Droplets. *Combust Sci Technol* 1976;14:147–54. doi:10.1080/00102207608547524.
- [96] Batchelor GK. *An Introduction to Fluid Dynamics*. Cambridge: Cambridge University Press; 2000. doi:10.1017/CBO9780511800955.
- [97] Liu AB, Mather D, Reitz RD. Modeling the Effects of Drop Drag and Breakup on Fuel Sprays. 1993. doi:10.4271/930072.
- [98] Schiller L, Naumann Z. A drag coefficient correlation. *ZVerDeutschIng* 1933;77:318–20. doi:10.1016/j.ijheatmasstransfer.2009.02.006.
- [99] O'Rourke P, Amsden A. The TAB Method for Numerical Calculation of Spray Droplet Breakup. *SAE Tech. Pap.*, 1987, p. 872089. doi:10.4271/872089.
- [100] Sarathy SM, Westbrook CK, Mehl M, Pitz WJ, Togbe C, Dagaut P, et al. Comprehensive chemical kinetic modeling of the oxidation of 2-methylalkanes from C7 to C20. *Combust Flame* 2011;158:2338–57. doi:10.1016/j.combustflame.2011.05.007.
- [101] Luo Z, Som S, Sarathy SM, Plomer M, Pitz WJ, Longman DE, et al. Development and validation of an n-dodecane skeletal mechanism for spray combustion applications. *Combust Theory Model* 2014;18:187–203. doi:10.1080/13647830.2013.872807.
- [102] Lebas R, Menard T, Beau PA, Berlemont A, Demoulin FX. Numerical simulation of primary break-up and atomization: DNS and modelling study. *Int J Multiph Flow* 2009;35:247–60. doi:10.1016/j.ijmultiphaseflow.2008.11.005.

- [103] Kadocsa A. Modeling of Spray Formation in Diesel Engines. BUDAPEST UNIVERSITY OF TECHNOLOGY AND ECONOMICS, 2007.
- [104] Smallwood G, Gulder O. Views on the structure of transient diesel sprays. At Sprays 2000;10:355–86. doi:10.1615/AtomizSpr.v10.i3-5.70.
- [105] Fuel/Engine Interactions n.d. <http://books.sae.org/r-409/> (accessed April 28, 2015).
- [106] Petranović Z, Edelbauer W, Vujanović M, Duić N. Modelling of spray and combustion processes by using the Eulerian multiphase approach and detailed chemical kinetics. Fuel 2017;191:25–35. doi:10.1016/j.fuel.2016.11.051.
- [107] Su L, Li X, Zhang Z, Liu F. Numerical analysis on the combustion and emission characteristics of forced swirl combustion system for DI diesel engines. Energy Convers Manag 2014;86:20–7. doi:10.1016/j.enconman.2014.05.023.
- [108] Wei S, Wang F, Leng X, Liu X, Ji K. Numerical analysis on the effect of swirl ratios on swirl chamber combustion system of DI diesel engines. Energy Convers Manag 2013;75:184–90. doi:10.1016/j.enconman.2013.05.044.
- [109] Reitz R. Development and testing of diesel engine CFD models. Prog Energy Combust Sci 1995;21:173–96. doi:10.1016/0360-1285(95)00003-Z.
- [110] Naber J, Siebers DL. Effects of Gas Density and Vaporization on Penetration and Dispersion of Diesel Sprays, 1996. doi:10.4271/960034.
- [111] Siebers DL. Scaling Liquid-Phase Fuel Penetration in Diesel Sprays Based on Mixing-Limited Vaporization, 1999. doi:10.4271/1999-01-0528.
- [112] Idicheria C a, Pickett LM. Quantitative Mixing Measurements in a Vaporizing Diesel Spray by Rayleigh Imaging. SAE Int J Engines 2007;1:776–90. doi:10.4271/2007-01-0647.
- [113] Pickett LM, Kook S, Williams TC. Visualization of Diesel Spray Penetration , Cool-Flame , Ignition , High- Temperature Combustion , and Soot Formation Using High-Speed Imaging. SAE Int J Engines 2009;2:439–59. doi:10.4271/2009-01-0658.
- [114] Pickett LM, Manin J, Genzale CL, Siebers DL, Musculus MPB, Idicheria C a. Relationship Between Diesel Fuel Spray Vapor Penetration/Dispersion and Local Fuel Mixture Fraction. SAE Int J Engines 2011;4:764–99. doi:10.4271/2011-01-0686.

- 
- [115] Pickett LM, Genzale CL, Bruneaux G, Malbec L-M, Hermant L, Christiansen C, et al. Comparison of Diesel Spray Combustion in Different High-Temperature, High-Pressure Facilities. *SAE Int J Engines* 2010;3:156–81. doi:10.4271/2010-01-2106.
- [116] Pickett, L.M., Genzale, C.L., Manin, J., Malbec, L.-M. and Hermant L. Measurement Uncertainty of Liquid Penetration in Evaporating Diesel Sprays. ILASS-Americas, Ventura, California: 2011, p. Paper No. 2011-111.
- [117] Petranović Z, Edelbauer W, Vujanović M DN. The O'Rourke droplet collision model for the Euler–Eulerian framework. *Proc. 26th Conf. Liq. At. Spray Syst.*, 2014.
- [118] Vujanović M, Petranović Z, Edelbauer W, Baleta J, Duić N. Numerical modelling of diesel spray using the Eulerian multiphase approach. *Energy Convers Manag* 2015. doi:10.1016/j.enconman.2015.03.040.

## **CURRICULUM VITAE**

Zvonimir Petranović was born on July 15<sup>th</sup> in 1986 in town of Koprivnica, Republic of Croatia. He finished the elementary school in his hometown of Križevci, Republic of Croatia. He attended and finished Air technician high school Rudolf Perešin in Zagreb, Republic of Croatia. He was enrolled in the Department of Mechanical Engineering and Naval Architecture at University of Zagreb in 2005 where he completed his master's degree in 2012. His Master thesis entitled "Numerical simulations of spray process during high pressure fuel injection into diesel engine" was done in cooperation with AVL List GmbH, Advanced Simulation Technologies, Graz, Austria. In September 2012 he was enrolled in the doctoral program as a research assistant on the Process and Energy Engineering chair, Faculty of Mechanical Engineering and Naval Architecture, University of Zagreb. The proposed title of his PhD thesis is "Numerical modelling of spray and combustion processes using the Euler Eulerian multiphase approach". He gained knowledge in numerical simulations, advanced use of the CFD code FIRE<sup>®</sup>, programming of the user defined functions and compiling with the existing code, numerical simulations of IC engines, etc. He contributed to the CFD code FIRE<sup>®</sup> through: parameterization of spray atomization models; modification and implementation of the O'Rourke collision model for the Eulerian size – of – classes spray model; validation and enhancement of the WAVE secondary breakup model; enhancement and development of the Spray-Nozzle interface for MPI simulations; enhancement and development of mesh independency for the Spray-Nozzle interface; implementation of Homogenous gas phase reactions for multiphase simulations and Nozzle interface for ELSA simulations; development of inlet boundary condition from the rate of injection diagram. All of his work is currently available for industry through the modified AVL FIRE's graphical user interface.

During his stay at the University of Zagreb he was a teaching as assistant for several courses such as Numerical modelling of combustion and radiation processes, Numerical modelling in aeronautics 2, and Numerical methods in continuum mechanics. He was a corresponding person for several student seminars regarding the numerical simulations of internal combustion engines. Currently, he is one of the corresponding persons for two BSc thesis regarding the injector flow and non-reactive spray process.

During his scientific work he was involved in an international project financed by AVL-AST GmbH entitled "Numerical modelling of combustion processes and formation of pollutant emissions". The results of his scientific research were published in 5 CC indexed international journals and he published dozen of research papers on internationally recognized conferences

(more information can be found on website: <https://bib.irb.hr/lista-radova?autor=335816>). He is a reviewer in several scientific papers for the respected international Journals such as: Energy Conversion and Management, Applied Thermal Engineering, International Communications in Heat and Mass Transfer and International Journal of Heat and Fluid Flow, International Journal of Spray and Combustion Dynamics, and SAE World Congress 2017.

Since 2013 as the member of the Local organizing Committee he helps with organization of several conferences in the series of “Conference on sustainable development of energy, water and environment systems (SDEWES)”. Since 2013 he is a member of the Faculty Council and a member of the student Council. Since 2014 he is the member of the Croatian section of the Combustion Institute. Since 2015 he is the vice president of the student Council, member of the Committee for e-learning and member of the Faculty disciplinary Committee.

He is a winner of international award “Paul Eisenklam Travel Awards for Young Researchers” given by the ILASS-EUROPE for year 2016. He finished his master study with Magna Cum Laude award given for excellent grades. He is a winner of Student Scholarship from National foundation for the support of student living standard in 2011.

He has good English language knowledge, both spoken and written. He has basic German language knowledge.

## ŽIVOTOPIS

Zvonimir Petranović rođen je 15. srpnja 1986. godine u Koprivnici, Republika Hrvatska. Završio je osnovnu školu Vladimira Nazora u Križevcima. Nakon završetka osnovne škole 2001. godine upisao je srednju zrakoplovnu školu Rudolf Perešin u Zagrebu. Nakon završetka srednje škole 2005. godine upisao je fakultet strojarstva i brodogradnje Sveučilišta u Zagrebu. Diplomirao je s pohvalom za visoki prosjek na procesno energetsom smjeru, usmjerenje energetika 2012 godine obranivši diplomski rad pod nazivom “Računalna simulacija stvaranja spreja prilikom visokotlačnog ubrizgavanja goriva u dizel motor”. Rad je financiran i izrađen u suradnji s tvrtkom AVL List GmbH Graz, Republika Austrija. U rujnu 2012 upisao je poslijediplomski doktorski studij na Fakultetu strojarstva i brodogradnje Sveučilišta u Zagrebu, procesno energetska usmjerenje. Predložena tema doktorskog rada pod nazivom “Numerical modelling of spray and combustion processes using the Euler Eulerian multiphase approach” obranjena je u studenom 2015. godine. Tijekom izrade doktorskog rada i boravka na poslijediplomskom studiju stekao je napredna znanja u numeričkim simulacijama, korištenju računalnog programa dinamike fluida AVL FIRE<sup>®</sup>, objektnog programiranja, itd. Njegov rad direktno je odražen na industriju jer je prilikom rada implementirao i unaprijedio nekoliko modela unutar računalnog programa FIRE<sup>®</sup> kao što su: parametrizacija modela raspadanja goriva prilikom visokotlačnog ubrizgavanja, implementacija O’Rourke modela sudaranja kapljica za Eulerovo sučelje, validacija i unaprjeđenje sekundarnog modela raspadanja za Eulerovo sučelje, unaprijeđene sučelja koje se koristi za preslikavanje podataka dobivenih računalnom simulacijom kroz sapnicu na ulaznu selekciju simulacije spreja, unaprjeđenje takvog sučelja za višeprosorsko računanje, implementacija modula za računanje kemijskih reakcija odnosno procesa izgaranja za Eulerov višefazni pristup, razvoj sučelja sapnica-sprej za ELSA simulacije.

Prilikom svog boravka na Fakultetu strojarstva i brodogradnje držao je vježbe na nekoliko predmeta kao što su modeliranje izgaranja i zračenja, numeričke metode u mehanici kontinuuma te numeričke metode u zrakoplovstvu 2. Bio je jedna od odgovornih osoba za vođenje nekoliko desetaka seminarskih radova u području numeričkih simulacija motora s unutarnjim izgaranjem. Bio je jedna od odgovornih osoba za dva završna rada u području strujanja fluida kroz sapnice malog promjera te pojave procesa spreja prilikom visokotlačnog ubrizgavanja.

Prilikom svoga znanstveno-istraživačkog rada uključen je u međunarodni projekt financiran od strane AVL AST d.o.o pod nazivom „Numeričko modeliranje procesa izgaranja”  
*Faculty of Mechanical Engineering and Naval Architecture*



i stvaranja štetnih emisija“. Rezultati njegova istraživanja objavljena su u 5 rada indeksirana u CC/SCI bazama te u desetak istraživačkih radova objavljenih na međunarodno priznatim konferencijama (više informacija može se pronaći na <https://bib.irb.hr/lista-radova?autor=335816>). Trenutno je prijavljen kao evaluator u međunarodno priznatim časopisima visokog faktora odjeka kao što Energy conversion and Management, Applied Thermal Engineering, International Communications in Heat and Mass Transfer, International Journal of Heat and Fluid Flow, International Journal of Spray and Combustion Dynamics, te je bio evaluator za SAE Svjetski Kongres koji će se održati 2017. u Detroitu.

Od 2013. član je lokalne organizacijske skupine na SDEWES konferencijama „Conference on sustainable development of energy, water and environment systems“. Od 2014. član je Jadranske sekcije instituta za izgaranja. Od 2013. član je Fakultetskog vijeća Fakulteta strojarstva i brodogradnje, Sveučilišta u Zagrebu. Od 2015. potpredsjednik je studentskog zbora Fakulteta strojarstva i brodogradnje, Sveučilišta u Zagrebu, član je vijeća za e-učenje i član je stegovnog suda.

Dobitnik je nagrade „Paul Eienklam Travel Awards for Young Researchers“ za 2016. godinu koju dodjeljuje ILASS Europe (European Conference on Liquid Atomization and Spray Systems). Za odličan uspjeh na diplomskom studiju Fakulteta strojarstva I brodogradnje u Zagrebu, dobio je “Magna Cum Laude” pohvalu. Također, 2011. Godine dobio je jednogodišnju stipendiju za porast studentskom standardu u kategoriji deficitarnih zanimanja.

Dobro koristi Engleski jezik, kako u pismu tako i u govoru. Ima osnovno znanje Njemačkog jezika